Thermal Interactions in Laminar Heterogeneous Flames of Non-Volatile Metal Suspensions

Jan Palečka

Department of Mechanical Engineering

McGill University

Montreal

August 2022

A thesis submitted to McGill University in partial fulfillment of the requirements of the degree of Doctor of Philosophy

TABLE OF CONTENTS

ABSTRACT

The characteristic feature of non-volatile solid fuel suspensions is the absence of a continuous premixed gas flame front. Instead, the reaction is localized to or near the surface of individual particles. This "flame-within-a-flame" structure gives rise to a multi-faceted combustion process, whose dynamics are governed by a range of underlying mechanisms. To understand the combustion of solid fuels, fundamental studies often explore the different "facets" of the process. This approach is used in the present thesis which examines two such mechanisms — front coupling and heat locking — and interprets them via simple formulations based on thermal considerations.

Front coupling governs the thermal interaction of reaction fronts formed by the combustion of two or more dissimilar fuels. Experiments were conducted in a novel Hele-Shaw cell apparatus in aluminum-propane-air mixtures, in which aluminum burns with the products of the propane-air front. In each run, the propagation of a quasi-2D flame in a thin high-aspect-ratio long rectangular channel between two parallel windows was observed. The unimpeded line-of-sight of the diagnostics allowed the visualization of the thermally coupled fronts, corresponding to the combustion of propane and aluminum, respectively. The coupling behaviour exhibits a strong dependence on the aluminum front rather than on the propane-air one. High-speed recording also showed several types of frontal instabilities affecting flame coupling/decoupling.

Heat locking occurs when particles ignite and burn diffusively at temperatures higher than their surroundings. In low-thermal-diffusivity media, the fast reaction "locks" heat in steep temperature gradients around the particles. This transition into the so-called "discrete

regime" leads to a fundamental switch in flame physics. Experiments were performed in a remotely operated module (built by Airbus Defence and Space) aboard sounding rockets and parabolic flights, as part of the Percolating Reactive Waves (PERWAVES) project, in collaboration with the European Space Agency (ESA) and the Canadian Space Agency (CSA). In each test, flames in suspensions of micron-size iron particles in xenon/oxygen gas propagated in transparent tubes. During the flight aboard the ESA MAXUS-9 rocket (April 2017), the flame speed of suspensions in 20%- and 40%-oxygen gas was measured. Despite their particles burning three times faster and at higher temperatures, flames in 40%-oxygen mixtures had the same speed as those in the less reactive 20%-oxygen mixture, confirming that flame combustion is controlled by inter-particle heat diffusion rather than by the rate of chemical reaction, in accordance with discrete flame theory. The frontal structure of the flames close to the propagation limit was investigated in a second sounding rocket campaign aboard the ESA TEXUS-56 in November 2019. High-speed imaging of the flames from the rocket flight and from a prior parabolic flight campaign aboard the National Research Council (NRC) Falcon-20 aircraft in May 2019 indicates that, close to their lean propagation limit, flames may exhibit a percolation-like behaviour.

ABRÉGÉ

L'absence de front de flamme de gaz prémélangé continu est une des caractéristiques majeures des suspensions de combustibles solides non volatils. Au contraire, la réaction est localisée à ou près de la surface des particules individuelles. Cette structure de " flamme dans la flamme " donne lieu à un processus de combustion à multiples facettes, dont la dynamique est régie par une série de mécanismes sous-jacents. Pour comprendre la combustion des carburants solides, les études fondamentales explorent souvent les différentes " facettes " du processus. Cette approche est utilisée dans la présente thèse qui examine deux de ces mécanismes, le couplage frontal et le verrouillage thermique, et les interprète grâce à des formulations théoriques simples basées sur des considérations thermiques.

Le couplage frontal régit l'interaction thermique des fronts de réaction formés par la combustion de deux carburants différents ou plus. Des expériences ont été menées dans un nouvel appareil Hele-Shaw dans des mélanges aluminium-propane-air, dans lequel l'aluminium brûle avec les produits du front propane-air. Dans chaque test, la propagation d'une flamme quasi-2D dans un long conduit rectangulaire à rapport hauteur/largeur élevé entre deux fenêtres parallèles a été observée. La ligne de visée sans entrave des diagnostics a permis de visualiser les fronts correspondants respectivement à la combustion du propane et de l'aluminium et couplés thermiquement. Le comportement de couplage présente une forte dépendance au front aluminium plutôt qu'au propane-air. L'enregistrement à grande vitesse a également montré plusieurs types d'instabilités frontales affectant le couplage/découplage de la flamme.

Le verrouillage thermique se produit lorsque les particules s'enflamment et brûlent dans

un régime contrôlé par la diffusion à des températures supérieures à celles de leur environnement. Dans les milieux à faible diffusivité thermique, la réaction rapide "verrouille" la chaleur dans des gradients de température abrupts autour des particules. Cette transition vers le régime dit "discret" conduit à un basculement fondamental de la physique de la flamme. Des expériences ont été réalisées dans un module téléopéré (construit par Airbus Defence and Space) à bord de fusées-sondes et de vols paraboliques, dans le cadre du projet Percolating Reactive Waves (PERWAVES), en collaboration avec l'Agence spatiale européenne (ESA) et l'Agence spatiale canadienne (ASC). Dans chaque test, des flammes dans des suspensions de particules de fer micrométriques dans du gaz xénon/oxygène se sont propagées dans des tubes transparents. Lors du vol à bord de la fusée ESA MAXUS-9 (avril 2017), la vitesse de flamme de suspensions dans des gaz à 20% et 40% d'oxygène a été mesurée. Bien que leurs particules brûlent trois fois plus vite et à des températures plus élevées, les flammes dans les mélanges à 40% d'oxygène avaient la même vitesse que celles dans le mélange moins réactif à 20% d'oxygène, confirmant que la combustion des flammes est contrôlée par la diffusion de chaleur inter-particules plutôt que par la vitesse de réaction chimique, conformément à la théorie des flammes discrètes. La structure frontale des flammes proches de la limite de propagation a été étudiée lors d'une deuxième campagne de fusées-sondes à bord de l'ESA TEXUS-56 en novembre 2019. L'imagerie à grande vitesse des flammes pendant le vol de la fusée et une précédente campagne de vols paraboliques à bord de l'avion Falcon-20 du Conseil national de recherche (CNR) en mai 2019 indique que, près de leur limite de propagation, les flammes peuvent présenter un comportement de type percolation.

ACKNOWLEDGEMENTS

I would like to start by thanking my supervisor, Prof. Jeffrey Bergthorson for the many years of guidance, advice, support, and trust, as well as for all the incredible opportunities I have had in his research group.

My thanks also go to Dr. Samuel Goroshin, who has also supervised me for many years, and who has inspired me for the PhD in this exciting field. Thanks to him and his endless curiosity, I was permanently exposed to new concepts, ideas, and solutions I would have hardly thought of myself. I also came to value, especially after the years, the sometimes harsh criticisms in the good old "Russian-school" tradition. They were very useful.

My thanks also go to Profs. David Frost and Andrew Higgins whose many advices helped me to progress in my work and studies.

I would also like to thank the many fellow students I have had the pleasure to work with, to suffer with, and to party with. Specifically Michael Soo, Philippe Julien, Sam Whitely, Alex Wright, Kartik Mangalvedhe, Antoine Durocher, Keena Trowell, Michelle McRae, Santino Salvo, James Vickery, and many others.

Chtěl bych taky poděkovat celé své rodině, která při mě stála po celá ta léta, která jsem se rozhodl strávit tak daleko od domova. Chtěl bych poděkovat rodičøum, Zuzaně, Petrovi a jeho rodině.

And my sincerest thanks go to Nina who has been an incredible support during all these years and has always given me so much care and love.

CONTRIBUTIONS TO ORIGINAL KNOWLEDGE

Several contributions have been made to the advancement of the field of combustion of non-volatile suspensions.

Technical contributions:

1) Building and use of a novel Hele-Shaw apparatus for the direct visualization of the frontal structure of flames in metallic suspensions.

2) Development of a flame tracking algorithm for metallic flames propagating in the Hele-Shaw apparatus.

3) Development of an algorithm to track the combustion and determine particle ignition from high-speed videos.

4) Development of alternative algorithm for discrete flame computations based on the tracking of the flame front.

Scientific contributions:

1) Critical concentration of suspension: Confirmation of the existence of a critical concentration required for the stabilization of an aluminum front in the wake of the stoichiometric propane-air front. This concentration is shown to increase for fuel-rich propane-air flames, as the reaction of both fronts becomes weaker, and to decrease as more oxygen is available for the second (aluminum) front in fuel-lean propane-air flames.

2) Thermal coupling dependence on second front: in a micron-sized aluminum-propane-air

flames, as the equivalence ratio of the first fuel-lean propane-air front is lowered, the separation between the fronts decreases and the flame speed increases. The propagation of the flame is controlled by the stronger coupling through the increased heat transfer from the second front rather than by the weakening heat production of the first front.

3) Interaction of thermal coupling and instabilities: the thermally coupled flame decouples in the strained region of the flame crest, while the coupling is maintained in the cusp region.

4) Confirmation of the discrete propagation regime in suspensions: the speed of flames propagating in quiescent mixtures of micron-sized iron in low-diffusivity oxygen/xenon gas is independent of the combustion time of particles, which can be only explained by the discrete regime of combustion.

5) Heat locking and percolating flames: the propagation of flames in iron suspensions in oxygen-xenon gas transitions from a parabolic front shape to a rough discrete surface of a percolating flame as the concentration of iron is lowered.

CONTRIBUTION OF AUTHORS

Contributions of co-authors and participants on the projects are listed by publication:

Chapter 2 Publication [1]: Palečka, J., Park, J., Goroshin, S. & Bergthorson, J. M., Aluminum-propane-air hybrid flames in a Hele-Shaw cell. Proc. Combust. Inst. 38, 4461–4468 (2021).

I assisted with the supervision of the McGill capstone project team, which developed and built the dispersion cone and the chamber of the Hele-Shaw cell, and performed flow analyses on ANSYS to determine an appropriate shape of the diffuser. With the help of Honours and Summer undergraduate student, J. Park, I conducted experiments involving gas flames, aluminum flames, and hybrid aluminum-propane flames. I wrote the publication and produced the graphical material. J. Park used my codes to provide flame speed data and to determine the separation of the fronts. S. Goroshin and J.M. Bergthorson provided corrections and edits with improved the discussion, writing, and analysis of the data.

Chapter 3 Publication [2]: Palečka, J., Sniatowsky, J., Goroshin, S., Higgins, A. J. & Bergthorson, J. M., A new kind of flame: Observation of the discrete flame propagation regime in iron particle suspensions in microgravity. Combust. Flame 209, 180–186 (2019)

I took part in the final phase of the preparation of the MAXUS-9 sounding rocket campaign along with S. Goroshin and A.J. Higgins, who also supervised the scientific team prior to the start of my PhD. I was part of the science team during the launch and conducted the

experiment, along with S. Goroshin, remotely during the flight. I performed the analysis of the post-flight data and, along with S. Goroshin and J. Sniatowsky, I performed the single-particle time measurements and analysis. I co-wrote the publication with S. Goroshin and prepared the graphical material. I also participated in the post-flight calibration, performing data analysis and selecting parameters to be calibrated. J.M. Bergthorson co-supervised the later stage of the project and his edits, comments, and contributions helped to improve the analysis.

Chapter 4 Publication: Palečka, J., Goroshin, S. & Bergthorson, J. M., Heat-locking, and limits of flame propagation in discrete flames, *Ready for submission*

I reduced some equations to more compact forms using special functions and interpreted some features in the regular regime. I developed an alternative to the previously used code for calculations in the random regime. In the experimental part, I co-led the work of the scientific team in the transition from the MAXUS-9 to the TEXUS-56 campaign, and developed a code for reliable tracking of burning particles. I co-led the activities of the science team before, during, and after the TEXUS-56 flight, similar to the MAXUS-9 campaign. I also participated in a parabolic flight campaign (May 2019) and led the McGill team during a second campaign (November 2021), attempting a post-calibration of data affected by a malfunction of the apparatus during the TEXUS-56 flight. I co-wrote the publication with S. Goroshin, and J.M. Bergthorson's edits and comments helped to improve and focus the analysis.

LIST OF TABLES

LIST OF FIGURES

CHAPTER 1
Introduction and comprehensive review of literature

1.1 Combustion of powders: a growing but fragmented field

The combustion of solid fuels has long been one of the main drivers of human development. Wood, peat, and coal have provided cheap, readily available, and high-intensity energy to power the pits, kilns, and furnaces from the bronze age until the industrial revolution. Especially in the form of small particles, whose large area-to-volume ratio ensures high rates and efficiency of the reaction, solids have continued to support high-power applications through their use in propellants, slurry fuels, and explosives [8, 9], as well as in material synthesis and processing technologies [10, 11]. Even today, amidst global efforts to reduce the carbon footprint of the energy sector, the combustion of metallic powders can offer the solution to an efficient energy storage: metal powders can act as efficient energy carriers, which can be burned to produce power, reduced back to metals thanks to renewable energy, traded as an energy commodity, and safely stored until the next use, all in a zero-carbon sustainable cycle [12, 13]. Suspensions may even drive space exploration, as metals and oxygen are often the only abundant propellants available on planets or asteroids [14] and can be used in metal-oxygen powdered rockets [15]. As a downside to the high reactivity, suspensions of reactive powders can cause serious accidents in countless industries handling fine powders, such as mining, pharmaceuticals, food processing [16, 17], chemical and metallurgical industries, or transportation [6].

Nevertheless, the combustion of solid fuel suspensions remains relatively poorly understood. While progresses in gas combustion, fluid dynamics, and quantum physics, among others, allow us to build complex power plants, wind turbines, solar panels, or jet engines with high precision, most industrial applications involving the combustion of powders still rely on empirical formulations or highly-fitted models with many adjustable parameters, which offer little fundamental insight and cannot be used outside of restricted operating conditions [6]. As for industrial safety, the limited understanding of the seemingly haphazard behaviour of reactive powders may lead to inadequate protective measures or to the use of costly excessive safety factors in the design and operating conditions of powder-handling facilities and appliances.

This, however, does not stem from a lack of scientific effort. On the contrary, significant work has been undertaken to provide a fundamental understanding of the processes that govern the combustion of suspensions since the early days of combustion science, starting with detailed review articles from the 1960's and 1970's that describe a large volume of work concerning the combustion of coal [18], metals [19], solid propellants [20], or compact powders [21]. Since then, research has focused on the investigation of the combustion of many solid systems. Despite all this effort, the field remains largely fragmented into isolated fields, which often focus on specific fuels or applications [6].

1.2 Combustion of suspensions: a multifaceted problem

The lack of a unified theoretical understanding analogous to gas flames is due to the variety and complexity of processes involved in solid combustion, as well as to the large degree of coupling between different length and time scales.

With the exception of soot formation and a few other phenomena [22], which involve multi-phase processes, the combustion of gaseous reactants is a single-phase homogeneous phenomenon, in which activated reactions occur through collisions at the molecular level. While the reactions may involve thousands of steps — between almost as many possible species — they usually happen within a short time scale (10^{-3} s) and are confined to a thin reaction zone (~ 0.1 mm). In comparison, characteristic lengths of molecular and thermal transport are on the order of a millimetre, while various hydrodynamic phenomena occur on much larger scales [23]. This opens the possibility for carefully designed experiments, in which the different effects can be, to some extent, de-coupled. The studies, often performed in laminar conditions on specially designed burners, provide a fundamental background for the understanding of complex real-life applications, for example those involving turbulent combustion.

The situation is very different for particulate fuels, in which the bulk of the solid is in the form of nano- to micron-sized particles. Chemical reactions occur at the interface between the particle/droplet and the gas, and their rates directly depend on an intricate interplay of transport and surface phenomena, phase changes, and complicated flows [24, 25]. The latter in turn respond directly to variations in large-scale temperature, concentration, and flow fields through a complex feed-back. As a result, the heterogeneous combustion of solid suspensions is a complicated multi-faceted process, which, even for laminar flames, strongly depends on the multi-scale nature of the interactions. Thus, while studies of the combustion of single isolated particles provide useful input parameters, they cannot explain the dynamics of burning suspensions. Instead, it is useful to isolate and explore the different "facets", i.e., the key mechanisms, which govern the combustion process in suspensions. The purpose of

this thesis is to examine two such mechanisms — front-coupling and heat-locking — from a fundamental perspective. The work does not concentrate on the specificities of the fuels used but tries instead to capture the underlying physics, which may be responsible, to varying degrees, for characteristic features observed in many systems. The following sections, as well as the presented publications, are therefore formulated with this goal in mind.

1.3 Why metals to study flames in non-volatile suspensions?

The heterogeneous nature of suspensions, which is responsible for the characteristics of their combustion, varies according to the volatility of the fuel. For example, plastics, such as polymethyl methacrylate (PMMA), exhibit the same behaviour as droplets of hydrocarbon sprays [26], as they melt and vaporize at low temperatures, and mix with the surrounding air in the preheat zone [27]. The combustion process thus occurs entirely in the gas phase.

Other more complex fuels, such as coal, contain refractory (i.e., high-boiling-temperature) fuel fractions (char) along with high-volatility components. The result is a complex flame in which some fractions burn heterogeneously while others volatilize and undergo homogeneous combustion with air [28, 29]. While such flames have the potential to exhibit front coupling, they do not usually offer sufficient control of parameters for fundamental studies of the phenomenon.

Finally, many metals have high melting and boiling points, and do not significantly vaporize in the preheat zone [30]. In addition, the oxidation of metal vapours is defined by low-activation energies already at room temperature [31] and, close to the flame temperature, premixing of gaseous metal and oxygen is precluded, and the reaction is thus confined to the vicinity of individual particles. Thus, despite having a combustion temperature above

the boiling point, metals such as aluminum or iron can be used in model mixtures for the exploration of fundamental processes in heterogeneous flames and have been chosen for experiments in this thesis.

1.4 Particle ignition: a key feature of heterogeneous combustion

A key concept in heterogeneous combustion is particle ignition. Some confusion exists in the literature concerning the term, as it has been used to describe various processes that bring particles to reaction, irrespective of whether they are critical or not [6]. Heterogeneous ignition theory was developed by Vulis [32] and Frank-Kamenetskii [33] as an extension of Semenov's non-adiabatic thermal explosion theory [34] for closed reactors. The analysis has been recently extended to burning suspensions [3, 35]. The model examines the temperature (T_p) evolution of a fuel particle of radius r placed in an oxidizing environment at temperature T_g. The oxidizer diffuses towards the particle where it reacts with the fuel molecules. The rate of heat production, Q_r of the reaction therefore depends on the speed of each process, and can be expressed as $Q_\mathrm{r} \propto \frac{k\beta}{k+\beta}$, where k is the rate of surface reaction corresponding to a one-step Arrhenius reaction, $k \propto \exp\left(-\frac{E_\mathrm{a}}{RT_\mathrm{p}}\right)$, where E_a is the activation energy and R the gas constant, and $\beta \propto \frac{1}{r}$ is the mass transfer coefficient related to the diffusion process. As it heats up, the particle is subjected to growing heat losses $Q_\mathrm{l} \propto (T_\mathrm{p} - T_\mathrm{g})$. As the diagram in Fig. 1–1 shows, in an initially cold gas, the heat production from small particles will always be controlled by their heat losses to the surrounding ($Q_{\mathrm{l},1}$). However, for larger particles, heating ($r \geq r_\mathrm{cr}$) is no longer compensated, so upon reaching the critical inflection point at $T_\mathrm{p} = T_\mathrm{cr}$, the heat losses ($Q_{\mathrm{l},2}$) no longer control the rate of heat reaction, k. As a result, the particle temperature rapidly increases and transitions to an upper branch, where the particle

burns in a diffusion-controlled regime, as at $k \gg \beta$, $Q_r \sim \beta \sim \frac{1}{r}$. The particle then behaves like a "flame inside a flame", as its reaction rate is largely independent of the temperature of its surroundings and decreases mainly with the shrinking size of the reactive surface [6]. It is the sudden transition between the low-temperature kinetic and high-temperature diffusive regimes, which occurs at a critical point that defines particle ignition. When either the particle shrinks below a certain size or the supply of oxidizer becomes limited, such as in fuel-rich suspensions, the particle transitions back towards the kinetically controlled branch through extinction (at heat losses $Q_{l,3}$) [35].

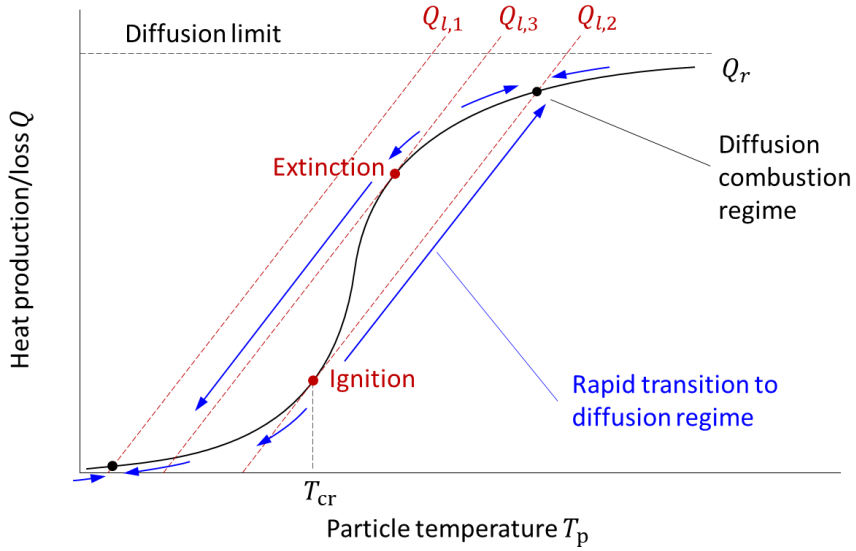

Figure 1–1: Process of particle ignition and extinction. Note that the curves are qualitative and do not reflect the effect of decreasing r on the shape of the Q_r and Q_l curves [3].

The combustion of a diffusively burning particle can occur in several different modes. The formulation made by Glassman and co-workers [30] and later improved by Steinberg *et al.* [36], is based on thermodynamic data. As previously discussed, in the diffusive regime,

the reaction of the particle is predicted to converge towards the stoichiometric adiabatic flame temperature, T_{ad}. When the latter exceeds the boiling temperature T_{b}, the metal evaporates and its vapours instantaneously react with the surrounding oxygen; a gas-phase homogeneous flame surrounds the particle at a stand-off distance, at which the outward flow of metal vapours equilibrates with inward diffusion of oxygen. Conversely, when $T_{\mathrm{b}} > T_{\mathrm{ad}}$, the oxidizer diffuses towards the particle, is adsorbed at the surface and reacts heterogeneously with the condensed metal. In addition, the phase of the products plays an important role. When the total predicted partial pressure of oxides/sub-oxides produced by the reaction at T_{ad} is high, the mostly gas-phase products are conveyed away from the particle through diffusion and Stefan flow. However, when their partial pressure is low, the mostly condensed products often remain at the surface, forming an oxide layer through which the reactants must diffuse to react. It should also be noted that condensed products, created by vapour combustion, may still deposit on the surface of the particle due to complex flows [37].

While this simplified formulation disregards many complex physical processes as well as the interaction with other particles in the suspension, it still provides a useful qualitative understanding of particle combustion. A more detailed description the combustion of fuels used in the present thesis can be found both for aluminum [38, 39, 40, 41, 42] as well as for iron particles [43, 44, 45, 46].

While particle ignition is linked to large rates of reaction at high temperatures, it is not the only way to achieve fast combustion. For example, particles suspended in dense clouds can burn at high rates even in a kinetically controlled regime [3, 35]. This is due to what has been referred to as the "cooperative mechanism (or effect)" [47, 48] or the "collective effect" [49], whereby the collective rate of heat production of particles is sufficient to raise the local

gas temperature, T_g, in the cloud. Through a feedback between T_g and the kinetic reaction rate, k, particles can achieve high rates of reaction without ever igniting. The resulting flame resembles a gas one, as any fluctuation in the temperature field is instantaneously reflected on the reaction rate of particles.

1.5 Stable propagation of metallic suspensions

The first to formulate the idea that a cloud of particles can undergo intense combustion with oxygen without any other flammable gases was Faraday in 1844 [19]. While this statement was formulated in connection with coal dust in mine explosions, it became obvious that it applied for metal powders as well. Since then, the bulk of the experimental research was mainly interested in the determination of the "explosibility" of different metallic suspensions. Experimental testing in metal and heterogeneous mixtures was (and still is) performed in closed bombs and vessels [50, 51, 52], with the explosive powder mainly assessed via the maximum attained pressure and the pressure rise. The susceptibility to ignite is measured through the Minimum Ignition Energy (MIE). Despite being performed in standardized conditions, the experiments often suffer from shortcomings of the approach [6]: powder dispersion is either too short to allow initial turbulence to decay or too long to avoid significant particle settling; the lack of visual access often prevents one from verifying the uniformity of the dispersion process and of flame propagation; pressure traces are not a reliable diagnostic for a system subjected to complex dynamics.

In parallel to testing in closed vessels, another stream of research — based on direct visual access to the flame and focused on the study of more fundamental aspects of combustion in suspensions — soon developed. In 1924, Nusselt [53, 19] realized that the combined

heat release of individually burning particles can significantly raise the temperature of the surrounding carrier gas and, similar to gas mixtures, could form and sustain a stationary conical Bunsen-type flame front. The first to overcome the challenges related both to the dispersion and stabilization of metal flames was Cassel at the US Bureau of Mines in 1948 [54], who measured flame speeds of Bunsen flames of, among others, aluminum, and calculated corresponding burning velocities. The work was followed by experiments on stabilized flames of metallic suspensions in Bunsen flames [55, 56, 57, 58], in lifted flames [59], and most recently, on flat counter-flow flames [60, 61], which, combined with PIV, provide the most reliable flame speed measurements [6]. While flame stabilization allows high levels of control and accuracy in testing, it is experimentally challenging in suspensions, which explains the relatively restrained number of institutions with the capabilities to do so. Moreover, experience has shown that a minimum burning velocity is required, which limits the method for suspensions below a certain particle size and to powder concentrations close or above stoichiometry.

An alternative approach is the study of freely propagating flames. For example, spherically expanding flames are often used in gas combustion[62, 63, 64], where a constant pressure environment can be achieved inside of large soap bubbles [65], filled with the reactive mixture, or in constant-pressure chambers with visual access [63]. Due to the practical constraints linked to suspensions, latex balloons were used to provide a quasi-constant pressure environment [66, 67]. As shall be seen in Section 1.7, transparent balloons allowed, for example, the direct observation of a variety of instability mechanisms [67]. However, the relatively large size of the experimental apparatus, the need to provide containment of the mixture after the flame bursts the balloon membrane, and the difficulties in focusing on fronts in complex

three-dimensional structure of the flame propagating in an optically thick medium could not satisfy the objectives of the present study.

Consequently, thermal interactions between fronts as well as the ones within them, which are the subject of this thesis, were studied in transparent tubes and channels. Compared to the previously described configurations, the constrained geometry of tubes/channels presents several challenges that make it unsuitable for many experiments. First, in the presence of gravity, flame propagation is affected by strong sedimentation of particles, which prevents the formation of uniform mixtures and induces strong recirculation cells in the tube. This is also compounded by strong buoyancy of product gases that usually dominate the dynamics of flame propagation. In addition, flames in tubes and channels often experience strong thermo-acoustic coupling, which prevents steady-state propagation. As will be explained later, these effects are avoided in microgravity experiments or are actually beneficial for our studies on the ground.

1.6 Microgravity: an indispensable experimental tool

Gravity plays an important role in the propagation of flames. It has been shown that buoyancy affects the flame stability, by stabilizing the propagation of downward flames, and enhancing hydrodynamic disruption of upward-propagating ones [68]. Microgravity research has played an important role in gas combustion, as it allows to observe conditions and experiments that would not be possible on the ground [69]. Early studies involved the study of the effects of buoyancy on flammability limits in drop towers [70]. The lower effect of buoyancy was also used to create conditions at which a slow flame extinguishes due to radiation losses [71]. Other studies — among many others — performed on different microgravity platforms,

examined flame instabilities [72, 73], cool flames [74] and probably most famously, proved the existence of so-called "flame balls" [75, 76], i.e., stationary spherical flames, which, at low gravity are sustained through the balance of heat and mass transfer.

However, the absence of gravity has a far greater impact and importance in the study of fundamental flame propagation in solid fuels, especially suspensions [6]. On the ground, gravitational effects, such as the buoyancy of hot combustion gases, particle sedimentation, and a general bulk instability of dust clouds often prevent a uniform, stable, and laminar dispersion of particles over a large range of sizes and fuel concentrations. This has been identified as a major cause for the difficulty in obtaining fundamental data on laminar flames in suspensions [6]. In this sense, microgravity research is crucial for the fundamental understanding of combustion behaviour in heterogeneous flames.

The earliest experiments involving suspensions of particles in microgravity were performed in small laboratory drop-towers [77, 78], which allowed limited times of lower-microgravity conditions. Further drop-tower tests were performed both by NASA [79] and the Japan Microgravity Center (JAMIC) [80]. The research was also expanded to parabolic flights [81, 82]. The tests mostly involved organic materials such as PMMA or coal, with some tests performed with metals. While not producing systematic results, combustion of metals (aluminum, magnesium, iron) in reduced environments was achieved in subsequent experiments [83, 84, 85, 86]. More fundamental studies of flames were performed only in the first years of the 21st century aboard the Falcon-20 parabolic flight aircraft jointly operated by the National Research Council of Canada and the Canadian Space Agency [87, 88].

1.7 Flame instabilities: a factor not to forget

Instabilities often affect flames in non-volatile solid suspensions in gaseous oxidizers. While the topic has received only limited attention, some insight can be obtained from other combustion systems. For instance, the deformation of an originally steady-state planar flame front in non-volatile suspensions is often caused by mechanisms with direct analogues in gas combustion, summarized in several reviews [89, 90, 68]. The effect of particle inertia and drag on flame dynamics has been studied in the context of sprays and volatile suspensions [91, 92, 93], and instabilities caused by the non-diffusive nature of the fuel have been described in condensed (gasless) systems [94, 95, 96]. Despite the merit of such comparisons, the unique features of non-volatile suspensions will require separate experimental and theoretical treatment [6].

In their seminal works, Darrieus [97] and Landau [98] showed that, when represented as thin interfaces between cold and hot gas, flames are unconditionally unstable, as gas expansion behind the flame enhances the growth of perturbations of all sizes. As shown in Fig. 1–2, conservation of mass between regions far upstream and downstream of the flame requires the widening of streamtubes to account for gas expansion in flame regions convex with respect to the unburnt gas, resulting in the decrease of flame speed. The inverse occurs in the concave regions, in which the gas flow accelerates. In the flame frame of reference, this corresponds to an acceleration/deceleration of the convex/concave region and a further wrinkling of the flame. While not applicable to small scales, the Darrieus-Landau (D-L) mechanism has been used to explain various patterns in the flame: the frequent formation of sharp cusps and crests, the convex curvature of flames in tubes, as well as the self-wrinkling large-scale

combustion [99]. The application of D-L has also been extended to both sprays and suspensions [4], where the kinematic (or velocity) slip of the particles can significantly alter flame dynamics. Theoretical studies by Korolchenko have shown that inertia can cause the particles to lag behind the accelerating gas and to deviate with respect to the gas streamlines, thus affecting the number density and reaction rate across the front. The hydrodynamic description also includes the effect of gravity [98], through the baroclinic Rayleigh-Taylor instability mechanism, contributes to the cellular nature of upward-propagating gas flames, while for flames propagating downward, gravity suppresses large cells. As discussed earlier, in suspensions, gravity may have a strong effect on particle settling [6], and depending on the particle mass, may strongly affect the formation of cells. Additional factors, such as the stabilizing effect of the large viscosity increase across the flame [100, 68], still need to be investigated for non-volatile suspensions.

While the simplicity of the D-L model has been addressed by Markstein [101] and others [102, 100, 103] to account for the effect of flame curvature and the internal structure of the flame [99]. Most importantly, it was found that the effect of hydrodynamic instability mechanisms can either be enhanced or opposed by diffusion phenomena. As shown in Fig. 1–2, mass diffusion has a destabilizing effect, as it tends to focus deficient reactants towards convex flame zones, thus accelerating them with respect concave ones and further deforming the flame. Inversely, thermal diffusion focuses heat into larger preheat zones for concave regions, which accelerate with respect to the convex ones. The effect of thermal and mass diffusion is represented by the ratio of their coefficients, α, and, D, respectively, called the Lewis number ($\mathrm{Le} = \frac{\alpha}{D}$). The thermal diffusivity is further expressed as $\alpha = \frac{\lambda_{\mathrm{gas}}}{c_{\mathrm{gas}}\rho_{\mathrm{gas}}}$, where λ_{gas} , c_{gas}, and ρ_{gas} are the gas thermal conductivity, heat capacity and density. A small

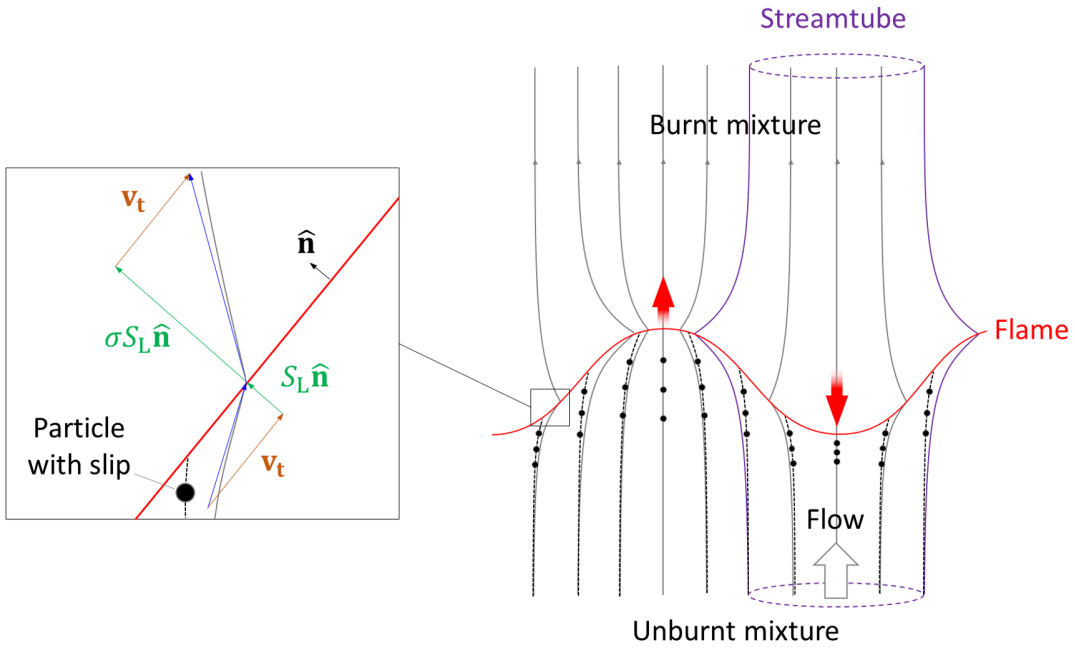

Figure 1–2: Hydrodynamic deformation of the flame, as introduced by Darrieus and Landau. Inset: the deviation of the gas streamlines is caused by the density jump across the infinitesimal flame sheet. Also represented, deviation of particle pathlines due to kinematic slip from deviating streamlines [4].

enough value of Le (about 0.5 for a density expansion of 6 [68]) gives rise to the thermo-diffusive (or diffusive-thermal) instability, as it allows the formation of even small cellular structures. Heat losses oppose the stabilizing effect of thermal diffusion and Le ≈ 1 close to quenching [68]. At moderate values of the Lewis number, the flame is stable. However, at sufficiently large Le, the imbalance of thermal and mass diffusion gives rise to planar pulsations and travelling waves along the flame surface [90]. While the high values of Lewis number are rather rare in adiabatic gas combustion, such as with heavy hydrocarbon fuels [73, 104, 105, 106], they can be observed in systems with heat losses, for example on burners [68]. On the other hand, in condensed systems, the non-diffusive nature of the reactants

allows the observation of various types of pulsating, spinning, spiralling, and travelling flames [94, 95, 96].

In non-volatile suspensions, the usually large density and negligible volume of the particles affects the heat capacity. The thermal diffusivity then becomes $\alpha = \frac{\lambda_{\mathrm{gas}}}{c_{\mathrm{gas}}\rho_{\mathrm{gas}}+c_{\mathrm{s}}B}$, where c_{s} and B are the particle heat capacity and particle concentration, respectively. Thus, fuel-rich suspensions are defined by small Lewis numbers [67], with in cellular flames appearing in both in spherical flames in inflatable balloons [67], as well as in flames propagating in tubes [107, 108]. In contrast, similar to gasless systems, fuel-lean suspensions are defined by the non-diffusive nature of the condensed fuel (limiting reactant), which leads to $\mathrm{Le} \to \infty$. A comprehensive study by Julien et al. [67] was performed in spherical flames propagating aluminum/oxygen/inert (nitrogen, argon, and helium) mixtures in elastic balloons. For progressively leaner systems, flames exhibited various combinations of pulsations and spiral patterns. Wright et al. [108] observed pulsations in flame of iron and in aluminum suspensions in oxygen/argon atmospheres. While aluminum exhibited instabilities even at 15% oxygen, iron instabilities formed only above an 42% oxygen. Pulsations have also been observed in the combustion of large PMMA particles in microgravity [109]. While the periodic change in speed was explained through successive heat absorption of particles and its radiation towards colder zones, the appearance of instabilities only in lean suspensions where such mechanisms are expected to be rather weak, is counter-intuitive [67, 6]. Moreover, tests showed that flame preheating through radiation only happens at large scales [67], which is probably due to the mean-free path of radiation being significantly larger than the vessel [6]. It has been suggested [67] that the observed pulsations may instead correspond to high-Le instabilities.

Some additional characteristics of non-volatile suspensions may significantly affect the stability of the flame. In oscillating multiphase systems, the transition between a high-temperature spike and low-temperature relaxation can be enhanced by a switch-like change in the reaction mechanism. In sprays, this role may be played by evaporation [110]. In non-volatile suspensions, theory predicts that the critical transition between low-temperature kinetically controlled and high-temperature diffusive regime of combustion can generate instabilities in some regions of the parametric space [35]. Instabilities have also been observed in a previous model of carbon/dust mixture [111], however with an arbitrary ignition temperature. Finally, most of the theoretical work so far has considered the development of instabilities of continuous fronts. As will be discussed in later sections, flame dynamics in suspensions are sometimes governed by the discrete nature of the sources and may significantly depart from continuous-front formulations, which are also used to describe instabilities. The effect of the flame discrete regime on high-Lewis-number instabilities has been recently examined by Mi et al. [112].

In most practical applications, the combustion process occurs in a confined environment, in which the coupling between acoustic waves in the combustion chamber and the heat released by the reaction often generates strong instabilities [113]. According to the Rayleigh mechanism [114], amplification of acoustic waves occurs if oscillations in pressure and in heat are in phase. The resulting thermo-acoustic instabilities have been extensively studied in the simplified case of laminar flames propagating in semi-open tubes, where the mixture is ignited at the open end and the flame propagates towards the closed end. As described by Searby [115], flames with a low laminar burning velocity remain unperturbed. Above a threshold, flames experience a primary acoustic instability, during which the hydrodynamic

cells are suppressed by acoustic fluctuations, and the flame becomes flat [116, 115]. The instability has been first described by Kaskan [117] as the periodic stretching of a flame anchored in boundary layer at the tube wall. However, more recent work has shown that it is more likely caused by velocity coupling [93, 118, 119]. At high laminar burning velocities, flame transitions to a much stronger secondary parametric instability, which results in a turbulent flame [116, 115]. Generally, the primary instability in the upper part of the tube and the secondary instability closer to the middle [115].

Thermo-acoustic coupling often appears to lead to stronger instabilities in two-phase mixtures. The explanation is often found in the slip (kinematic and sometimes thermal) between the gas and the solid phases. In sprays and volatile fuels, a complete evaporation of the droplets/particles before the reaction zone is assumed [91, 92, 93], with slip affecting particle distribution in the preheat zone. This results in the modulation of the fuel flux at the flame. In less volatile suspensions, particles enter the flame in a mostly condensed state, and their point-like combustion directly interacts with the acoustic field. This is of particular interest in solid rocket motors. Historically, fine metal particles were added to rocket motors to provide viscous damping to acoustic oscillations [20]. However, through so-called distributed combustion, where a particle continues to burn far from the propellant surface, such suspensions may instead significantly enhance the instability [120, 121]. Fundamental studies were also conducted with burning suspensions in tubes. Thermo-acoustic instabilities were first described by Cassel [54] in mixtures of dextrin in oxygen-enriched gas, and later identified in burning metal suspensions Aslanov [122] and Goroshin [123]. Most of the flames exhibited the onset of the primary acoustic instability above a critical

concentration. In general, suspensions of smaller particles appear to be more prone to instabilities. High concentrations in the small fractions also lead to the appearance of the secondary instability, characterized by stronger oscillations, and pronounced wrinkling of the flame front. The propensity of smaller particles to the primary instability was explained through the mechanism introduced by Kaskan [117]. It was speculated that in suspensions with larger particles, larger concentrations were needed for the flame to penetrate the sound boundary layer and to become anchored there. Further tests [122, 108] showed that the onset and strength of instabilities varies with the volatility of the fuel, with the more volatile aluminum particles experiencing an onset at the lowest critical concentration, while iron flames display no instabilities even for high particle concentrations. A possible coupling with high-Le thermo-diffusive instabilities was also reported [108].

Instabilities often prevent measurements of fundamental quantities such as the flame speed, and present a remarkable challenge to an efficient and safe use of burning suspensions in many applications. At the same time, they are a key phenomenological tool, which can be used to probe fundamental mechanisms that govern the combustion of suspensions, as well as to verify many theoretical conjectures about the structure and dynamics of flame fronts. The importance the author attributes to this topic is reflected by the relative length of this section.

1.8 Flames can propagate with multiple fronts

A typical flame consists of a multitude of reactions sometimes involving thousands of species. In a gas flame, the process is usually confined into a very thin zone ($\sim 0.1\,\mathrm{mm}$). Only in rare occasions and extreme conditions, delays associated with the evolution (often

slow decomposition) of a species lead to the widening of the flame zone and to the appearance of multiple fronts [124]. As mentioned in previous sections, in heterogeneous flames, physical processes can result in staged reactions and in the occurrence of multiple heat release zones. For example, coal flames involve the premixing and combustion of volatile fuel vapors with air, which is followed by a more gradual reaction of less volatile fractions [18]. It has been suggested that binary mixtures of fuels, which show sufficient differences either in chemical composition or in combustion properties (mainly particle size), could lead to the formation of multi-frontal flames, especially if the reactions can occur sequentially [125].

The dynamics of such multi-frontal flames have first been investigated by Khaikin [126] in a model flame consisting of two Arrhenius-type sequential steps, i.e., with the second reaction consuming the product of the first one. The study found that, depending on the relative values of the pre-exponential kinetic, heat release, and activation parameters, thermal energy production could either occur 1) in a single prominent heat release zone, with a high rate of the second step leading to essentially merged reactions, 2) in two distinct zones, with a significant delay between the production and consumption of the intermediate product, or 3) in systems in which the reactions are controlled by the heat transfer from the second to the first. Subsequent models [127, 128, 129, 130, 5] have confirmed and studied these various structures, which were dubbed the "merged", "separation", and "control" regimes, respectively.

The two-step approach was also applied in the study of propagation of flames in binary fuel mixtures [125]. The simplified model considers only the energy equation with each heat release step corresponding to the reaction of one fuel fraction with an abundant oxidizer. Each step is initiated at a pre-defined ignition temperature and proceeds at a constant rate

over a specific time interval. The simplified nature of the model allows a full analytical treatment of the system. Along with the adaptation of the model to account for heat losses [5], the analysis provided a straightforward explanation for the existence of the three propagation regimes in terms of thermal coupling between the two reaction fronts. As Fig. 1–3 shows, the results can be interpreted in terms of the amount of the second fuel fraction in the mixture, ϕ, which increases both the heat production from the second reaction and heat capacity of the mixture. At $\phi = 0$, the mixture contains only fuel 1 and burns as a single reaction system, coinciding with flame speed predictions for one-step adiabatic flames [130]. As ϕ is raised, the addition of the second fraction causes only an increase in the heat capacity of the mixture and a decrease in the flame speed. Below a critical concentration, the heat production is first insufficient to raise the temperature to allow the ignition of the second front to occur ($\phi < \phi_{\mathrm{II}}$), and then, for $\phi > \phi_{\mathrm{II}}$), while the flame may burn, it is unable to match the speed of the products leaving the first reaction zone. The fronts are thus uncoupled and remain separated. At ($\phi < \phi_{\mathrm{IIe}}$, the fronts become thermally coupled, as the second reaction is finally able to stabilize far in the wake of the first combustion zone. As ϕ is further raised, the increased heat transfer from the second front quickly reduces the distance between the front and raises the speed of the overall flame in the "control" regime. Finally, at ($\phi = \phi_{\mathrm{IIm}}$), the reactions merge and become overlapped at higher concentrations. The analysis helped to explain observations in experiments involving methane-air Bunsen flames, seeded with increasing proportions of aluminum micron-sized powder [131]. At low concentrations, the aluminum acted similar to an inert additive, reducing the flame speed. However, above a critical concentration, a second much brighter aluminum front formed and stabilized on top

of the methane-air one. Similar observations were made in flames in iron suspensions, which, in addition, allowed the direct observation of the two-front structure [132].

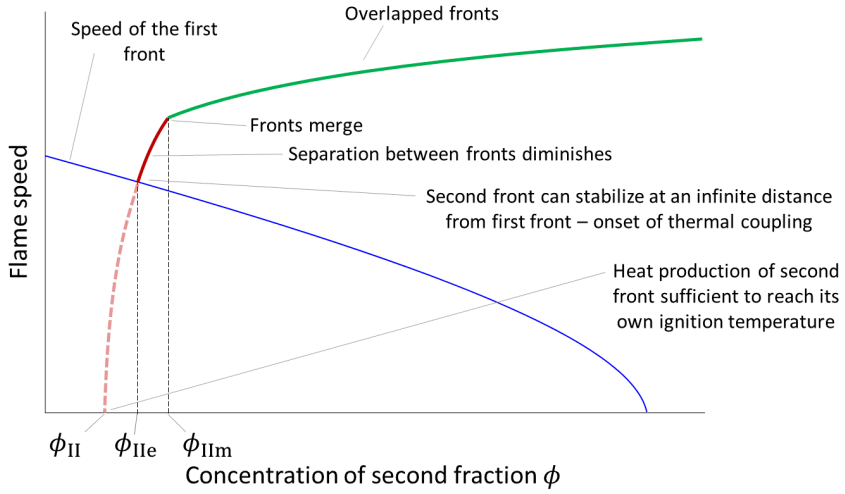

Figure 1–3: Process of thermal coupling explained through the model in [5].

Theoretical results [5] also showed that heat losses to cold walls can lead to both uncoupling of the flames and quenching. However, the latter, occur earlier than the former, depending on the concentration ϕ. This provided a clear explanation to the experimental observations of flame propagation in aluminum-methane-air mixtures in transparent tubes , equipped with quenching metallic plates forming narrow channels, in which the flame was subjected to intense heat losses [133]. At low concentrations, a dim methane-air flame, seeded with slowly reacting aluminum, propagated through the tube and quenched in small enough channels. At higher aluminum concentrations, the bright metal front extinguished upon reaching the channels — the heat losses causing thermal uncoupling and frontal separation – and only a methane-air reaction front entered and emerged from the channels. Once

back in the tube, the aluminum front appeared again in the wake of the methane-air front. Finally, at high concentration, no uncoupling occurred, with the flame either propagating or quenching as a whole.

1.9 Scope of the thesis

The papers in this manuscript-based thesis have been assembled in a logical rather than a chronological order. The primary hypothesis on which the work is based is that simple thermal analysis can explain many features of flame propagation in combustible suspensions and possibly other solid fuels. Therefore, the objective of the study is to systematically examine flame propagation and frontal structures of representative suspensions, and to show that the seemingly complex behaviour can be explained qualitatively in terms of previously developed models based solely on the energy equation, and on concepts such as thermal coupling, discrete heat release, and thermal locking. The work is inscribed in a wider effort aimed at uncovering fundamental features of heterogeneous combustion, which could guide future research [6].

The first publication, presented in Chapter 2, pertains to the study of thermal coupling in multi-frontal "hybrid" flames. It represents a continuation of the author's previous work on binary flame propagation [133, 5]. The difficulty to directly observe the behaviour of binary-front flames was solved through the conception and building of a novel apparatus in heterogeneous combustion — the Hele-Shaw cell. The technique, adapted from experimental research in fluid flows and gas combustion, will be presented, along with results pertaining to the propagation and structure of flames in aluminum-propane-air mixtures. Thermal coupling is also shown to lead to complex interactions between the fronts, which manifests

particularly in the presence of acoustic instabilities. Details about the experimental setup and the analysis can be found in Appendix A.

The second and third publications focus on thermal effects caused by the discrete nature of sources in heterogeneous systems. The experimental studies were performed in microgravity environments aboard European Space Agency (ESA) rockets — the MAXUS-9 in April 2017 and the TEXUS-56 in November 2019. The flight campaigns were the results of Phase I and Phase II of the project entitled "Percolating Reactive Waves in Particulate Suspensions" (PERWAVES), conducted in collaboration with ESA, the Canadian Space Agency (CSA), and Airbus Defence and Space in Germany. Additional information about the apparatus and the analysis can be found in Appendix B, as well as in a dedicated publication [134].

Chapter 3 discusses the first phase of the PERWAVES project, centred around the flight of the MAXUS-9 rocket. The publication is preceded by an introduction, which provides the context of the research in discrete flames. The experiments performed during the microgravity flights are analyzed. Despite the complexity of the experiment leading to relatively high uncertainties, the results prove the existence of the discrete regime of flame propagation.

The implications of discrete behaviour are explored in Chapter 4. The introduction of purely discrete concepts such as phase transitions and percolation provide a useful context to discuss the effect of heat locking on flame propagation, especially close to its limit. The publication, which is ready for submission, discusses the many ways through which heat locking can affect the propagation of a mixture of burning particles arranged both in regular matrices and in random systems. Finally, the work explores the different behaviours exhibited by discrete flames in suspension in microgravity.

CHAPTER 2
The Hele-Shaw cell and thermal coupling

2.1 Hele-Shaw cells and observation of flame dynamics

The thermal coupling mechanism is investigated in the first manuscript presented in this thesis, it examines experimentally the propagation of flames in aluminum-propane-air mixtures. As described earlier, such hybrid metal-hydrocarbon-air flames exhibit complex two-frontal structures, which have been explained via the mechanism of thermal coupling between fronts corresponding to the reactions of the gaseous and of the metal fuel, respectively [5]. Due to the diversity of fuel fractions in many industrially produced powders, such multi-frontal structures are likely to play a role in many applications and require fundamental investigation.

A way to probe the flame is to observe its behaviour in the presence of destabilizing effects such as heat losses. As mentioned in the introduction, flames propagating in aluminum-methane-air mixtures in tubes and forced through narrow channels with higher heat losses displayed complex front-coupling and separation dynamics [133]. However, while clearly demonstrating the two-front structure, the 3D shape of the flame did not allow direct observations of the coupled structure. Similar difficulties prevented direct studies of the two fronts in spherically expanding flames [135].

A geometry, which avoids the difficulties associated to the 3D structure of heterogeneous flames, is provided by the so-called Hele-Shaw cell. The apparatus consists of two parallel

closely spaced glass plates, which enclose a thin test section. It was first used by H. S. Hele-Shaw to provide a visualization of flow streamlines, during which he discovered that below a certain spacing, viscous effects maintain laminar conditions at any flow velocity. The cell has then been used in experiments involving potential flows, and led to the discovery of viscous fingering, also known as the Saffman-Taylor instability [136], which occurs when a less viscous fluid displaces a more viscous one, and which results in the deformation of the fluid interface and the formation of one or more protruded "fingers".

Flame studies in the Hele-Shaw geometry, albeit theoretical, have first been proposed by Joulin & Sivashinsky [137] who observed that heat losses tend to reduce hydrodynamic instabilities, while momentum losses, through the Saffman-Taylor mechanism, may instead destabilize flames. Since then, the Hele-Shaw cell has been increasingly used to study the propagation of flames [138, 139, 140, 141, 142, 143]. Apart from the geometry confining the growth of instabilities to two dimensions and thus allowing an easier spectral analysis of the most unstable wavelengths, the use of the apparatus is motivated by three main reasons. First, the geometry resembles that of confined "crevice" spaces in many applications, such as between pistons and cylinders, in which incomplete combustion can cause the formation of pollutants [138]. Indeed, flames subjected to instabilities and losses in Hele-Shaw cells have been shown to deform up to the point where the flame ceases to exist in concave regions through which unburnt and partially burnt fuel escapes [144]. A second use of the Hele-Shaw pertains to the possibility of combining variations of heat and momentum losses by changing the thickness of the channel with other factors that cause various types of instabilities such as the direction of flame propagation with respect to gravity in the

Rayleigh-Taylor mechanism, the flame temperature and density variation for the Darrieus-Landau mechanism, or the mixture composition and Lewis number Le for the thermodiffusive mechanism. Resulting parametric studies provide a guidance [145] for the interaction of these effects in more complex geometries. Finally, the confinement of Hele-Shaw cell often leads to thermo-acoustic effects[142], which have been observed to deform the flame by the primary and secondary mechanism, as described in the introduction [115].

The first manuscript, presented below, is the first study of its kind, which aims to take advantage of the dynamics present in the Hele-Shaw cell to probe complex multi-frontal flames. Note: the "Hele-Shaw" designation has been used by extension of experiments performed in gas combustion, as possible effects of Hele-Shaw flows are most likely weak in the current geometry.

2.2 Publication: Aluminum-propane-air hybrid flames in a Hele-Shaw cell, *Proceedings of the Combustion Institute* [1]

Jan Palečka, Judy Park, Samuel Goroshin, Jeffrey M Bergthorson

Department of Mechanical Engineering, McGill University,

817 Sherbrooke Street West, Montreal, Quebec H3A 0C3, Canada

Received 8 November 2019; accepted 20 September 2020

Available online 16 December 2020

2.2.1 Abstract

This paper introduces a novel Hele-Shaw cell apparatus to be used for the study of propagation and stability phenomena in heterogeneous flames. In particular, the apparatus is used to experimentally examine the coupling/decoupling of dual-front flames propagating in suspensions of micron-size aluminum particles in propane-air gas mixtures at varying gas equivalence ratios and aluminum concentrations. The results show that the thermal coupling that exists between the primary propane-air flame front and the secondary aluminum flame front is a strong function of the rate of reaction, and of the temperature, of the secondary front and much less dependent on the reaction rate or temperature of the primary front. It is also shown that flame instabilities in hybrid aluminum-propane-air flames significantly increase the flame surface area, enhance the propagation rate, and can also exhibit complex interactions with front coupling.

Keywords: Heterogeneous combustion; Hele-Shaw cell; Dual-front flames; Aluminum suspensions

2.2.2 Introduction

The Hele-Shaw cell, i.e., a narrow channel with a large width-to-thickness aspect ratio and transparent walls which allows the visual observation of a quasi two-dimensional flame, has become increasingly popular for the study of complex flame shapes and dynamics [1–3]. While impacting flame propagation through boundary layers, heat and momentum losses to the channel walls can sometimes enable the study of flames that are otherwise difficult to stabilize on burners or that result in complex 3-D shapes in tubes or for spherical flames. The relatively simple geometry of the Hele-Shaw cell allows the comparison of experimental results with theoretical models in the study of the evolution of intrinsic instabilities and of their effects on the speed and the surface area of a self turbularizing flame [4–7]. Several papers have investigated how gas expansion, buoyancy-driven convection, and momentum losses by friction to the cell walls affect the flame through the hydrodynamic Darrieus-Landau, Rayleigh-Taylor, and Saffman-Taylor instability mechanisms [4–8]. The effect of the ratio between the mixture thermal and molecular diffusivities, α and D, i.e., the Lewis number, $\mathrm{Le} = \alpha/D$, has been investigated in [6] and the flame interaction with the channel acoustics was studied in [3].

Our recent experiments have shown that, similar to gaseous combustion, flames in solid fuel suspensions — particularly of metal particles — also demonstrate a wide variety of flame instabilities. Pulsating, cellular, and spiral spinning isobaric flames were noticed in aluminum dust clouds confined in rubber balloons [9] and cellular flame structures have been observed in the combustion of micron-size iron suspensions in tubes [10]. The interaction of acoustic oscillations with metal flames was investigated in an early work [11] and recently in [12]. The shapes and dynamics of unstable flames in particulate suspensions are, however,

even more difficult to study than in gaseous flames due to an intense light scattering in the preheat and the combustion zones, which, in combination with the very strong luminosity of metal flames, makes the flame surface difficult to localize.

Due to a relatively low optical thickness of the dust mixture across the narrow channel of the Hele-Shaw cell, the intensity of the pre-flame light scattering is greatly reduced, which facilitates the visualization of complex flame structures that are otherwise obscured by the light scattering in flames on burners and in tubes. As shown in this paper, the Hele-Shaw cell is especially useful in investigating complex flames in hybrid metal-hydrocarbon fuel mixtures encountered in many practical applications. The formation of the thermally coupled double-flame front structure in binary fuel mixtures has been predicted theoretically [13,14] and was observed experimentally [15,16] when methane-air Bunsen flames stabilized on a burner were seeded with progressively increasing concentrations of aluminum particles, as illustrated in Fig. 1(b). The formation of the secondary aluminum dust flame coupled to the primary hydrocarbon flame was manifested by a rapidly increased flame brightness and temperature when the aluminum concentration reached some critical threshold. Another indirect evidence of the linked double-front flame structure was obtained in methane-aluminum flame quenching experiments [17] when the aluminum front decoupled from the methane front, quenched in a narrow channel, and subsequently re-appeared in the wide tube (Fig. 1(c)). Thermal coupling was also used to interpret results in spherically expanding flames in balloons [18]. The novel Hele-Shaw cell adapted for the investigation of two-phase flames described in the following paragraphs has allowed the direct visualization of the flame structure and the study of a complex coupling/decoupling behaviour of gaseous and aluminum flame fronts in

propane-aluminum hybrid mixtures over a wide range of gaseous and metal fuel concentrations.

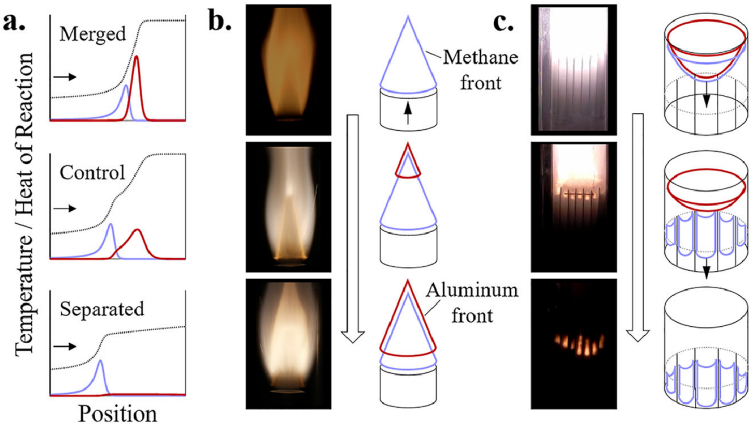

Figure 2–1: (a) Diagrams of the flame structure in the 'merged', 'control', and 'separated' regimes; (b) and (c) Examples of flame coupling in a Bunsen burner configuration (adapted from [15]) (b) and decoupling in quenching plates (adapted from [17]) (c) in flames of aluminum suspensions in methane-air gas mixtures.

2.2.3 Experimental methods

2.2.3.1. Hele-Shaw cell for the study of flames in suspensions

The novel Hele-Shaw apparatus, presented in Fig. 2, consists of an experimental cell, a particle dispersion system, and an ignition system. The metallic powder is fed into the apparatus by an actuator-driven piston, originally developed for the use in flame tubes [10,13]. The particles are dispersed via the impingement of a concentric thin air-knife sonic jet from a 50-µm slot (Fig. 2 inset). The resulting turbulent mixture is conveyed through an expanding 3D-printed diffuser, which allows a uniform distribution during the expansion of the flow into the high-aspect ratio (1 cm × 20 cm) cross-section of the 50 cm-long vertical cell. The entry of the latter is divided into 1.27-cm-wide channels, formed by a set of parallel plates, which laminarize the flow. Upon reaching the upper open end of the cell, the mixture is

ignited by an electrically heated tungsten filament, which forms a loop over the central part of the channel. Immediately after ignition, the flow in the cell is stopped by cutting the gas supply and shutting a solenoid-operated slide gate which isolates the cell from the diffuser. Thus, the flame propagates down into a quiescent two-phase fuel-air mixture until it reaches the closed end of the cell. Visual access to flame propagation is provided by a Robax glass window, placed both on the front and on the back of the cell.

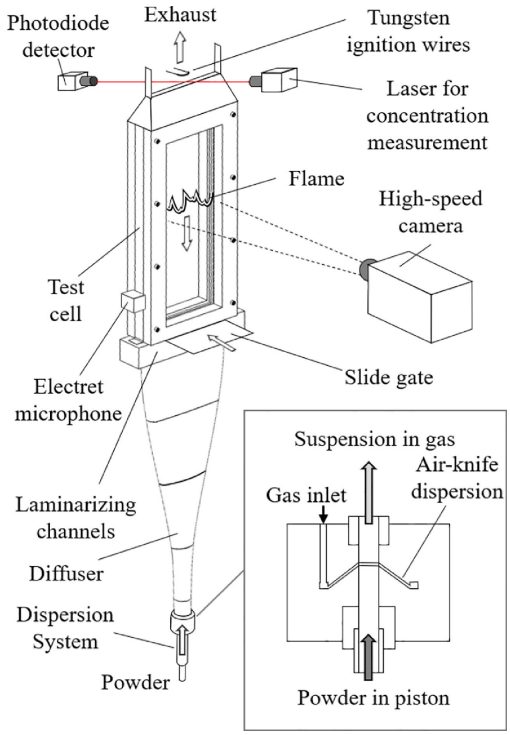

Figure 2–2: Diagram of the experimental Hele-Shaw apparatus used for quasi-2D flame observation in heterogeneous flames.

2.2.3.2. Aluminum powder and gas mixtures

The mixtures consist of airborne suspensions of micron-sized spherical aluminum particles. The powder is produced by Valimet Inc. (Stockton, CA) under the code H-2 and has an arithmetic mean diameter (d_{10}) of 3.5 to 3.8 µm (Fig. 3). The concentration of the metallic suspension is measured by a calibrated laser attenuation system, placed right above the open end of the cell, and described in [17]. Once the voltage signal reaches the value corresponding to the target concentration, the test is initiated. The particles are dispersed in propane-air gas mixtures at different equivalence ratios. While the uncertainty in the gas composition is solely a function of the mass-flow controllers and is relatively negligible ($< \pm$ 2% of ϕ), the time and spatial variations of the powder concentrations between the point of measurement and the channel in the cell can lead to uncertainties of 50-100 g/m^3. Thus, only the relative nature of concentration measurements is considered.

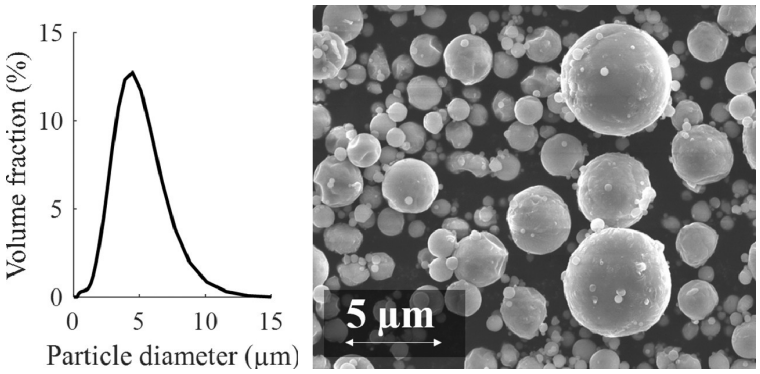

Figure 2–3: Aluminum powder: size distribution (obtained on a Horiba LA-920 Particle size analyzer) and scanning electron microscope images.

2.2.3.3. Diagnostics

A Photron SA5 high-speed camera records flame propagation through the front window. Neutral density filters attenuate the large luminosity of the aluminum combustion process and are aimed to prevent the saturation of the camera sensor. The luminosity of the flame is a strong function of the rate of reaction and temperature of the aluminum flame front, which itself prominently depends on the particle concentration and on the type and proportion of oxidizer in the gas. The combination of the frame rate, the filtering, the shutter speed, and the aperture are carefully tailored to the specific gas mixture.

An electret microphone (1063-ADA), placed in a sealed cavity inside the cell structure and connected to the channel through a thin orifice, is used to capture pressure variations within the cell. The 333-MHz readings are synchronized with the trigger of the high-speed videos on the data acquisition system.

2.2.4 Results and discussions

2.2.4.1. Flame propagation in the Hele-Shaw cell

Flame propagation was studied in propane-air mixtures with concentrations of aluminum suspensions, B_{Al}, up to $400\,\mathrm{g/m^3}$. Aluminum reacts both with oxygen and with products of the propane-air reaction, mainly carbon dioxide and water, albeit at a reduced rate. Thus, the equivalence ratio, ϕ, of the propane-air gas rather than of the overall mixture was used as an independent variable in the experiments, ranging from 0.5 to 1.2.

A typical propagation of a hybrid flame at $\phi = 1.0$ and a concentration above $150\,\mathrm{g/m^3}$ is presented in Fig. 4(a). As both pressure variations and the evolution of the position of the leading front with time indicate (Fig. 4(b)), the downward propagation can be divided

into three stages. First, in a quasi-steady phase (1–2 in Fig. 4(a) and (b)), the flame speed is constant and the front develops characteristic structures — first small-scale wrinkling (1), followed by large-scale cells (2). Close to the mid-plane of the channel (3), the flame propagation becomes unstable and its oscillations couple with the pressure field (Fig. 4(c)). The frequency of oscillation is usually in the range of 180 to 240 Hz (Fig. 4(d)), slightly higher than the cold 1/4 wavelength resonant frequency of 173 Hz. Much like some gas [3,19], and metal [12] flames, the hybrid flames then usually experience a phase of acoustic instabilities, in which the fronts flatten and decelerate (3 in Fig. 4(a) and (b)) and then the flame curvature increases and the pulsating flame accelerates (4 in Fig. 4(a) and (b)). During propagation, the hybrid flames are subjected to a variety of instabilities, which result in both large hydrodynamic structures and in smaller thermodiffusive wrinkling, which is probably caused by low Lewis numbers due to the presence of powder in the mixture [9]. A dedicated study of these phenomena is reserved for a future publication. Due to space limits, the present paper focuses solely on effects associated with front coupling in hybrid flames. As can be noted in Fig. 4(a) and (c), the flame has a clear two-front structure, with periodic coupling and decoupling occurring in phase with the variations in pressure. This is discussed in more detail in Section 3.4.

2.2.4.2. Frontal structure

As Fig. 5 shows, both variations of the aluminum concentration, B_{Al}, and of the gas equivalence ratio, ϕ, have a significant impact on the structure of the flame. The effect of B_{Al} is illustrated in Fig. 5(a)-(c) for $\phi = 1.0$. Similar to previous experiments for stabilized flames [15,16] and flames in tubes [17] in methane-air gas mixtures, at low Al concentrations

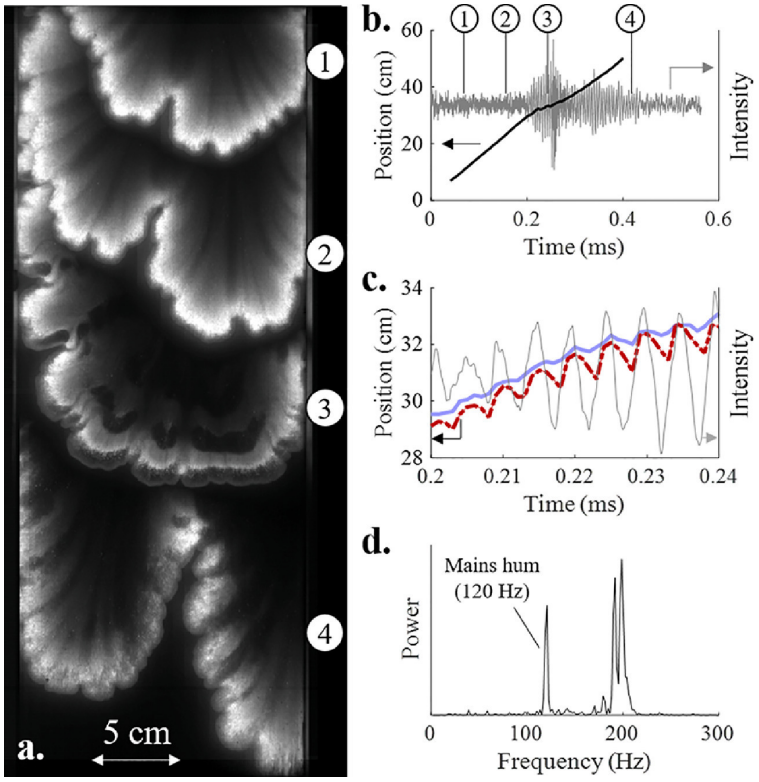

Figure 2–4: Hybrid aluminum-propane-air flames in the Hele Shaw cell: (a) consecutive frames of a flame in the cell, pressure readings and flame position over time – (b) overall and (c) shorter interval with the position of the propane (solid line) and the aluminum (dash-dotted line) front, and (d) corresponding frequencies of oscillations (with 120-Hz mains hum).

(Fig. 5(a) and (b)), only a relatively dim propane-air front, followed by a faint brush of aluminum particle streaks, propagates through the channel. At higher concentrations, the light intensity of the more numerous particles increases at a finite distance from the gas front (Fig. 5(b)). It is worth noting a much sharper increase in intensity at the flame cusps regions (Fig. 5(b)), whose preheat zones are relatively thicker due to the focused thermal diffusion from the negatively stretched flame. Upon reaching the flame, the low-Stokes-number particles (St $\approx 10^{-2}$) and the gas carried by affected streamlines thus burn at a

higher rate. Above a critical concentration, the combustion of aluminum particles leads to the formation of a second much brighter front (Fig. 5(c)), which couples to the propane-air flame front and propagates at a relatively constant distance behind it. Similarly, changes in ϕ of the propane-air mixture, illustrated in Fig. 5(c)-(e), lead to large variations in the luminosity of the two-front flames. While, for the same camera settings, the second front mostly saturates the screen at $\phi = 0.7$, it is dimmer at lower aluminum concentrations at $\phi = 1.0$, and much dimmer at even higher aluminum concentrations for $\phi = 1.2$. Such variations in brightness make the choice of appropriate optical filtering difficult. As a result, the second front may appear only as a very dim region on the frame and is often hard to identify (Fig. 5(b) and (e)). Such cases are reported as 'faint Al front' in the figures.

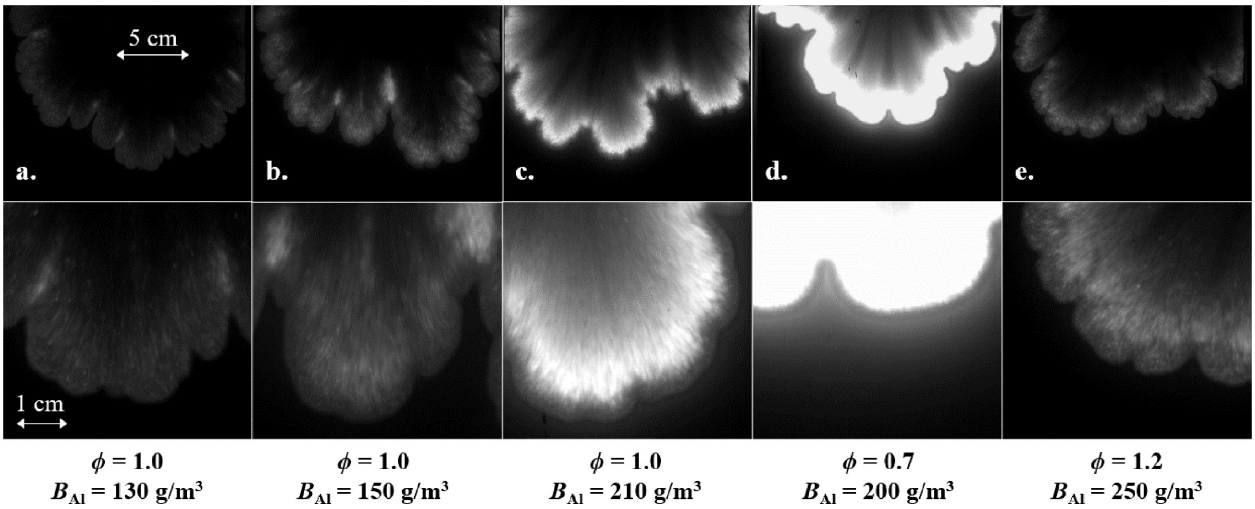

Figure 2–5: Flame front structure at different equivalence ratios, ϕ, and aluminum concentrations, B_{Al}. For the sake of comparison, the photographs of the full flames have been taken with exactly the same camera conditions, while the detailed views have been enhanced to illustrate specific features of each flame.

The frontal structure at different ϕ and B_{Al} is presented in Fig. 6. The critical concentration at which front coupling occurs decreases with decreasing equivalence ratio. This

trend continues even below the equivalence ratio $\phi_{\mathrm{q,gas}} = 0.58$, at which pure gas propane-air flames are observed to quench in both literature [20] and in the current apparatus. Thus, the addition of aluminum promotes the propagation of the propane front below its quenching conditions. Perhaps slightly surprisingly, even low concentrations (at $\phi = 0.5$ in Fig. 6(a)), at which no front coupling occurs, are sufficient to enhance the propagation of the propane-air front. In this case, the flame starts and propagates close to the side of the cell and, only when it reaches approximately the third of the cell, expands in the lateral direction.

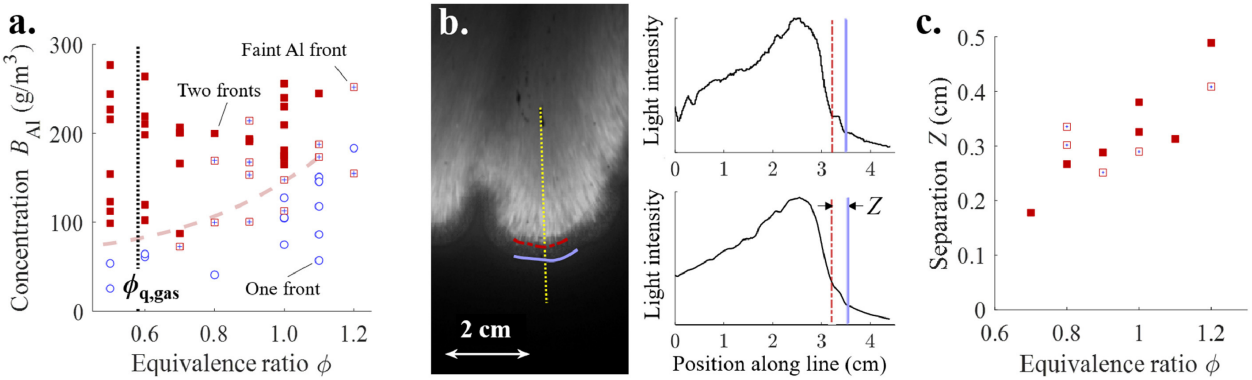

Figure 2–6: Dual-front structure: (a) onset of the second front in aluminum-propane-air flames, (b) process for finding distance between fronts, Z, with instantaneous (top) and average (bottom) intensity profiles along the line, and (c) separation Z for different equivalence ratios.

The results in Fig. 6(a) are also in relative agreement with findings in methane-air Bunsen flames [15], where coupling appeared at lower concentrations for $\phi = 0.8$ than for stoichiometric mixtures. This similarity is to be expected, as differences in the combustion process in methane-air and propane-air mixtures are unlikely to significantly affect flame coupling of aluminum with similar combustion products and temperatures.

To ensure consistency of data, the determination of the distance between the fronts, identified as Z (or also as χ) in previous theoretical work [13,14], has been performed only

on non-saturated flames for identical camera settings. The process is described in Fig. 6. To trace the outline of the aluminum front (Fig. 6(b)), an image segmentation process using Otsu's thresholding method was performed on each frame. The gradient of the traced curve was then used to determine the normal line to the furthest point of the traced front (Fig. 6(b)), which always lies on a positively stretched convex part of a cell. Then, the pixel intensity of the flame image is taken along the normal line (Fig. 6(b), top right), on which the location of the aluminum and propane fronts are visible as a sharp change in slope at roughly 15% and 30% of maximum intensity, respectively, between which there is a plateau in intensity. The process is performed every 10 ms of flame propagation, and yields a relatively noise-free mean intensity profile (Fig. 6(b), bottom right) from which Z is determined as the distance between the two points where the magnitude of slope changes sharply (Fig. 6(b)).

Front coupling can be analyzed through the separation between the two fronts, Z. As previous experiments have shown [15], the separation is not caused by an 'ignition delay' of single aluminum particles after they cross the propane front. Z should be rather viewed as the expression of the relative strength of thermal coupling between the two flame fronts. As Fig. 6(c) indicates, Z increases from about 2 mm to 5 mm between $\phi = 0.7$ and 1.2. Thus, a decrease in the proportion of oxygen in the gas weakens the coupling link between the fronts.

2.2.4.3. Flame speed

The flame speed, S_{T}, of the hybrid flames (Fig. 7(a)) was measured through the position in time of the leading point of the gas front before the onset of acoustic coupling (constant-speed phase 1-2 in Fig. 4(a) and (b)). In heterogeneous flames, which exhibit large variations in surface area and in luminosity, this method offers the highest consistency. Comparison

with the propagation of propane-air gas flames in the Hele-Shaw cell (grey-blue band in Fig. 7(a-(c)) suggests that — whether it leads to the formation of a second front or not — the addition of the powder enhances the propagation speed of the propane-air flame. This occurs in part through an increase in the surface area of the front, A_{T}, which is 2-4 times larger than the cross-section area of the channel, A_{L} (Fig. 7(b)). To some extent, this effect can be accounted for, by considering the rescaled burning rate, $S_{\mathrm{F}} = S_{\mathrm{T}}(A_{\mathrm{L}}/A_{\mathrm{T}})$ [23]. The resulting comparison with gas flame, presented in Fig. 7(c), is in agreement with our previous findings in Bunsen burner flames [15], in which the addition of aluminum powder led to a reduction of the burning velocity in both stoichiometric and methane-lean flames at $\phi = 0.8$. However, for lower equivalence ratios, the burning rate, SF, increases significantly. This is in accordance with the predictions of previous models [13,14], which have shown that, during the so-called 'control' regime of combustion of a coupled flame, the second front controls the propagation characteristics of the overall flame. Thus, as oxygen becomes more available at lower ϕ, the reaction rate of the aluminum front increases, the coupling is strengthened, and the overall flame propagation speed is determined by that of the secondary aluminum front. The effect becomes even more important below $\phi_{\mathrm{q,gas}} = 0.58$, where the pure gas propane-air front cannot exist on its own.

2.2.4.4. Flame coupling and acoustic oscillations

As Fig. 7 indicates, flame stretch induced by frontal instabilities, and its interaction with coupling, plays an important role in the propagation of hybrid flames. This becomes especially true once the flame spontaneously develops acoustic oscillations close to the mid-plane of the cell. This has been shown to lead to a visible de-coupling of the fronts(Fig. 4). A

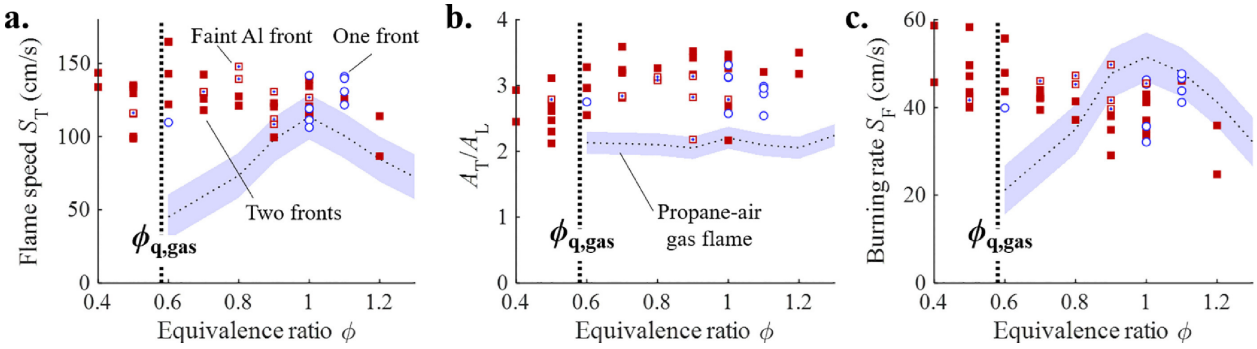

Figure 2–7: Flame speed: (a) The propagation velocity, S_T vs equivalence ratio, (b) ratio of the flame surface area, A_T to the cross-sectional area of the channel, A_L, (c) normalized flame speed, $S_F = S_T\,(A_L/A_T)$ vs. equivalence ratio,ϕ . The aluminum concentration of the experiments is 50–400 g/m^3.

closer look at the dynamics of this phenomenon is provided in Fig. 8, which shows a coupled flame ($B_{Al} = 210\,g/m^3$ and $\phi = 0.8$) at the onset of thermo-acoustic fluctuations. As the consecutive frames (Fig. 8(a)), microphone readings (Fig. 8(b)) and the position of the fronts (Fig. 8(c)) show, the fluctuations in pressure lead to the weakening of the coupling, which causes the detachment of the aluminum front, while having only a small effect on the gas front. The distance Z increases in the more positively stretched parts of the flame, i.e., crests. For strong enough oscillations, this can lead to a complete frontal separation and the disappearance of the aluminum front in the wake of the leading gas front, which is followed by a sudden reappearance of a brightly burning aluminum front close to the propane front and the recovery of the initial two-front profile of the flame. Thus, in convex regions of the flame, de-coupling can be caused by pressure variations. The reaction rate of particles in aluminum suspensions is particularly susceptible to oscillations as has been observed in tubes [11,12], as well as in experiments in the current cell in mixtures without propane.

Thus, when the hybrid flame reaches the mid-plane, pressure and velocity variations disrupt the aluminum front and only the gas front seem to proceed.

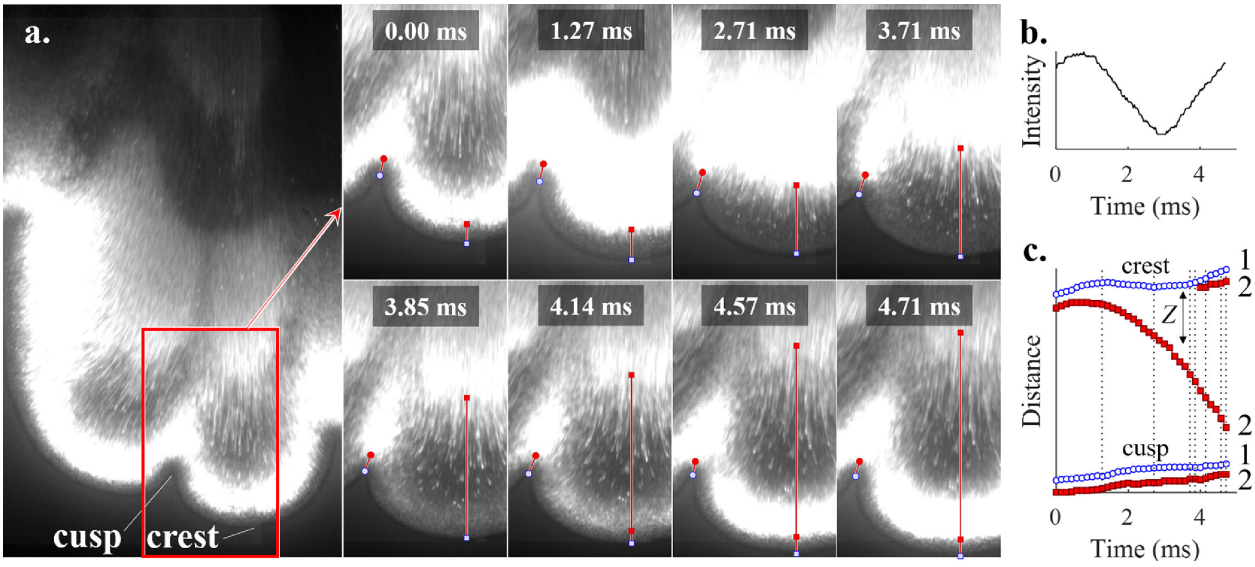

Figure 2–8: Decoupling/recoupling in a hybrid flame ($\phi = 1.0$): (a) frames indicate one cycle of instabilities which shows the decoupling and subsequent re-coupling between the fronts. (b) Corresponding pressure readings, and (c) position of the propane (1) and aluminum (2) fronts at the crest and the cusp (dotted lines correspond to times of individual frames in the figure). Here 0 ms corresponds to the first frame..

A different behavior is observed in the negatively stretched region at the flame cusps, where no such separation occurs, and the two-front structure is maintained throughout the oscillation (Fig. 8(a) and (c)). It is suspected that the difference with the crest can be explained by a more favourable heat diffusion from the negatively strechted front to the streamlines leading to the cusp, which provides higher local rates of reaction. Thus, even when the flame is subjected to pressure oscillation, the strong coupling is maintained at the cusps.

2.2.5 Summary

A novel Hele-Shaw cell permitting observation of flames in solid fuel suspensions has been built and tested in the study of hybrid propane-aluminum flames. The most important features of a hybrid flame observed in this study can be summarised as follows:

- A critical concentration of aluminum in suspension is required to achieve flames with coupled aluminum and propane-air fronts.
- The front coupling is a strong function of the propane-air equivalence ratio, ϕ. Lower aluminum concentration is required for flame coupling at lower ϕ, which demonstrates that the coupling is more dependent on the amount of residual oxygen that is available for the reaction with aluminum, rather than the temperature of the primary hydrocarbon flame.
- At lower propane-air equivalence ratios, the flame propagates in a control regime, i.e., its speed is defined by the speed of the aluminum flame front behind the gaseous flame.
- The coupling/decoupling between propane and aluminum flame fronts is strongly correlated with the acoustic pressure field if the coupling is weak.

It has also been observed that the seeding of propane-air mixtures even with small amounts of metallic powder exacerbates the formation of instabilities and increases the flame surface area, which in turn may expand flame propagation limits and increase the flame speed. Moreover, once such a cellular flame undergoes thermoacoustic instabilities, variations in stretch and thermal diffusion lead to varying responses of the coupled flame fronts and result in complex flame configurations. Further work with additional optical diagnostics (IR high-speed camera,spectroscopy) is planned to elucidate the complex physics

of these multi-front flames.

2.2.6 Acknowledgments

The authors would like to thank A. Higgins, J. Sniatowsky, and M. Soo for their contributions. Funding was provided by the Canadian Space Agency through the Flights and Fieldwork for the Advancement of Science and Technology (FAST), in collaboration with the European Space Agency on the PERWAVES project. Student work was also partially supported by the Panda Faculty Scholarship of the Trottier Institute for Sustainability in Engineering and Design (TISED), the Doctoral Research Scholarships Program for International Students(DS) of the Fonds de recherche du Quebec – Nature et Technologie (FRQNT), and the Natural Sciences and Engineering Research Council NSERC Undergraduate Summer Research Award (USRA) program.

2.2.7 References

[1] J. Sharif, M. Abid, P.D. Ronney, Proceeding of the First Joint U.S. Section Combustion Institute. Meeting, NASA, Washington DC, 1999.

[2] J. Wongwiwat, J. Gross, P.D. Ronney, in: Proceeding of the Twenty-fifth ICDERS, 2015, pp. 3–8.

[3] F. Veiga-López, D. Martínez-Ruiz, E. Fernández-Tarrazo, M. Sánchez-Sanz, Combust. Flame 201(2019) 1–11, doi:10.1016/j.combustflame.2018.12. 005.

[4] G. Joulin, G. Sivashinsky, Combust. Sci. Technol. 98 (1–3) (1994) 11–23, doi:10.1080/00102209408935393.

[5] S.H. Kang, S.W. Baek, H.G. Im, Combust. Theory Model. 10 (4) (2006) 659–681, doi:10.1080/ 13647830600636049.

[6] D. Fernandez-Galisteo, V. Kurdyumov, P.D. Ronney, Combust. Flame 190 (2018) 133–145, doi:10.1016/j. combustflame.2017.11.022.

[7] D. Martínez-Ruiz, F. Veiga-López, D. FernándezGalisteo, V.N. Kurdyumov, M. Sánchez-Sanz, Combust. Flame 209 (2019) 187–199, doi:10.1016/j. combustflame.2019.07.019.

[8] S.H. Kang, H.G. Im, S.W. Baek, Combust. Theory Model. 7 (2) (2003) 343–363, doi:10.1088/1364-7830/ 7/2/308.

[9] P. Julien, J. Vickery, S. Goroshin, D.L. Frost, J.M. Bergthorson, Combust. Flame 162 (11) (2015) 4241–4253, doi:10.1016/j.combustflame.2015.07. 046.

[10] F.D. Tang, S. Goroshin, A. Higgins, J. Lee, Proc. Combust. Inst. 32 (2009) 1905–1912, doi:10.1016/j. proci.2008.05.084.

[11] S.V. Goroshin, V.G. Shevchuk, N.D. Ageev, Combust. Explos. Shock Waves 17 (6) (1981) 595–600, doi:10.1007/BF00784247.

[12] A. Wright, A.J. Higgins, S. Goroshin, Combust. Sci. Technol. 188 (11–12) (2016) 2178–2199, doi:10.1080/ 00102202.2016.1211877.

[13] S. Goroshin, M. Kolbe, J.H.S. Lee, Proc. Combust. Inst. 28 (2) (2000) 2811–2817, doi:10.1016/ S0082-0784(00)80703-1.

[14] J. Palecka, S. Goroshin, J.M. Bergthorson, Combust. Sci. Technol. 190 (9) (2018) 1557–1579, doi:10.1080/ 00102202.2018.1459583.

[15] M. Soo, P. Julien, S. Goroshin, J.M. Bergthorson, D.L. Frost, Proc. Combust. Inst. 34 (2) (2013) 2213– 2220, doi:10.1016/j.proci.2012.05.044.

[16] P. Julien, M. Soo, S. Goroshin, D.L. Frost, J.M. Bergthorson, N. Glumac, F. Zhang, J. Propuls. Power 30 (4) (2014) 1047–1054.

[17] J. Palecka, P. Julien, S. Goroshin, J.M. Bergthorson, D.L. Frost, A.J. Higgins, Proc. Combust. Inst. 35 (2) (2015) 2463–2470, doi:10.1016/j.proci.2014.06.116.

[18] J. Vickery, P. Julien, S. Goroshin, J.M. Bergthorson, D.L. Frost, J. Loss Prevent. Process Ind. 49 (2017) 472–480, doi:10.1016/j.jlp.2017.05.027.

[19] G. Searby, Combust. Sci. Technol. 81 (4–6) (1992) 221–231, doi:10.1080/00102209208951803.

[20] J. Jarosinski, J. Podfilipski, T. Fodemski, Combust. Sci. Technol. 174 (1) (2002) 167–187, doi:10.1080/ 713712915.

[21] M.W. Beckstead, Combust. Explos. Shock Waves 41 (5) (2005) 533–546, doi:10.1007/s10573-005-0067-2.

[22] M. Soo, S. Goroshin, N. Glumac, K. Kumashiro, J. Vickery, D.L. Frost, J.M. Bergthorson, Combust. Flame 180 (2017) 230–238, doi:10.1016/j. combustflame.2017.03.006.

[23] J.F. Driscoll, Prog. Energy Combust. Sci. 34 (1) (2008) 91–134, doi:10.1016/j.pecs 2007.04.002.

2.2.8 Further reading

S. Goroshin, I. Fomenko, J.H.S. Lee, Symp. Combust. 26 (1996) 1961–1967, doi:10.1016/S0082-0784(96) 80019-1.

CHAPTER 3
Discrete flames in microgravity

3.1 Discrete flames in heterogeneous systems

The previous manuscript examined how the complexity of heterogeneous combustible systems gives rise to thermal coupling between reaction fronts. However, the structure of a single front is far from homogeneous. The presence of "flames within a flame" leads to complex interactions within the front itself. Due to the low activation energy of the reaction of metal vapours with oxygen, no long-distance chemical interactions are expected [6]. Instead, the propagation of the flame in heterogeneous systems has long been recognized to be dependent on thermal interactions. The interplay between localized heat production by particles, thermal dissipation/diffusion in the inter-particle medium and surroundings, and the activation of subsequent combustion events has been shown to lead to the "discrete" regime of combustion.

Early models of heterogeneous flames were often based on a continuous formulation, i.e., on the averaging of the reaction term in terms of the spatial coordinate [146, 147]. However, under closer inspection, many fronts in reactive powder compacts, composite propellants, or pyrotechnics exhibit a strongly non-continuous behaviour [6]. Detailed observations have been performed in gasless solid combustion [148]. While appearing smooth from a distance, flame fronts in fact involved corrugated front structures, whose shape was strongly correlated with the micro-structure of the reaction media. Large variations of temperature were

measured across the front, often with peak regions forming "hot spots" burning far above the combustion temperature predicted for the mixture [148]. In addition, the speed of the advancing fronts was far from uniform, often consisting of a series of quick jumps followed by relatively long hesitations of the front, which were attributed to sequences of rapid combustion events preceded and followed by long ignition delays in a "relay-race" regime [149]. Moreover, the reaction front did not always propagate in the axial direction; instead, initiations of hot spots were sometimes observed to form successive waves lateral to the front [148].

Different modelling approaches were used to capture these discrete characteristics of the flame, which were understood to be caused by the heterogeneous nature of the mixture and the confinement of the reaction to discrete locations. Modelling approaches included one-dimensional formulations involving chains of reacting particles [148], as well as two-dimensional models, often based on the simplification of the medium into a regular lattice of sites, or cells, whose activation was determined by often complex rules [6]. Three-dimensional models were also used to study the propagation in propellant mixtures [150]. In other areas, such as excitable systems or spray combustion, techniques based on cellular automata [151] or percolation-type models [152] were also used to describe the propagation of reactive fronts. In general, models claim to achieve agreement with experiments. However, such statements are sometimes difficult to assess. In many cases, described phenomena occur in mixtures with complex morphologies, in which reactants can melt, evaporate, diffuse or interact in other ways in processes that require a large number of parameters, whose determination is not always clear and may sometimes appear even arbitrary [6]. Moreover, experimental detection of the discrete flame propagation regime and the degree to which the discrete structure alters flame propagation is often difficult and often depends on the selected sensitivity threshold of

the diagnostics. Agreement may therefore arise for some combination of parameters, while it is non-existent in others. Other claims include the existence of a percolation behaviour (see Section 4.1) which is inferred from the result of simulations. However, such properties may not be observed in the complicated experiments but are rather the result of the simplified model, which is based on phenomenological consideration rather than on actual physics [6].

A fundamental verification of heterogeneous effects caused by the discreteness of sources must rather be conducted in simple experimental settings, which allow straightforward analytical treatment. In non-volatile metallic suspensions, phase changes and the combustion reactions occur at the level of single particles, which, in narrow size distributions, can be characterized well by a limited number of relatively uniform properties (ignition temperature, combustion time, and others). Igniting and burning particles (or groups thereof) thus form easily identifiable discrete "hot spots", which interact through the scalar temperature and oxygen concentration fields in the gas phase. Shoshin *et al.* [153, 154] performed a systematic study of the role of discrete sources on flame propagation. In the model, the flame propagates through a system of particles (either placed on regular matrices or randomly distributed) in an inert conductive medium. Each particle ignites when its temperature (in equilibrium with the surrounding gas) reaches an ignition temperature, T_{ign} and delivers heat at a constant rate over a characteristics combustion time, t_{c}. The model assumes that heat diffuses away from the particle independently from other sources in a constant-thermal-diffusivity (α) process [6]. This linearization of the energy equation neglects the increase of α with temperature. To some extent, it can be argued that in a real mixture, this effect is largely negated by gas expansion, which increases the inter-particle distance with temperature. The model, which is discussed more detail in Section 4.2, shows that

the discrete behaviour in flames can be expressed through a non-dimensional discreteness parameter, $\chi = \frac{t_c}{t_d}$, where $t_d = \frac{l^2}{\alpha}$ is the characteristic time for inter-particle diffusion, with l being the average inter-particle distance. For $\chi \gg 1$ and large fuel concentrations, the flame speed practically coincides with the speed of a continuous flame approximation, while for discreteness parameter values below unity ($\chi < 1$), the flame speed predicted by the discrete flame theory is significantly lower than for the case where the reaction source uniformly spread over the domain. Moreover, inter-particle diffusion becomes the limiting process of propagation, as $t_d > t_c$, so the propagation speed is practically independent of the combustion time, i.e., the reaction rate of particles, $\dot{\omega} \propto 1/t_c$. Thus, unlike in classical continuous models, discrete lean flames with fuels with different reactivities – caused for example by variations of fractions of available oxygen in the gas - and comparable thermal diffusivities should have similar flame speed. A note should be made about the discreteness parameter χ, which appears as τ_c in Publication 2 as well as in some previous work [87, 155, 156, 157]. The χ notation, used in Publication 3, follows the logic of the original formulation of the theory [154].

Some evidence of discrete behaviour was observed in laboratory experiments. Flames propagating through lean aluminum dust clouds in balloons exhibit practically the same speed between mixtures with oxygen concentrations of 15 and 30%, respectively. This was later confirmed by flame speed independence on oxygen concentration (within the same 15 to 30%-oxygen range) in flames propagating through fuel-lean aluminum suspensions in tubes [108]. In addition, stabilized counterflow iron flames displayed the same burning velocity for oxygen concentrations of 30% and 40%. In many cases, the level of oxygen is limited

by the onset of disruptive thermo-acoustic or high-Lewis-number thermo-diffusive instabilities above a certain threshold [67, 108]. The sensitivity of the flame to oxygen concentration was further investigated in suspensions of iron in oxygen-xenon and oxygen-helium mixtures with several batches of particles of different sizes, in experiments performed in microgravity conditions (at gravity levels of $5 \times 10^{-2} g$) aboard a parabolic plane. With an estimated discreteness parameter of $\chi = 0.4$, mixtures of xenon were expected to burn close to discrete predictions. Conversely, with helium ($\chi = 3.2$) flames were expected to display a more continuous behaviour. While the discrete regime was confirmed in xenon, where flames with 40% and 21% O_2 were found to be satisfyingly similar, residual gravity caused a large scatter in the helium data, proving the need to perform experiments a lower gravities aboard orbital or suborbital platforms. The latter were used in experiments detailed in the second manuscript.

3.2 Publication: A new kind of flame: Observation of the discrete flame propagation regime in iron particle suspensions in microgravity, *Combustion and Flame* [2]

Jan Palečka, Jessica Sniatowsky, Samuel Goroshin, Andrew J. Higgins, Jeffrey M. Bergthorson

Department of Mechanical Engineering, McGill University,

817 Sherbrooke Street West, Montréal, Québec H3A 0C3, Canada

Received 24 April 2019; Revised 31 May 2019;

Accepted 12 July 2019

3.2.1 Abstract

The rate of flame propagation is generally understood to directly reflect the burning rate of a combustible mixture, as it is proportional to the square root of the overall reaction rate in the flame. However, in the case of heterogeneous mixtures composed of spatially separated discrete heat sources, such as suspensions of solid-fuel particles, theory suggests that the flame propagation speed may become insensitive to the reaction rate. Such a flame propagation regime, known as the "discrete flame" in the literature, is predicted to occur in suspensions of fast-burning metal particles and (or) low-conductivity gas media where the flame propagation becomes dominated by the heat transfer between fast-burning heat sources. In an attempt to experimentally confirm the existence of the discrete flame regime, flame fronts propagating in transparent glass tubes through iron particle ($d_{32} = 33\,\mu m$) suspensions in low-thermal-diffusivity oxygen/xenon mixtures were studied in a high-quality microgravity environment. The experiment was performed on board the European Space Agency MAXUS-9 sounding rocket that lifted off from the Esrange Space Center (Sweden) on April 7, 2017. In total, 41 combustion runs were completed in suspensions with 20% and 40% of oxygen content during the 12 min of microgravity. While the experimentally

determined combustion time of a single iron particle differs by a factor of more than three in mixtures with 20% and 40% oxygen content, the flames in these mixtures were found to propagate with practically equal speed in accordance with the predictions of the discrete flame theory.

Keywords: Microgravity combustion; Metal suspension; Discrete flame

3.2.2 Introduction

In heterogeneous combustion systems, such as thermite and self-propagating high temperature synthesis (SHS) powder compacts, composite metallized propellants, and particulate fuel suspensions in oxidizing gases, the reaction usually takes place at the phase boundaries, i.e., the reaction is localized in space. Despite the discrete nature of the heat sources, most theoretical models for flames in heterogeneous systems have been based, until recently, on approximating the heat-source term by a continuous function of spatial coordinates [1]. Flame models that assume the reaction to be continuous in space cannot capture or explain phenomena, such as front roughening and percolation behavior, that have been frequently observed in experiments examining heterogeneous flames [2,3]. In an attempt at capturing the discrete nature of the heat sources, several flame models have recently been proposed to describe the combustion of SHS powder compacts [4], propellants [5], and forest fires [6].

In these efforts, the reactive system is represented by an ensemble of internally homogeneous reactive "cells", "hot spots", or "particles" that are spatially separated within an inert, heat conductive media or that are in thermal contact with each other at localized points. Due to the complex morphology of reactive powder compacts, where reactive regions

and inert spaces are often of similar scale, the localization of reactive regions and the definition of rules for their interaction is rather difficult and often arbitrary. It should also be noted that, just as spatial averaging may not be justified in certain heterogeneous systems, the presence of heterogeneity in a system does not necessarily mean that the homogeneous flame approximation cannot be applied. Most of the proposed models for flame propagation in powder compacts, however, do not provide a criterion to determine the conditions when discrete effects must be accounted for or when the continuum assumption is appropriate, nor do they suggest parameters that may allow unambiguous identification of the discrete flame propagation regime in experiments [2,7].

In contrast, for a system of solid fuel particles in suspension within an oxidizing gas, the construction of a theory for flame propagation that includes explicit coordinates of the discrete sources is more straightforward and can be well justified on physical grounds. Since the solid particles have a density more than three orders of magnitude greater than the surrounding gas, the mean distance between reactive particles in fuel-lean particulate suspensions is about two orders of magnitude larger than the particle radius. Thus, each reacting particle can be considered as a point-like heat source in space. If the combustion of the particles is controlled by oxygen diffusion, they also react via a well-defined, on-off switch-like mechanism. The particles in this case start to react vigorously when each particle reaches its ignition temperature, and the reaction proceeds within a combustion time that is proportional to the diameter of the particle squared (e.g., [8]).

The discrete flame model of particle suspensions proposed in [9] allows the flame speed in a suspension of particles, regularly distributed in space, to be determined analytically.

The model, which assumes a constant ignition temperature, $T_{\rm ig}$, for the particles in suspension, also provides a simple approach for numerical modeling of flame fronts in 2D and 3D systems with randomly distributed particles, as performed in [10,11]. Due to the simplicity and transparency of this model, it can serve as a benchmark reference for modeling of discrete flames in more complex combustion systems. The discrete flame model for particulate suspensions predicts that the realization of a continuous or a discrete flame-propagation regime depends on a single dimensionless parameter, $\tau_{\rm c}$, representing the particle combustion time, $t_{\rm c}$ [s], normalized by the characteristic time for heat transfer between spatially separated particles, $t_{\rm h} = l^2/\alpha$:

$$\tau_{\rm c} = \frac{t_{\rm c}}{t_{\rm h}} = \frac{t_{\rm c}\alpha}{l^2} \tag{3.1}$$

where α [cm^2/s] is the thermal diffusivity of the gas and l [cm] is the average distance between particles in the suspension. For large values of the discreteness parameter ($\tau_{\rm c} \gg 1$), the flame speed and its dependence on the system parameters coincide with values and predictions of the corresponding homogeneous flame model. When $\tau_{\rm c} \ll 1$, the flame front propagates in a discrete regime displaying rather unusual properties.

In the discrete regime of flame propagation, the flame propagation speed becomes practically independent of the particle combustion time [9], but becomes sensitive to the distribution of particles in space. For a regular, lattice-like spatial distribution of particles, the discrete flame is unable to propagate below some fuel concentration value even in the absence of heat losses [10]. This regular-distribution fuel-concentration limit is almost twice as large as the so-called "thermodynamic" lean propagation limit, which is defined as when the flame temperature decreases below the ignition temperature of the particles and is the limit

of flame propagation in a continuous system. Propagation below the regular-distribution fuel-concentration limit is only possible through density fluctuations in a system with randomly distributed heat sources [12]. In the random system, the discrete flame propagation process becomes highly statistical in nature, demonstrating fluctuations of the flame speed both in space and over time. The average flame speed, through an equal size domain containing the same number of particles, also fluctuates over different numerical realizations [12].

At discreteness parameter values much less than unity, and for low fuel concentrations, the roughness of the flame front in two-dimensional simulations increases with time as a power-law according to the exact exponent $\beta = 1/3$ [13] and thus belongs to the so-called Kardar–Parisi–Zhang (KPZ) universality class that has been found to describe very different physical phenomena [14]. As can be seen in Fig. 1, the front roughness starts to decrease with an increase of the discreteness parameter and, for $\tau_c \gtrsim 10$, the flames in suspensions become practically indistinguishable from a continuous flame front.

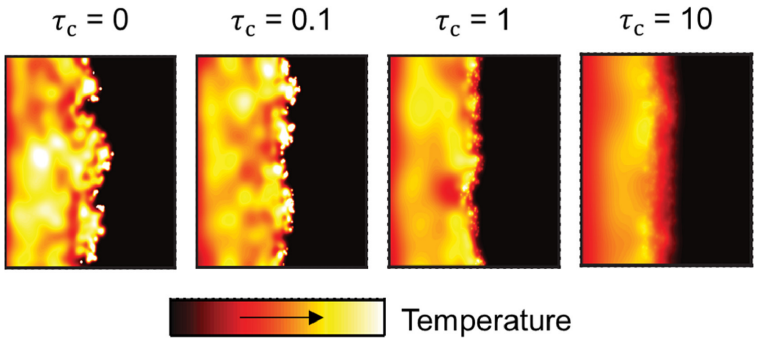

Figure 3–1: Discrete and continuous regime: evolution of the flame-front roughness in particle suspensions with change of the discreteness parameter, τ_c, for a constant value of the ratio T_{ig}/T_{ad} of 0.1, where T_{ad} is the adiabatic temperature (modified from Fig. 2 in [13]).

Fast-burning metal fuels, including aluminum, magnesium, titanium, and zirconium, in fuel-lean oxygen/nitrogen or oxygen/argon mixtures are estimated to be in the discrete flame propagation regime based on the available data for particle ignition temperatures and combustion times [9]. Experimental realization of lean metal flames with reliable identification of the discrete flame propagation regime appears, however, to be extremely difficult in the laboratory environment. Due to particle sedimentation and the limit on the minimal observable flame speed imposed by natural convection, only metal powders with particle sizes well below 10 µm can be used in terrestrial laminar flame experiments. Flames in suspensions of small particle sizes are, however, prone to thermo-acoustic and pulsating thermo-diffusive instabilities, often resulting in a very narrow set of parameters and a short time window that permit observation of an unperturbed flame [15]. In addition, small particle sizes make it difficult to observe the flame micro-structure and, thus, do not permit the estimation of important discrete flame properties, including the flame roughness and its growth rate. Even the low-gravity environment that can be obtained on parabolic-flight aircraft was found to be insufficient, since the frequently occurring g-jitters, at the level of tens of mg's, distorted, and often quenched, slow moving flames in suspensions of large particles [16]. Simple scaling arguments [17] show that front-disrupting buoyancy-driven flows of hot combustion products can be effectively suppressed at sufficiently high-quality microgravity ($10^{-4} - 10^{-6}g$), which are only provided by experiments in space on orbital platforms or suborbital sounding rockets.

Despite these experimental challenges, which resulted in a relatively large scatter in the data, a weaker dependence of the flame speed on particle combustion time — than would be predicted by continuum theory — was observed in both ground-based experiments with

fuel-lean aluminum suspensions [18] and in low-gravity experiments with iron suspensions in oxygen/xenon mixtures [11], indicating the discrete flame propagation regime. Additional evidence for the discrete regime has been obtained for flames in aluminum [15] and iron [19] suspensions. Ultimately, however, only experiments in space on orbital platforms or sub-orbital sounding rockets can provide the quality microgravity environment needed to observe the very slow discrete flames in suspensions of relatively large particles needed for flame front visualization.

This paper describes experimental results obtained during the Percolating Reactive Waves in Particulate Suspensions (PERWAVES) microgravity combustion experiment performed aboard the European Space Agency MAXUS-9 sounding rocket. Flames in suspensions of iron particles were studied in mixtures of oxygen and xenon with 20% and 40% of oxygen. The experiment was intended to provide a rigorous test for the hypothesis that — in the discrete regime — the flame propagation speed in the two mixtures should be practically independent of the particle reaction time.

3.2.3 Discreteness parameter of flames in iron particle suspensions in oxygen/xenon gas mixtures

A chemically pure (99.8% metal base) spherical iron powder, supplied by TLS Technic GmbH & Co. (lot 0881/1/2) and sieved to a narrow particle-size distribution with a mean particle diameter around 28 µm and a Sauter diameter (d_{32}) around 33 µm (Fig. 2), was used for in-flight experiments. Despite a longer combustion time in comparison to light metals, the discreteness parameter of an iron particle suspension in oxygen/xenon gas mixture is estimated to be below unity due to the large density and low ignition temperature of iron, and the low thermal diffusivity of xenon. Relatively low combustion temperatures lead to a

combustion mode occurring mostly heterogeneously on the particle surface, generating only small amounts of nano-oxides at elevated oxygen concentrations (see below). This makes iron a preferable solid fuel for operations on microgravity flight platforms [16].

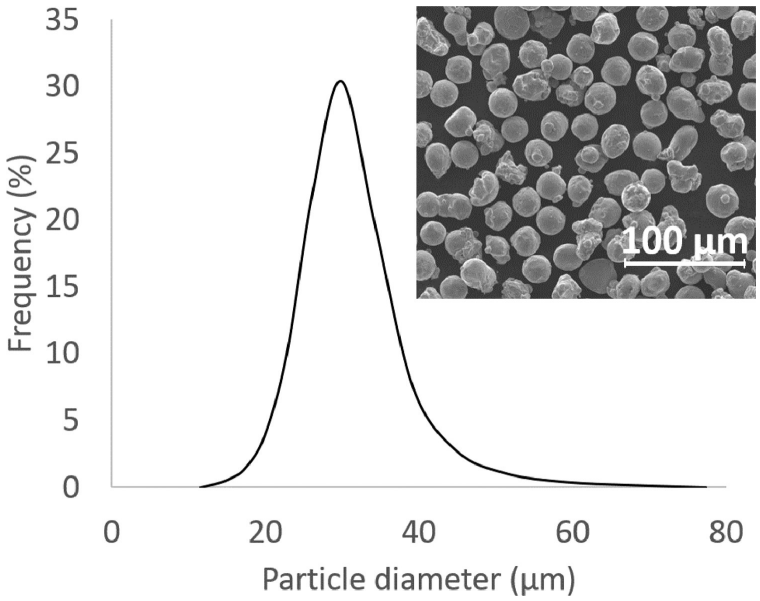

Figure 3–2: Particle size: scanning electron microscope photograph of the iron powder and the particle size distribution obtained with a HORIBA LA-920 Particle size analyzer.

Besides the thermal diffusivity and the distance between particles, the only combustion property defining the discreteness parameter, τ_c, in (1) is the particle combustion time, t_c. It is reasonable to assume that the combustion time in a fuel-lean particulate suspension is close to the combustion time of a single particle [8,20]. The combustion time of individual iron particles was measured experimentally using the simple ground-based laboratory apparatus shown in Fig. 3(a). A very small amount, less than 0.1 mg, of iron powder was injected through a miniature tubular furnace having a temperature of about 800 K into a quartz tube (length = 300 mm, ID = 12 mm) preheated to about 1100 K by a semi-cylindrical ceramic

heater. A bleeding flow, at 1 cm^3/s, of O_2/Xe mixture was used to maintain a constant gas composition in the tube prior to and during the experiments.

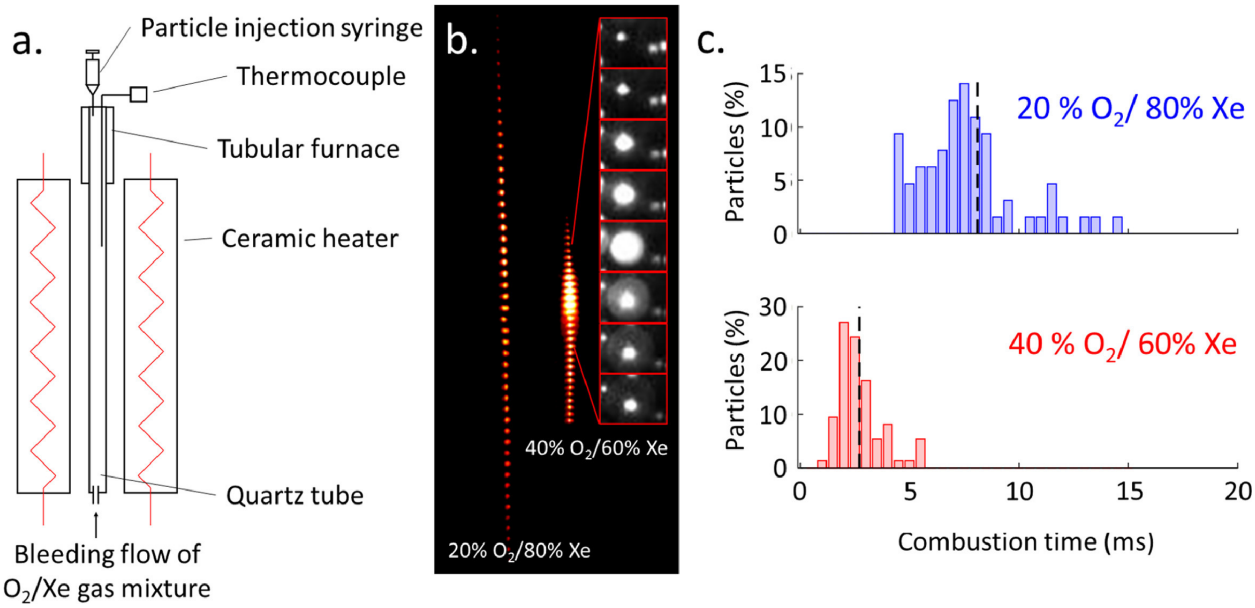

Figure 3–3: Particle combustion time measurements: (a) ground-based experimental set-up for measuring particle combustion time; (b) composite traces of particle combustion (artificially colored for more clarity) at 20% (left) and 40% (right) oxygen content in oxygen/xenon mixtures with zoomed images selected to illustrate the significant change in size of the burning zone around the particle in the 40%-O_2 mixture; (c) distribution of particle combustion times as a percentage from the total number measured. The dashed black lines indicate the respective mean values of combustion times, which are 8.1 ms for the 20%-O_2 mixture and 2.7 ms for the 40%-O_2 mixture.

Fast injection of the powder sample was performed by a syringe through a 0.1-mm ID hypodermic needle using about 1 cm^3 of the same gas mixture as in the tube. As cold gas from the powder injection was mixing with the hot gas in the tube, numerous particle ignition and combustion events were observed within about 30-40 mm of the tube midsection. The particle combustion process was filmed at 5000 fps by a Photron SA1 high-speed digital camera equipped with macro-lenses. An example of particle combustion traces composed

from multiple frames is shown in Fig. 3(b). As can be seen, the width of the particle images at 40% O_2 is blurred for a considerable part of the combustion time, and is much wider than at 20% O_2, indicating vapor- or gas-phase combustion. The presence of Fe_2O_3 nano-oxides in the combustion products and FeO molecular lines protruding over the continuous spectra acquired during the flight experiments in 40% O_2 mixtures (see discussion in Section 4) reinforces this conclusion. On the other hand, the narrow sharp particle images, the absence of FeO molecular lines in spectra, and the absence of nano-size combustion products point to a particle combustion mode driven by a purely heterogeneous surface reaction in mixtures of 20% O_2.

The histograms of the measured combustion times, plotted using about 200 particle combustion events, are shown in Fig. 3(c). They yield average combustion times of about 2.7 ms in 40% O_2/60% Xe and about 8.1 ms in the 20% O_2/80% Xe mixtures. An observed threefold decrease in combustion time with doubling of the oxygen concentration, as compared to the factor of two predicted by diffusion-limited particle combustion theory, can be explained by the onset of the vapor/gas-phase combustion for at least a part of the total particle combustion time in mixtures with 40% oxygen. Although thermodynamic calculations indicate that the combustion temperature of particles in 40% O_2 is about 2898 K, which is about 236 K below the iron boiling point of 3134 K, the iron vapor pressure at this temperature is almost 0.5 bar and may be sufficient to cause the formation of a diffusion flame lifted above the particle surface. The zoomed images in Fig. 3(b) (right), which capture in detail the evolution of the light trace of the particle from its ignition to a sharp decrease in light intensity, provide visual evidence of a lifted diffusion flame enveloping the particles. A larger

surface area of the lifted flame, in comparison to the particle surface area, accelerates the particle combustion rate.

Table 1 displays the calculated values of the discreteness parameter, τ_c, for both experimental mixtures. The distance between particles, l, is estimated at a fuel concentration of $B = 1\,\mathrm{g/L}$, and the thermal diffusivity, $\alpha = \lambda_{gas}/(\rho_{gas}c_{gas} + Bc_s)$, is based on the thermal conductivity of the gas mixture, λ_{gas}, with a density, ρ_{gas}, and on the specific heat capacities of the gas, c_{gas}, and of the solid fuel, c_s. At the same fuel mass concentration and the same type of metal fuel, l is a constant and is independent of the oxygen concentration. As can be seen, estimated values of the discreteness parameter, τ_c, in iron-oxygen/xenon suspensions are well below unity, indicating that the combustion front is predicted to propagate as a discrete flame.

Table 3–1: Estimation of the value of the discreteness parameter, τ_c,for suspensions of iron particles ($d_{32} = 33\,\mu\mathrm{m}$) in O_2/Xe mixtures at the fuel concentration of about $1\,\mathrm{g/L}$ (close to the stoichiometric concentration for mixture with 20% oxygen) with the specific heat capacity of iron, $c_s = 0.45\,\mathrm{J/g\ K}$.

Mixture	λ_{gas}, W/cm K	ρ_{gas}, g/L	c_{gas}, J/g K	α_{gas}, cm^2/s	t_c, ms	l, cm K	τ_c
20% O_2/80% Xe	$7.5 \cdot 10^{-5}$	4.6	0.21	0.053	8.1	0.053	0.15
40% O_2/60% Xe	$9.9 \cdot 10^{-5}$	3.8	0.28	0.065	2.7	0.053	0.063

3.2.4 PERWAVES MAXUS-9 combustion module

The PERWAVES combustion module was one of four experiments flown on the MAXUS-9 sounding rocket launched by the European Space Agency. The design of the PERWAVES combustion module, built by Airbus, is illustrated in Fig. 4 and is based on a semi-open

tube concept tested previously in reduced-gravity parabolic-flight experiments with different metal suspensions over several years [16]. The goal of the experiment was to observe flame propagation in suspensions of iron particles in oxygen/xenon gas, which were created in transparent quartz tubes.

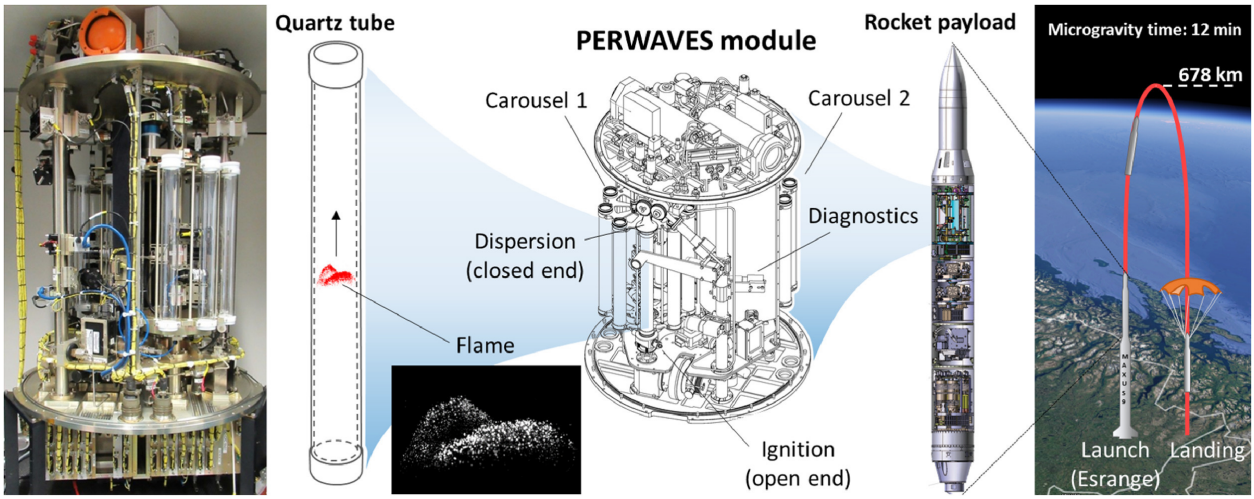

Figure 3–4: Schematics of the PERWAVES experiment: flight module with an image of the flame in the tube, the positioning in the flight payload, and the rocket flight trajectory.

For each experimental run, the 30-mm ID and 332-mm long tube was filled with an iron suspension by a powder-dispersion system comprised of a piston, driven by a step motor, and a rotating wheel with a rough surface. The wheel delivered powder into a narrow channel, where it was dispersed by a fast flow of O_2/Xe gas. After expansion in a conical diffuser, the flow of particles entered the quartz tube at the rate of about 70 cm^3/s that was maintained for 6 s. The motor step rate determined the powder mass feeding rate. After the entire tube was uniformly filled with the suspension, the filling process was stopped. Following an additional 0.4 s-delay, during which time the iron particles and gas came to rest, the suspension was ignited from the other – open – end of the tube. This was achieved by

the injection and the subsequent ignition, using an electrical spark, of approximately 1 cm^3 of propane gas. Thus, the experiment permitted the unobstructed observation of flames propagating in quiescent iron-powder suspensions from the open ignition end to the closed dispersion end of the quartz tube. The interior of the module was flushed with argon prior to launch and the environment outside the tubes was maintained at 1 atm.

The detailed design and the operation of the apparatus will be published elsewhere. Here we just mention that it has two independently operated carousels each containing nine tubes. Each carousel is equipped with individual powder dispersion and ignition units and is supplied with two different dispersing O_2/Xe gas mixtures containing either 20% or 40% of oxygen. The carousel rotates and connects a fresh tube to the dispersion and the ignition units after two combustion runs, since the tubes become less transparent due to combustion product deposition on the tube wall.

Flame propagation was recorded by two cameras operated at 60 Hz. A Basler ace acA2000-50gm camera, with a resolution of 2048 × 280 pixels, had a field of view spanning the entire tube length and was used for flame speed measurements, and another camera (Basler ace acA1300-60gm) was focused on a narrow 3 cm × 3 cm (1024 × 1024 pixels) section for detailed observations of the front structure. A third camera (Basler ace acA1300-60 gm), operated at 10 Hz with a resolution of 1024 × 824 pixels, was focused upon a thin laser light sheet and was used for estimations of relative fuel concentrations by recording, and later counting, laser-illuminated particles. An Ocean Optics fiber spectrometer with a field-of-view of about 2 mm and spectral resolution of 1.5 nm recorded flame spectra at a rate of 20 spectra per second. The experimental setup was designed to run in a fully automatic mode starting with high fuel concentrations and decreasing concentration by pre-programmed steps

until no flame propagation event was observed. The operators on the ground were, however, allowed to override the pre-set automatic procedure by observing flame propagation events on monitors and sending commands to increase, decrease, or maintain the current powder concentration via radio-link between the ground control station and the payload. This was, in fact, done during the flight of MAXUS-9.

3.2.5 Experimental results

The MAXUS-9 mission lifted off from the Esrange Space Center in Kiruna, Sweden on April 7, 2017 at 11:30 CEST. It carried about 600 kg of recoverable scientific payload comprised of four different experimental modules. The PERWAVES experimental sequence started shortly after payload separation from the booster and lasted about 12 min in a high-quality microgravity environment. In total, 25 flame-propagation events were observed in both carousels. However, only 16 tests showed sufficiently long steady-state flame propagation to be processed for the flame-speed determination.

The flame temperatures determined by polychromatic fitting [21] of the continuous flame emissivity spectra to Planck's law are shown in Fig. 5. As can be seen, in mixtures with 20% O_2, the measured flame temperature correlates well with thermodynamic prediction of the temperature of diffusively burning particles that coincides with the temperature of the stoichiometric mixture. The larger scatter of the temperature data for mixtures with 40% oxygen suggests that the emission spectra are not grey. The system of FeO molecular bands seen superimposed on top of the continuous spectra (Fig. 5), and the strong dependence of the emission and scattering coefficient on wavelength usually attributed to metal nano-oxides [22], can cause such deviation.

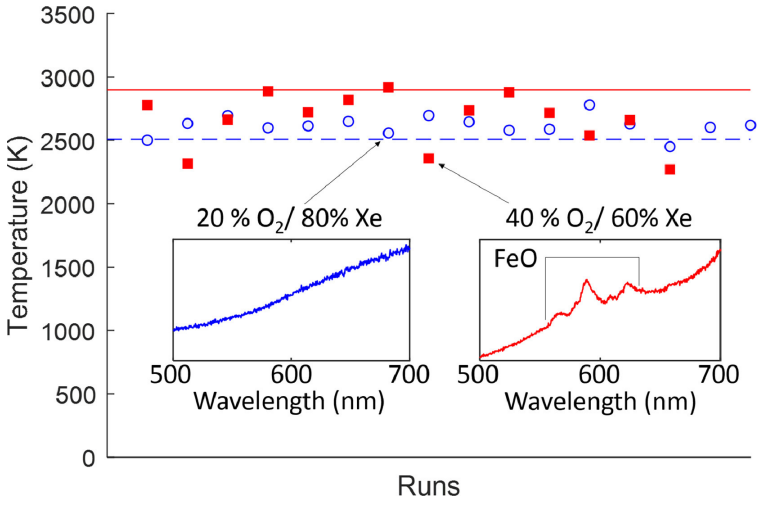

Figure 3–5: Flame temperatures: temperatures determined experimentally from spectrometer measurements (symbols) and calculated using the FactSage thermodynamic software (lines) in mixtures with 20% (blue circles and dashed line) and 40% (red squares and solid line) oxygen content. Examples of the emission spectra show appearance of the vapor-phase FeO in mixtures with 40% O_2.

Indeed, electron microscope photographs of products collected from the PERWAVES exhaust system filters (Fig. 6) show that the products of combustion in the 40% O_2 mixture contain a large amount of Fe_2O_3 red-oxide nano-particles generated by the vapor-phase combustion of iron droplets. In contrast, the products of combustion in 20% O_2 mixtures demonstrate no trace of nano-particles and consist primarily of FeO/Fe_3O_4 black oxide with particle sizes similar to the size of the initial iron powder, suggesting a mode of pure heterogeneous combustion. The results from the spectrometer (Fig. 5) and product analysis (Fig. 6) during the microgravity experiment are consistent with the observations of single-particle burning events obtained during the ground-based combustion-time measurements (Fig. 3). These results collectively suggest pure heterogeneous combustion in 20% oxygen

mixtures and the formation of a lifted diffusion flame around the particle for part of the combustion duration in 40% oxygen mixtures.

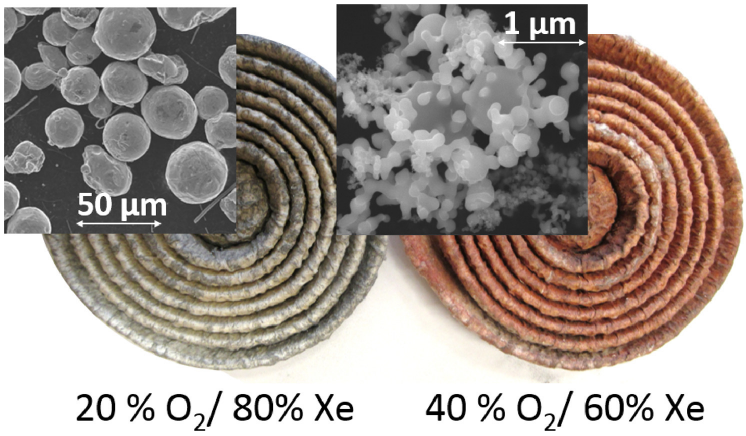

Figure 3–6: Combustion products: Filters with collected products from mixtures with different oxygen content and electron photographs showing the presence of the iron nano-oxide particles in the products from 40% O_2 mixtures.

The concentration of iron particles in the suspension was determined for each run via a particle-counting system, composed of a laser sheet illuminating a section of the tube and a CCD camera. The counting was performed over around 40 frames prior to ignition. This allowed a relatively accurate prediction of the run concentration mean with a typical standard deviation in the mean at or below 7%. With the assumption that the width of the counting volume is equal to a half-width of the laser sheet intensity profile, and taking the middle value of the camera sensitivity threshold, the absolute fuel mass concentration was estimated to be roughly 0.7–1.1 g/L for all flight combustion runs. The particle count, however, was found to be a continuously decreasing function of the camera sensitivity threshold without any well-defined plateau. The strong dependence of the particle count on the camera sensitivity

can be related to a complex Gaussian laser beam intensity profile, exacerbated by the far-field Fraunhofer diffraction from the light-sheet-forming slit. This dependence of the particle count on camera sensitivity makes identification of the counting volume somewhat arbitrary.

To overcome this uncertainty, the particle counting system was calibrated in post-flight laboratory tests with iron suspensions of a known mass concentration. The latter was determined from the measured powder mass feeding rate, the gas flow rate, and the gravitational sedimentation speed of particles relative to gas. Reusing the tubes inevitably leads to particle and product deposition on the wall, causing lower counts on subsequent tests. The measurements in the latter were replaced by estimations based on the linear fits of data pertaining to runs in clean tubes. In-situ observations of the particle flow in the tube with a telescope-microscope optical system indicated a complete absence of particle agglomeration and showed that the speed of particles in the suspension relative to gas coincides with the calculated sedimentation speed of individual particles. The calibration demonstrates a linear relationship between particle count and the absolute particle concentration with a slope that is practically independent of the camera sensitivity threshold. The application of the ground calibration to the particle count flight data yields a concentration range from 0.5 g/L to 1.0 g/L, which is in a good agreement with the aforementioned rough estimations from direct particle counts. Uncertainties in mass concentration have been attributed to four major sources: the choice of pixel intensity used to distinguish individual particles on the 8-bit frames recorded by the particle-counting camera; the calibration process (illustrated in the Supplementary material); the deviation in the particle size distribution and the associated uncertainty in the particle slip velocity with respect to the gas flow; and measurement biases estimated for the readings by the aforementioned particle size analyzer.

It needs to be noted that mass concentrations in the flight experiments from MAXUS-9, obtained from the calibration procedure, are well below nominal concentrations that can be derived from the known powder mass-feeding and gas flow rates. This indicates that in microgravity, unlike at normal gravity conditions, a large part of the powder mass supplied by the dispersion system does not enter the combustion tube. An explanation for this behavior may lie in the phenomenon of trapping of heavy dust particles by a vortex flow in the absence of gravity, predicted by recent theoretical studies [23,24]. Numerical analysis indicates that the rapid expansion of the flow in a wide-angle conical diffuser, connecting the narrow dispersion channel with the combustion tube, leads to the formation of either a symmetrical or an asymmetrical vortex pair [25], and such flows may exist in the narrow dispersion channel feeding the combustion tube. As shown in [23], particles with a finite inertia are not necessarily centrifuged away from the vortex system. Indeed, in the absence of gravitational sedimentation, these particles can have various equilibrium positions inside the vortex, becoming effectively trapped. This occurs when the value of their Stokes number is within a given range [23,24]. For some particles that escape circulation due to centrifugal force, the motion in the vortex may also facilitate their deposition on the wall of the diffuser, further reducing the outgoing fuel concentration. The gravity on Earth induces a vertical particle sedimentation velocity that largely exceeds the vortex circulation speed. This effectively pulls the particles out of the vortex flow, and thus prevents their accumulation during ground-based testing of the apparatus. A detailed numerical simulation of the particle-laden flow dynamics in the PERWAVES microgravity apparatus is planned in the near future and its results will be reported separately.

The other key measurements in the experiment are obtained by tracing the flame position over time. Typical examples of flame trajectories and flame images in mixtures with 20 and 40% O_2 are shown in Fig. 7. The observed flame speeds were on the order of 1 cm/s, well below the 5–6 cm/s flame speed that has been observed in parabolic flight experiments [16]. The light intensity of the burning particles is much greater in the mixture with 40% O_2 (see Fig. 7), indicating hotter and faster combustion, consistent with the ground-based tests shown in Fig. 3 and the temperature measurements reported in Fig. 5.

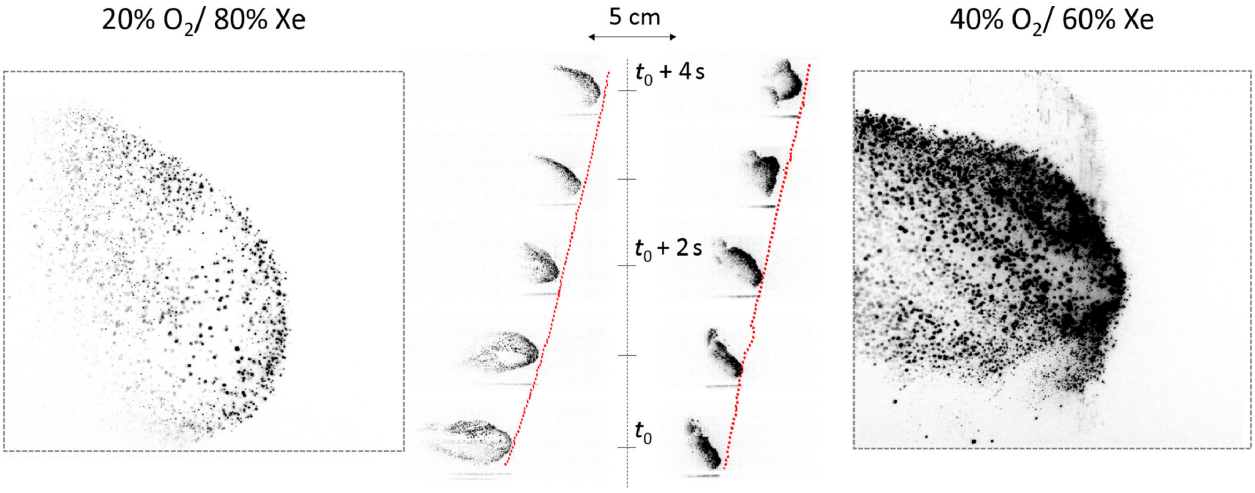

Figure 3–7: Flame propagation: typical flame trajectories and flame images in O_2/Xe mixtures with 20% and 40% oxygen content. Negative images are used for clarity.

The average flame speeds in each run shown in Fig. 8(a) were derived from the linear parts of the flame trajectory. A systematic algorithm discarded portions of unsteady acceleration caused by ignition. In a majority of cases, the data reflects between 40% and 90% of overall flame propagation time and the reported flame speed represents the mean of the slopes of different linear parts of the trajectory, weighted by the relative length of the corresponding time interval. The error bars on Fig. 8(a) represent data within two standard

deviations from the mean. As can be seen from the results, there is practically no correlation between the flame speed and the estimated particle concentration.

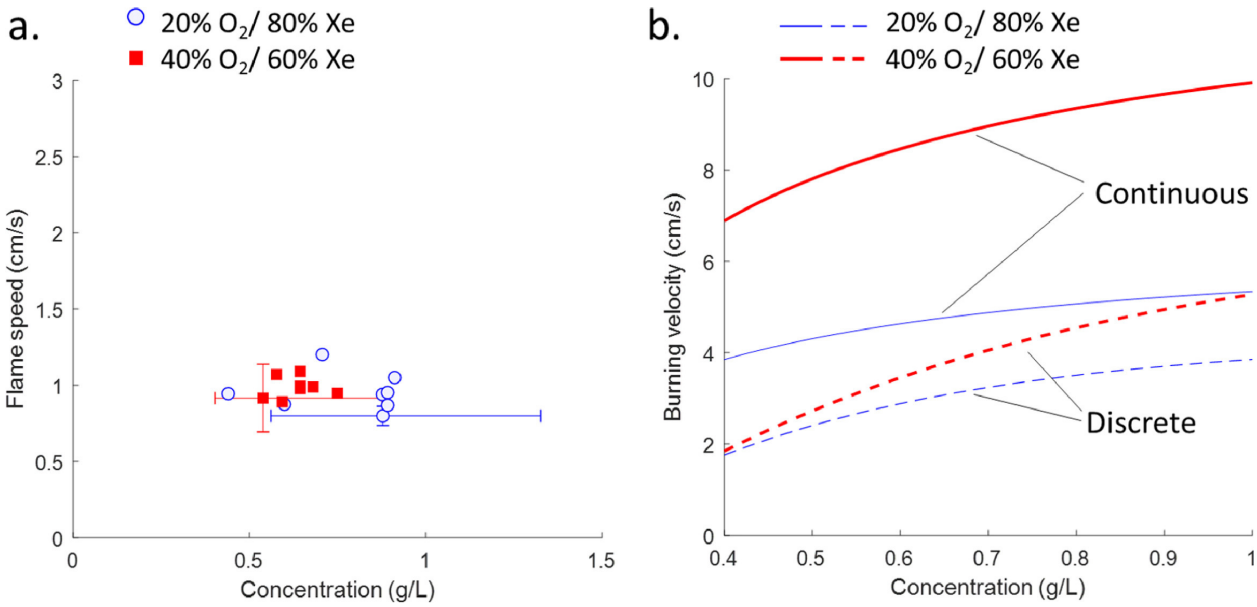

Figure 3–8: Flame speed: (a) experimental flame propagation speeds in suspensions of iron particles in O_2/Xe gas mixtures at 20% and 40% oxygen content with respect to iron concentration; (b) burning velocities predicted by the continuous and discrete flame.

3.2.6 Discussion and conclusion

Since the inception of combustion science in the 19th century, it has been understood that the flame propagation speed directly reflects the overall rate of the combustion reaction in the flame, i.e., that faster burning fuels have higher flame speeds and vice versa. The classical 20^{th} century thermal flame theories [26] show that the square of the burning velocity v^2 [cm^2/s^2] is directly proportional to the thermal diffusivity α [cm^2/s] of the mixture and to the overall reaction rate in the flame (or inversely proportional to the characteristic

combustion time, t_c [1/s]): $v^2 \propto \alpha/t_c$. This relation can be derived from dimensional analysis alone [27].

The discrete flame theory for flames in particulate suspensions, however, predicts that the influence of the reaction rate on the flame speed diminishes with a decrease of the value of the discreteness parameter and disappears when $\tau_c \to 0$ [9]. Thus, testing the sensitivity of the flame speed to the reaction rate, while keeping the thermal diffusivity and the distance between particles approximately constant, provides a direct diagnostic tool for the identification of the flame propagation regime. Changing oxygen concentration in the Xe/O_2 mixture from 20 to 40% increases thermal diffusivity by about 1.2 times, while decreasing the particle combustion time by more than 3 times. Correspondingly, the continuum theory of flame propagation predicts an increase in the flame speed in 40% oxygen mixtures versus 20% oxygen mixtures by about $\sqrt{1.2 \times 3} = 1.9$ times. In Fig. 8(b), the dependence of the flame speed on iron particle concentration is plotted as predicted by continuum theory and the discrete flame model. Both theories assume that particles start to react when the gas reaches some externally prescribed ignition temperature, assumed to be 900 K, and continues to react with a constant rate over the average measured combustion time. While the continuum flame model formulation is based on some uniform average density of heat sources throughout the combustion zone, the discrete flame model assumes a regular, lattice-like, distribution of the heat sources in space and employs their exact coordinates explicitly.

As can be seen in Fig. 8(a), the experimentally measured flame speeds at 20% O_2 and 40% O_2 indeed are close to each other, as predicted by the discrete flame propagation theory. When the propagation of the flame becomes constrained by inter-particle thermal diffusion,

rather than combustion time, the influence of particle combustion time and, hence, oxygen concentration on flame speed is greatly diminished. Thus, in the discrete flame propagation regime, the average inter-particle spacing, $l \sim B^{-1/3}$, rather than the combustion time, is the more relevant parameter influencing flame speed. Revisiting the classical dimensional analysis reviewed at the beginning of this section, the flame speed in this regime is expected to have a $v \sim \alpha/l$ dependence, as reflected in the curves that derive from discrete flame theory in Fig. 8. For flames propagating in mixtures of particles of the same size and at the same concentration, l is constant. The slight difference in the discrete curves at the two oxygen concentrations is due to the 20% increase in thermal diffusivity for the 40% O_2 mixture, since low-diffusivity xenon is displaced by higher-diffusivity oxygen.

This work has experimentally demonstrated the discrete flame propagation regime in a solid-fuel suspension. These discrete flames are predicted to have unusual properties, such as front roughness and percolation-like behavior. Future microgravity experiments with faster and high-resolution imaging systems will enable further elucidation of the physics of this new kind of flame.

3.2.7 Acknowledgments

We thank F. Tang for his crucial contributions to this project, A. Wright for his help with preparations for the flight, as well as the collaborators from Airbus Defence and Space and the European Space Agency, specifically A. Verga. Funding: This project is undertaken with the financial support of the Canadian Space Agency through the Class Grant and Contributions Program (contract number CSA-9F007052073) and through the Flights

and Fieldwork for the Advancement of Science and Technology (FAST) Grant Program under contract numbers 15FASTB16 and 18FAMCGA11, as well as with the support of the European Space Agency through the European Programme for Life and Physical Sciences in Space (ESA-ELIPS AO-2009-0918).

3.2.8 Supplementary material

Supplementary material associated with this article can be found, in the online version, at doi:10.1016/j.combustflame.2019.07. 023.

3.2.9 References

[1] A.G. Merzhanov, Self-propagating high-temperature synthesis: twenty years of search and findings, Combustion and plasma synthesis of high-temperature materials, Wiley, New York (1990), pp. 1–53.

[2] A.S. Mukasyan, A.S. Rogachev, Discrete reaction waves: gasless combustion of solid powder mixtures, Progr. Energy Combust. Sci. 34 (3) (2008) 377–416.

[3] A. Rogachev, A. Mukas'yan, Experimental verification of discrete models for combustion of microheterogeneous compositions forming condensed combustion products (Review), Combust. Explos. Shock Waves 51 (1) (2015) 53–62.

[4] O. Rabinovich, P. Grinchuk, B. Khina, A. Belyaev, Percolation combustion: Is it possible in SHS? Int. J. Self Propag. High Temp. Synth. 11 (3) (2002) 257–270.

[5] A.R. Kerstein, Percolation model of polydisperse composite solid propellant combustion, Combust. Flame 69 (1) (1987) 95–112.

[6] G. Caldarelli, R. Frondoni, A. Gabrielli, M. Montuori, R. Retzlaff, C. Ricotta, Percolation in real wildfires, Europhys. Lett. (EPL) 56 (4) (2001) 510–516.

[7] S.A. Rashkovskiy, A.Y. Dolgoborodov, Structure and behavior of gasless combustion waves in powders, Combust. Sci. Technol. 189 (12) (2017) 2220–2241.

[8] R.A. Yetter, F.L. Dryer, Metal Particle Combustion and Classification, Microgravity Combustion: fire in free fall, Academic Press, London, 2002, pp. 419–478, doi:10.1115/1.1508155.

[9] S. Goroshin, J.H. Lee, Y. Shoshin, Effect of the discrete nature of heat sources on flame propagation in particulate suspensions, Proc. Combust. Inst. 27 (1) (1998) 743–749.

[10] F.-D. Tang, A.J. Higgins, S. Goroshin, Effect of discreteness on heterogeneous flames: propagation limits in regular and random particle arrays, Combust. Theory Model. 13 (2) (2009) 319–341.

[11] S. Goroshin, F.D. Tang, A.J. Higgins, Reaction-diffusion fronts in media with spatially discrete sources, Phys. Rev. E – Stat. Nonlinear Soft Matter Phys. 84 (2) (2011) 027301.

[12] F.-D. Tang, A.J. Higgins, S. Goroshin, Propagation limits and velocity of reaction-diffusion fronts in a system of discrete random sources, Phys. Rev. E 85 (2012) 036311.

[13] F. Lam, X. Mi, A.J. Higgins, Front roughening of flames in discrete media, Phys. Rev. E 96 (2017) 013107.

[14] M. Kardar, G. Parisi, Y.C. Zhang, Dynamic scaling of growing interfaces, Phys. Rev. Lett. 56 (9) (1986) 889–892.

[15] A. Wright, A.J. Higgins, S. Goroshin, The discrete regime of flame propagation in metal particulate clouds, Combust. Sci. Technol. 188 (11–12) (2016) 2178–2199.

[16] S. Goroshin, F.D. Tang, A.J. Higgins, J.H.S. Lee, Laminar dust flames in a reduced-gravity environment, Acta Astronaut. 68 (2011) 656–666.

[17] P.D. Ronney, Premixed-gas flames, Microgravity combustion: fire in free fall, Academic Press, London (2002), pp. 35–82.

[18] P. Julien, J. Vickery, S. Goroshin, D.L. Frost, J.M. Bergthorson, Freely-propagating flames in aluminum dust clouds, Combust. Flame 162 (11) (2015) 4241–4253.

[19] M. McRae, P. Julien, S. Salvo, S. Goroshin, D.L. Frost, J.M. Bergthorson, Stabilized, flat iron flames on a hot counterflow burner, Proc. Combust. Inst. 37 (3) (2019) 3185–3191.

[20] M. Soo, X. Mi, S. Goroshin, A.J. Higgins, J.M. Bergthorson, Combustion of particles, agglomerates, and suspensions a basic thermophysical analysis, Combust. Flame 192 (2018) 384–400.

[21] S. Goroshin, J. Mamen, A. Higgins, T. Bazyn, N. Glumac, H. Krier, Emission spectroscopy of flame fronts in aluminum suspensions, Proc. Combust. Inst. 31 (2) (2007) 2011–2019.

[22] H.G. Wolfhard, W.G. Parker, Temperature measurements of flames containing incandescent particles, Proc. Phys. Soc. Sect. B 62 (8) (1949) 523–529.

[23] J.R. Angilella, Dust trapping in vortex pairs, Phys. D: Nonlinear Phenom. 239 (18) (2010) 1789–1797.

[24] J.R. Angilella, R.D. Vilela, A.E. Motter, Inertial particle trapping in an open vortical flow, J. Fluid Mech. 744 (2014) 183–216.

[25] I.V. Kravchenko, S.A. Patlazhan, R. Muller, V.G. Sultanov, The origin of extensional flow in a channel with sudden contraction and expansion, J. Phys.: Conf. Ser. 774 (1) (2016).

[26] Y. Zeldovich, G. Barenblatt, V. Librovich, G. Makhviladze, The mathematical theory of combustion and explosions, 1985, Consultants Bureau, New York, U.S., 1985.

[27] L. Landau, E. Lifshitz, Fluid mechanics, Pergamon Press, London, U.K., 1959.

CHAPTER 4
Heat locking and discrete propagation limit

4.1 Flame extinction due to heat locking

The last manuscript presented in this thesis is the result of the next phase of the PERWAVES project. While the previous publication presented an experimental proof of the discrete regime, the publication 3 concentrates on how locked heat, present in discrete flames, affects the limits of propagation. The discussion will be carried out via the theoretical model, developed by Shoshin *et al.* [153] and Goroshin *et al.* [154]. The latter allows one to see how, in heterogeneous systems, localized heat release from particles modifies the fundamental mechanisms of flame propagation, and the nature of its propagation limit. It is however important to first discuss the general concepts of phase transitions and of percolation. These topics are useful in the interpretation of discrete systems in general.

Phase transitions play an important role in the analysis of reactive frontal phenomena, including flames [158, 159]. In a macroscopic system, a phase is a set of states with relatively uniform composition and properties [160], which change significantly during the transition. Phase transitions are most often associated with changes in properties of matter, like variations of density and heat capacity at interfaces between solids, liquids, and gases, or of magnetic susceptibility between paramagnetic and ferromagnetic phases at the Curie temperature. The concept is also used to explain phenomena such as the emergence of superconductivity or superfluid transitions in certain materials. The term has been used both for

closed systems, which ultimately converge to an equilibrium, as well as in open ones, where the constant supply of external energy, reactants, particles, etc. leads to currents through the systems, which drive its temporal evolution and keep it away from equilibrium [161]. Such non-equilibrium systems often involve the transition from an unstable or metastable phase to a more stable one, which occurs through an interface or a front [162].

Phase transitions are associated with changes in the system's free energy potential, F, which represents the available work a system can deliver at a constant temperature. All thermodynamic properties can be represented in terms of F and of its partial derivatives with respect to temperature, such as entropy $S = -\frac{\partial F}{\partial T}$ or the heat capacity, $c = -T\frac{\partial^2 F}{\partial T^2}$. During the phase transition, the free energy potential loses its analycity, as one or more of its derivatives, and consequently some of the thermodynamic properties, become discontinuous. Starting with Ehrenfest in 1933, phase transitions have been classified by the order of the lowest discontinuous derivative. Modern classification generally differentiates between first-order (or discontinuous) and second-order (or continuous) phase transitions, for which the discontinuity concerns derivatives of order 2 and up [160].

The discontinuity of the first derivative of the energy means that a system must accumulate/release some latent heat to cross a first-order transition. This results in a range of energy input values, over which both phases coexist in the system, such as in the vapour dome region of the liquid-to-gas transition [160]. The presence of multiple phases leads to violent dynamics, which make the system difficult to analyze. In a similar fashion, if a propagating front undergoes a first-order transition, there is a range of parameters/point for which the front may or may not propagate, leading to the coexistence of the propagated/extinct phases [163]. Similar to the liquid-gas system, the dynamics of the system in

the transition region entirely depend on its local fluctuations. For example, a single event can decide whether a flame propagates further or not [164]. To ensure a fully propagating phase, the system must acquire a finite amount of latent energy. In waves propagating in disordered material, this may be in the form of a lowered activation threshold or a larger heat release. First-order connectivity has also been investigated in the context of several percolation mechanisms [165, 166].

Second-order transitions are smooth processes, in which the absence of a latent heat makes the analysis more straightforward [160]. The behaviour of the system can be described through the evolution of a thermodynamic function, called the order parameter, which undergoes a fast transition, e.g., from low to high values, when the control variable crosses a critical value. Thus second-order transitions are critical phenomena. As it approaches the critical point, the order parameter, A, obeys a power law of the form: $A \sim |T_c - T|^{-\alpha}$. Here the temperature T is the control variable, with T_c being the critical point, and α is a constant critical exponent, related to the variable, A. Remarkably, phase transitions of seemingly dissimilar systems have been found to give rise to identical values of critical exponents. A useful concept for the description of the behaviour is the correlation length, ξ, which is a measure of how the local fluctuations in one part of the system affect those in another. As the system approaches the phase transition, the correlation length diverges to infinity. This explains why, at the critical point, the properties of the system do not depend on the microscopic details but are rather defined by more universal dynamics. Systems that share such common dynamics are grouped into universality classes.

The most iconic system of second-order transitions is the percolation transition, which is purely geometrical and which examines the interconnectivity of a system. In the most

classical sense, the theory examines the formation of connecting clusters in a regular lattice of sites (particles), which are connected randomly with a probability p. When $p = 0$, no connections are formed and all sites are disconnected. As the p is raised, connections are randomly added to the system, connecting contiguous sites. A network of interconnected sites is called a cluster. Below a threshold value, increases in p lead to the formation of many small, disconnected clusters. However, when the probability reaches a critical values, $p = p_c$, an infinitesimal increase in connections leads to the formation of a single large cluster which spans the entire domain from one side to the other. As p is further raised, this cluster quickly grows, engulfing all surrounding clusters. Thus, within a relatively short span of p values, the domain is mainly composed of a large cluster with a few small independent clusters interspersed in the remaining space. The phase transition at the percolation threshold $p = p_c$ has been shown to be of second order, with critical exponents describing the behaviour of the number of clusters, the size of the largest cluster or the correlation length [167], being defined by specific exponents. The behaviour of many physical systems can be successfully represented via both the classical site percolation model [168] or any of its variations such as bootstrap [169], first passage [152], invasion [170] or directed percolation [161], in which connection rules are added or modified, and which may form their own universality classes [161, 168].

4.2 Publication: Heat locking and limits of flame propagation in discrete flames, *Ready for submission*

Jan Palečka, Samuel Goroshin, Jeffrey M. Bergthorson

Department of Mechanical Engineering, McGill University,

817 Sherbrooke Street West, Montréal, Québec H3A 0C3, Canada

Intended submission: Combustion and Flame

4.2.1 Abstract

The discrete nature of sources in heterogeneous flames burning in non-volatile fuel suspensions of reactive particles leads to the phenomenon of heat locking, which causes the flame to deviate — often significantly — from classical theory based on continuous sources. The different aspects of heat locking are explored via a simplified physical model and the different phenomena, resulting from heat locking, are described both for flames propagating in lattices of regularly spaced particles, as well as for mixtures with random particle distribution. In regular lattices, the discreteness of burning hot-spot sources often leads to unstable propagation. Conversely, in random systems, the propagation involves phase-transition phenomena, with percolating behaviour such as percolation. Flame dynamics are explored and the emergence of percolation processes is discussed in the context of so-called discrete flame regime, in which the particle combustion time is below the characteristic time of heat transfer between particles. In the discrete flame, the portion of the heat released by combustion is concentrated in the space near each particle and is locked out of the global heat transfer across the flame, resulting in the appearance of a specific flame propagation limit. It was predicted that fluctuations in inter-particle distance in a random suspension will partially mitigate this internal heat loss and may result in the emergence of a percolating flame.

Observations of percolating flame behaviour were indeed made during reduced-gravity experiments aboard the Falcon-20 parabolic-flight aircraft and the TEXUS-56 sounding rocket launched in Fall 2019. Flames in suspensions of iron particles (d_{32} = 33 µm) in 40% O_2 - 60% Xe gas mixtures in the 0.5 - 0.6 g/L fuel concentration range demonstrated an onset of the percolating behaviour, accompanied, for example, by the replacement of the frontal flame ignition envelope with a fractal-like structure.

Keywords: Microgravity combustion; Discrete flames; Heterogeneous flames; Percolation

4.2.2 Introduction

In heterogeneous systems, chemical reaction is localized either on the boundaries between reacting phases or within islands of premixed components separated by an inert medium. Spatial localization of the reaction can result in the phenomenon of ignition, which leads to the appearance of hot spots, i.e., regions at temperatures significantly above the rest of the medium and often above the adiabatic combustion temperature of the reactive mixture [1]. The discontinuous nature of the mixture also provides gaps of non-reactive space that the front must cross to activate further layers of reactants.Diffusion of thermal energy requires gradients, which "lock" some of the heat, and prevent it from participating in the activation of next reactive layers [2].

Despite the localized nature of the reaction and the appearance of hot spots, standard models of flame propagation in heterogeneous media have been customarily written in a homogeneous formulation. In the latter, the source term in the heat transfer equation is a continuous function of spatial coordinates and the ignition of sources is initiated via the rise

of a mean-field temperature. This approach effectively ignores the influence of local temperature gradients around hot spots on the heat transfer across the flame. To explain frequently observed rough structures of heterogeneous flame fronts incompatible with continuous flame models [3, 4], a number of phenomenological theories on the mechanism of flame propagation in heterogeneous systems started to appear at the beginning of the 1980's. The models were based on flame propagation between hot spots [5], in which an active heat source can trigger a neighbouring site through direct thermal influence or via some other contact mechanism. Flame propagation and its limits have been analyzed in terms of the then quickly developing percolation theory [6]. The initiation of sites was either performed randomly with a given probability on regular-grid lattices or through proximity to an active source for randomly distributed sites. A percolation-type description was applied, in a different context, to the combustion of sprays [7, 8], of propellants [9, 10], to coal devolatilization [11] and, more recently, to powder compacts in Self-Propagating High-Temperature Synthesis (SHS) [12-14].

Most of the developed combustion percolation models are written in the so-called site-percolation or bond-percolation [15] formulations, in which the probability of the initiation of a hot spot depends on the relative position of the latter with respect to a pre-determined number of closest neighbouring active hot spots and where the effect of the background mean-field temperature is ignored. The typical example of this approach is the classical "forest fire" model where the ignition of a tree depends on the proximity to one or more already burning randomly positioned neighbours [16]. Site-initiation by contact pre-determines the system's percolating behaviour and the existence of the percolation threshold, i.e., the critical value of the site initiation probability or the density of the discrete randomized sources at

which combustion can span through the domain of the infinite size as a fractal cluster. The rules, on which the contact process is based, however, do not always rely on a transparent physical mechanism and are often arbitrary in systems with complex meso-scale structures [17]. The neighbour-to-neighbour initiation rules that disregard the influence of the mean-field temperature also do not allow to recover a continuous flame behaviour, observed in some regions of the parametric space.

In contrast, the description of the heterogeneous flame propagating in a non-volatile solid-particle suspension first proposed by Shoshin *et al.* [18], and Goroshin *et al.* [19] provides a seamless transition from a discrete to a continuous flame propagation mode. This model, which was first developed to describe flames in a regular suspension formed by particles positioned at the nodes of a cubic lattice, has been further explored and extended by Tang *et al.* [20-22] to include suspensions with a random particle size distribution. It was shown that, in a certain range of parameters, a flame propagating in a random suspension starts to show an increasing front roughness [23] and the sensitivity of the propagation limit to the domain size [22]. It is important to underline that, unlike in the site or bond percolating formulations, the percolating-like flame behaviour in this model is not imposed by the sympathetic site initiation rule but emerges naturally with the same particle ignition criteria as in the continuous flame models. In the present paper, we will provide a brief review of the basic theoretical results of this model with an emphasis on indicating the suspension parameter space where the percolating flame behaviour is likely to be the most pronounced, which allows its experimental detection.

Unlike in combustion of propellants and powder compacts, where only the surface of the burning sample can be observed and the 3-D flame structure is mostly hidden, suspensions

of relatively large particles with sizes in the range of tens of microns are fully transparent, permitting the observation of the flame structure where the position of each reacting particle is fully definable. Hence, the combustion of non-volatile solid suspensions provides a unique experimental testing bed for developing theories of percolating reactive-diffusion fronts in 3-D space where direct observations of the dynamic percolating phenomena are practically non-existent [24]. In this paper we describe recent sounding rocket and parabolic flight microgravity experiments with flames in suspensions of iron particles in oxygen-xenon gas mixtures that provide evidence of the emerging percolating flame behaviour for the first time.

4.2.3 Theoretical considerations of the limit of flame propagation

4.2.3.1. Model for continuous and discrete flames

The effects of heat locking and dissipation will be described through the flame model developed by Shoshin *et al.* [18, 19] and expanded in subsequent papers [20-22], in which the reaction starts when the mixture reaches a pre-defined ignition temperature, $T_{\rm ign}$. Assuming one fraction (usually the oxidizer) is abundant enough so that its depletion in the reaction has a minor effect on the reaction rate, the temperature field can be described solely through the non-dimensional reaction-diffusion equation:

$$\frac{\partial \theta}{\partial \tau} = \nabla^2 \theta + R \tag{4.1}$$

with the non-dimensional temperature $\theta = \frac{T-T_0}{T_{\rm ad}-T_0}$, and $T_{\rm ad} = \frac{qB}{\rho c_{\rm p}} + T_0$ is the adiabatic temperature, respectively, T_0 is the initial temperature, q is the heat release per unit mass of fuel, B is the fuel mass concentration, ρ and $c_{\rm p}$ are the density and specific heat of the medium, respectively, and are assumed to be constant. Table 4–1 shows expressions for the

reaction rate term, R, both for a homogeneous (continuous) source, and for sources with discrete spatial positions. The non-dimensional discreteness parameter $\chi = \frac{t_c \alpha}{l^2}$ is defined as the ratio of the particle combustion time, t_c, and the characteristic time of heat diffusion between particles, $t_d = l^2/\alpha$, where l and α are the average inter-particle distance and the constant thermal diffusivity of the medium, respectively. χ is used to express the degree of heat locking in the mixture. As discussed in the next sections, two cases can be distinguished: when $\chi = 0$, an ignited particle releases all its thermal energy instantaneously, as expressed by the δ function, while for $\chi > 0$, the heat release proceeds at a constant rate for the duration of the particle combustion time t_c. It should be noted that both the time (τ) and space (x) variables are non-dimensional, obtained by scaling dimensional variables with t_d and l, respectively.

Table 4–1: The reaction term R for the different formulations discussed in the paper.

Nature of source	Reaction term
Continuous	$R = \begin{cases} 0, & \text{if } x < 0 \text{ and } x > \eta\chi. \\ \frac{1}{\chi}, & \text{if } 0 \leq x \leq \eta\chi \end{cases}$
Discrete ($\chi = 0$)	$R = \sum_{i=1}^{N} \delta(\mathbf{x} - \mathbf{x}_i)\, \delta(\tau - \tau_i)$
Discrete ($\chi > 0$)	$R = \sum_{i=1}^{N} \frac{1}{\chi} \delta(\mathbf{x} - \mathbf{x}_i)\, H(\tau - \tau_i)\, H[\chi - (\tau - \tau_i)]$

In the following section, both the analytical solutions as well as simulations aim to find the propagation speed of the flame, i.e., the eigenvalue of the problem. It is the latter that is

used to describe the various manifestations of heat locking in mixtures with discrete sources.

4.2.3.2. Flame propagation for continuously distributed sources

While it has now been widely accepted that models with a uniform distribution of the source term in space fail to capture essential physics of many segregated systems [2, 4], such "continuous" approaches offer a point of comparison, against which the effects of heat locking can be clearly displayed. For spatially continuous and homogeneous sources, equation (4.1) can be solved analytically [25, 26], providing an implicit equation for the flame speed, η:

$$\frac{\eta^2\chi}{\mu} = 1 - e^{-\eta^2\chi} \tag{4.2}$$

Here $\mu = \frac{qB}{c\rho(T_{\text{ign}}-T_0)}$ is the dimensionless concentration, and correspondingly $\frac{1}{\mu} = \theta_{\text{ign}}$ is the dimensionless ignition temperature, whereas $\eta = vl/\alpha_{\text{u}}$ is the dimensionless flame speed. In a previous publication [27], we have found that equation (4.2) can be modified to express the flame speed explicitly:

$$\eta^2 = \frac{1}{\chi}\left[W_0\left(-\mu e^{-\mu}\right) + \mu\right] \tag{4.3}$$

where W_0 represents the zero branch of the function in the real space.

4.2.3.3. Discrete systems of regular lattices of particles

The role of the discrete nature of heat sources for flames in suspension was first investigated by Shoshin *et al.* [18, 19] who considered the problem of a flame propagating in a system of regularly distributed point-like heat sources (particles) positioned at the nodes of an imaginary cubic lattice, as shown in Fig. 4–1. The figure depicts a flat flame consisting

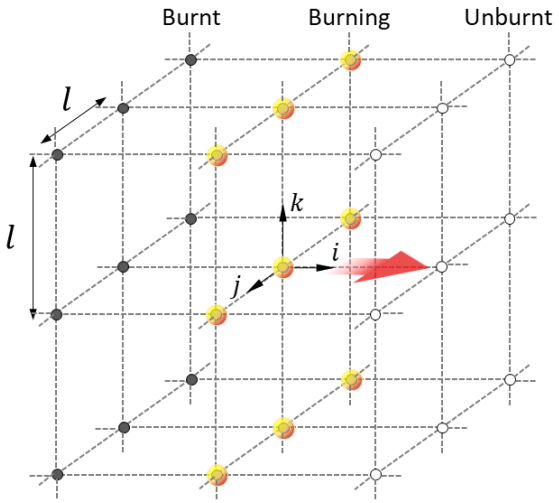

Figure 4–1: Representation of the lattice of equally spaced discrete sources along with the direction of flame propagation.

of one or multiple layers of simultaneously reacting particles, which propagates from left to right along the x-axis, with a fixed particle spacing of l. Each particle ignites when the temperature reaches some value, T_{ign}, and burns with constant heat output during an externally prescribed combustion time, t_{c}. It is assumed that a stable flame exists, i.e., that particles along the x-axis ignite at regular time intervals, τ, and the flame speed can be defined as $v = l/\tau$. It is also assumed that the heat generated by each particle propagates through the system independently of other sources, i.e., that the differential heat transfer equation is linear. Some justification for this assumption is provided by the fact that the gas expansion enlarges the distance between particles counterweighting, to a degree, the increase of the gas thermal diffusivity with temperature [19]. Assuming linearity of the heat diffusion equation, the temperature at any point in the domain can be expressed as the superposition of the incremental temperature increases provided by all reacted sources in the infinite system.

For fast-burning particles that closely resemble a δ-type source, both in space and in time, the contribution of all particles located at $\mathbf{x}_i$ and having ignited at times $\tau = \tau_i$ to the temperature field evaluated at point at $\mathbf{x}$ at time τ, is:

$$\theta(\mathbf{x}, \tau) = \sum_{i=1}^{\infty} \left[\frac{1}{4\pi (\tau - \tau_i)} \right]^{\frac{p}{2}} \exp \left[-\frac{|\mathbf{x} - \mathbf{x}_i|^2}{4 (\tau - \tau_i)} \right] \tag{4.4}$$

where p is the dimension of the domain. Equation (4.4) is independent of the way particles are arranged in the domain. For particles arranged in a three-dimensional regular lattice [19, 20], the temperature of the particle at the instant of ignition, θ_{ign} is:

$$\theta_{\text{ign}} = \frac{1}{\mu} = \frac{1}{(4\pi)^{\frac{3}{2}}} \sum_{i=1}^{\infty} \sum_{j=-\infty}^{\infty} \sum_{k=-\infty}^{\infty} \left(\frac{i}{\eta} \right)^{-\frac{3}{2}} \exp \left[-\frac{\eta (i^2 + j^2 + k^2)}{4i} \right] \tag{4.5}$$

In one-dimensional systems, the equation becomes:

$$\theta_{\text{ign}} = \frac{1}{(4\pi)^{\frac{1}{2}}} \sum_{i=1}^{\infty} \left(\frac{i}{\eta} \right)^{-\frac{1}{2}} \exp \left(-\frac{i\eta}{4} \right) \tag{4.6}$$

As can be seen from the solution of (4.6) plotted in Fig. 4–2, due to the finite time needed for the heat to propagate between particles, the flame speed remains finite even if the combustion time tends to zero.

In the present work, it has been found that the summation in eq. (4.6) can be expressed through the polylogarithm function, $\text{Li}_s = \sum_{k=1}^{\infty} z^k / k^s$ $(z, s \in \mathbb{C})$, such that the new expression relating the ignition temperature, θ_{ign}, and the flame speed, η, is:

$$\theta_{\text{ign}} = \sqrt{\frac{\eta}{4\pi}} \text{Li}_{\frac{1}{2}} \left(e^{-\frac{\eta}{4}} \right) \tag{4.7}$$

The expression simplifies the numerical determination of the flame speed. However, eqs. (4.6) and (4.7) only provide the steady-state prediction of the flame speed. As has been

shown in detail by Tang *et al.* [22], the behaviour of flames propagating through evenly spaced layers of particles is far more complex.

First, eq. (4.7) can be used to show that the flame speed monotonically decreases with increasing θ_{ign}, with $\eta \to 0$ as $\theta_{\text{ign}} \to 1$. However, previous studies of the temperature profile [20] have shown that propagation is virtually impossible above a critical value of the ignition temperature, $\theta_{\text{ign,cr}} \approx 0.568$. When $\theta_{\text{ign}} < \theta_{\text{ign,cr}}$, an unburnt particle experiences a rise in temperature until it ignites at $\theta = \theta_{\text{ign}}$. Thus, the time derivative, $\frac{\partial\theta}{\partial\tau}$, is positive at ignition. However, when $\theta_{\text{ign}} = \theta_{\text{ign,cr}}$, $\frac{\partial\theta}{\partial\tau} = 0$, i.e., the ignition occurs exactly as the temperature profile reaches a plateau. In the present work, the use of the polylogarithm is used to provide an analytical expression for the critical flame speed, η_{cr}, at ign, cr. Assuming η_{cr} to be constant:

$$\frac{\partial\theta}{\partial\tau} = 0 \to \frac{\partial}{\partial\tau}\left(\sum_{i=1}^{\infty}\left[\frac{1}{4\pi\left(\tau-\tau_i\right)}\right]^{\frac{1}{2}}\exp\left[-\frac{i^2\eta_{\text{cr}}}{4(\tau-\tau_i)}\right]\right) = 0 \tag{4.8}$$

which yields:

$$\frac{\eta_{\text{cr}}}{2} = \frac{\text{Li}_{\frac{3}{2}}\left(e^{-\frac{\eta_{\text{cr}}}{4}}\right)}{\text{Li}_{\frac{1}{2}}\left(e^{-\frac{\eta_{\text{cr}}}{4}}\right)} \to \eta_{\text{cr}} = 1.2... \text{ and } \theta_{\text{ign,cr}} = 0.568... \tag{4.9}$$

When $\theta_{\text{ign}} > \theta_{\text{ign,cr}}$, $\frac{\partial\theta}{\partial\tau}$ becomes negative, i.e., ignition is reached as the temperature of the particle is decreasing. This can be achieved only if the particle had already reached ignition conditions prior to the time predicted by the steady-state eq (4.7). As discussed in the next paragraph, when the particle is allowed to ignite simply when its temperature reaches ignition conditions, the unsteady simulations quickly result in oscillations and quenching. Interestingly, it has been numerically shown [20] that for example for $\theta_{\text{ign}} = 0.63$, when the particles are allowed to ignite at times predicted by the steady-state solution (when $\theta = \theta_{\text{ign}}$ and $\frac{\partial\theta}{\partial\tau} < 0$), i.e. when the temperature is decreasing, the flame propagates steadily even

above $\theta_{\text{ign,cr}}$. Thus, delaying particle ignition does not inhibit flame propagation. On the contrary, it seems to allow the flame (or wave) to reach the highly activated layers of unburnt particles in a stable manner. This may be of interest in systems with delays, for example due to gas-to-particle heat transfer or surface phenomena.

Previous work [20, 28-30] has shown that a flame propagating in layers of regularly spaced reacting material (particles, slabs, etc.) in an inert conducting medium loses stability even before reaching $\theta_{\text{ign,cr}}$. At low ignition temperatures, θ_{ign}, the flame is stable with steady-state speed predicted by eqs. (4.6) and (4.7). However, at $\theta_{\text{ign,bif}} \approx 0.512$, the flame dynamics undergo a Hopf bifurcation, manifested by the appearance of periodic oscillations. This is the first step of a period-doubling cascade that ends in chaotic behaviour around $\theta_{\text{ign}} = \theta_{\text{ign,qch}} \approx 0.534$. Beyond this value, irrespective of the method used for flame initialization, unsteady simulations always result in strong oscillations and flame quenching. Such strongly periodic behaviour is usually associated with rigid geometries, such as lattices or crystals, in which the imposition of inter-particle spacing leads to a lower-symmetry state, whose constraints may force the system to modulate its response, for example through excitations or oscillations [31].

4.2.3.4. Discrete regime in regular lattices with gradual heat release ($\chi > 0$)

Similar to equation (4.5), the model by Goroshin *et al.* [19] also provides an implicit expression for the speed of flames propagating in regular arrays of particles with finite combustion times ($\chi > 0$):

$$\theta_{\text{ign}} = \frac{1}{\mu} = \frac{1}{(4\pi\chi)^{\frac{3}{2}}} \sum_{i=1}^{\infty} \sum_{j=-\infty}^{\infty} \sum_{k=-\infty}^{\infty} \int_{\left(\frac{i}{\eta}-\chi\right)H\left(\frac{i}{\eta}-\chi\right)}^{\frac{i}{\eta}} \zeta^{-3/2} \exp\left(-\frac{i^2+j^2+k^2}{4\zeta}\right) d\zeta \qquad (4.10)$$

Similar to the $\chi = 0$ case, in a regular array, the 1D equation consists of a single summation [22]:

$$\theta_{\text{ign}} = \frac{1}{\mu} = \frac{1}{2\sqrt{\pi}\chi} \sum_{i=1}^{\infty} \int_{\left(\frac{i}{\eta}-\chi\right)H\left(\frac{i}{\eta}-\chi\right)}^{\frac{i}{\eta}} \zeta^{-1/2} \exp\left(-\frac{i^2}{4\zeta}\right) d\zeta \tag{4.11}$$

where H is the Heaviside step function. The integral in eq. (4.11) can also be expressed as the lower branch of the incomplete gamma function, $\gamma(s,x) = \int_0^x t^{s-1}e^{-t}dt$ (with the integration variable $t = \frac{i^2}{4\zeta}$), which yields:

$$\theta_{\text{ign}} = \frac{1}{\mu} = \frac{1}{4\sqrt{\pi}\chi} \sum_{i=1}^{\infty} i \left[\gamma\left(-0.5, \frac{i\eta}{4}\right) - \gamma\left(-0.5, \frac{i^2}{4\left(\frac{i}{\eta}-\chi\right)H\left(\frac{i}{\eta}-\chi\right)}\right)\right] \tag{4.12}$$

As demonstrated in [20] and as illustrated in Figure 4–2, the predictions of the model for $\chi \to 0$ coincide with the results of equations (4.6) and (4.7) for instantaneously burning particles ($\chi = 0$), described in the previous section. Conversely, at $\chi \gg 1$ and low θ_{ign} (Figure 4–2b), the flame speed closely approaches the continuous flame approximation. As described in [20], longer combustion times (increasing χ) lead to the increase of the limiting θ_{ign} and to the disappearance of chaotic behaviour. Thus, a more gradual release of chemical energy inhibits the growth of highly organized structures, responsible for the ultimate onset of chaos in regular lattices.

However, as Tang *et al.* [20] also reported, the convergence to the continuous solutions is not smooth for highly activated flames at θ_{ign}. Similar to instantaneously burning particles ($\chi = 0$), instabilities were found through both steady-state and unsteady considerations. First, the complex nature of the steady-state predictions is illustrated by all the solutions to eq. (4.11) displayed in Fig. 4–2a in the three-dimensional $\chi - \eta - \theta_{\text{ign}}$ space. The figure

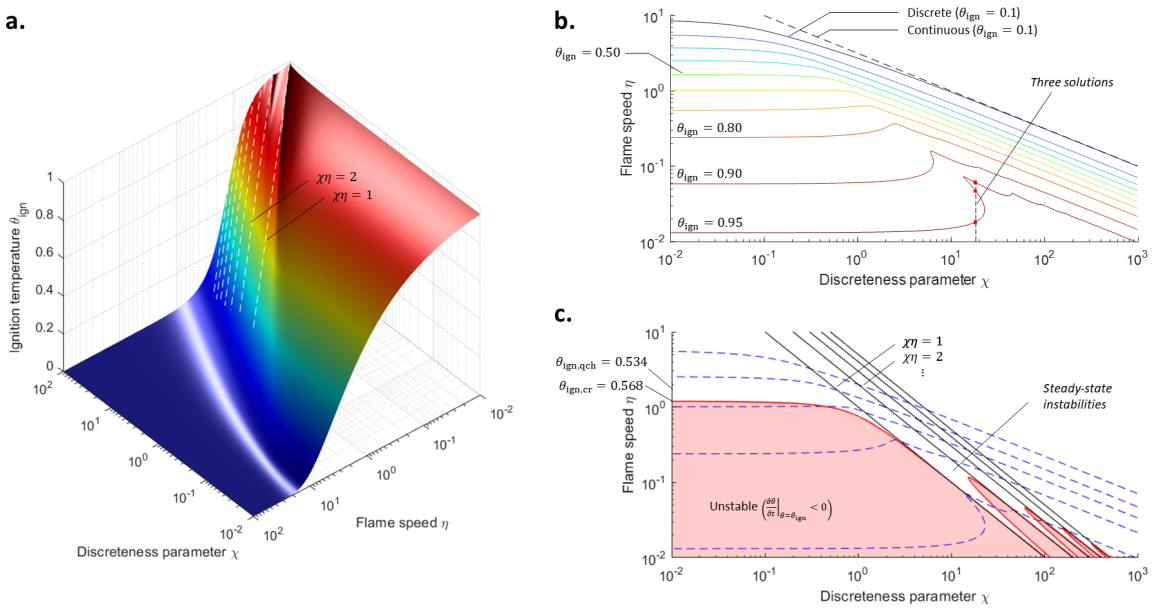

Figure 4–2: Map of discrete model: a. Three-dimensional representation of the steady-state solutions in the χ-η-θ_{ign} space with prominent ridges corresponding to $\chi\eta = \sigma$; b. Flame speed dependence on the discreteness parameter χ and the ignition temperature θ_{ign}, showing the convergence of the model towards continuous solutions at low θ_{ign} and the multiplicity of solutions at high θ_{ign}; c. location of different types of instabilities on the map and their relation to the $\chi\eta = \sigma$ curves, with flame speed curves as dashed blue lines.

confirms the convergence to the $\chi = 0$ case (eq. (4.6) and (4.7), as well as to the continuous model for high values of χ. However, the convergence is not smooth. On the contrary, a series of ridges appear in the parametric region of interest (whose effects were noticed in both [20] and [32]. The behaviour is further shown in Fig. 4–2b., which displays the constant-θ_{ign} curves extracted from the three-dimensional surface. In high-χ and θ_{ign} parametric regions, the system exhibits a pair of bifurcations, which lead to up to three predicted steady-state speeds in some cases.

To explain these ridges, in the present work, we "split" the contribution to θ_{ign} according to the value of the Heaviside term H into the contribution of σ closest particles, which are still burning when $\theta\left(x=0\right)=\theta_{\text{ign}}$, i.e., those at a distance $i/\eta<\chi$ (with $H\left(\frac{i}{\eta}-\chi\right)=0$), and those which have finished burning (with $H\left(\frac{i}{\eta}-\chi\right)=1$):

$$\begin{aligned}\sum_{i=1}^{\infty}\int_{\left(\frac{i}{\eta}-\chi\right)H\left(\frac{i}{\eta}-\chi\right)}^{\frac{i}{\eta}}\zeta^{-1/2}\exp\left(-\frac{i^2}{4\zeta}\right)\,d\zeta=&\sum_{i=1}^{\sigma}\int_{0}^{\frac{i}{\eta}}\zeta^{-1/2}\exp\left(-\frac{i^2}{4\zeta}\right)\,d\zeta\\&+\sum_{i=\sigma+1}^{\infty}\int_{\left(\frac{i}{\eta}-\chi\right)}^{\frac{i}{\eta}}\zeta^{-1/2}\exp\left(-\frac{i^2}{4\zeta}\right)\,d\zeta\end{aligned}\tag{4.13}$$

Thus, at the moment of ignition of a new particles, exactly σ previous particles are still burning. An increase in the discreteness parameter, i.e., the combustion time implies that, at $\frac{\sigma}{\eta}=\chi$, i.e., $\sigma=\eta\chi$, the number of still burning particles increases from $\sigma-1$ to σ. As Fig. 4–2a shows, the ridges, associated with regions of instability stem from these transition curves, defined by increasing values of the integer σ.

In addition, the analysis that was used to find the critical ignition temperature, $\theta_{\text{ign,cr}}$, beyond which the steady-state speed is maintained only when particles ignite when the temperature gradient is negative, can be extended to non-zero χ by finding the critical flame speed, η_{cr}, at which eq. (4.11) or (4.12) obey the condition $\frac{\partial\theta}{\partial\tau}=0$ at $\theta=\theta_{\text{ign}}$. The resulting χ - η curve is shown in Fig. 4–2c. This leads to a series of islands of instability, which were reported by Tang *et al.* [20]. Here we show that complex shape of these islands follows the pattern of $\chi\eta=\sigma$ condition. Tang has also reported that, at larger values of χ, unsteady simulation exhibit again flame quenching before the ignition has even reached $\theta_{\text{ign,cr}}$. At $\chi>5.6$, numerical simulations show a new sensitivity of the flame propagation to disturbances. For small values of θ_{ign}, the insertion of a disturbance results in a few oscillations in

the flame speed, which rapidly decay towards a stable steady-state. For larger θ_{ign}, no decay is observed and the oscillations persist. Finally, for θ_{ign}, the amplitude of flame oscillations grows with time in an unbounded way, which leads to the quenching of the flame. This has been reported as the actual quenching limit, $\theta_{\text{ign,qch}}$ for $\chi > 5.6$ by Tang *et al.* [20]. While the value of $\theta_{\text{ign,qch}}$ was reported numerically in [20], the general shape of the curve also seems to loosely follow the pattern traced by the $\chi\eta = \sigma$ curves. This observation could potentially shed light on the nature of the oscillations. A hypothesis is that the complex dynamic response of the flame, as it approaches seemingly "continuous" conditions, may be linked to the location of the source: while the heat is produced more continuously in time, the release occurs at spatially discrete positions. A smooth convergence to the continuous flame model could then be achieved by gradually spreading the source in space. More importantly, even with continuously burning sources, spatial heterogeneity can still display heat-locking behaviour which significantly alters flame behaviour close to propagation limits. It is also worth noting the similarity of the high-activation high-Lewis number conditions to the ones encountered in pulsating diffusive-thermal instabilities [33], which have been also observed in solid flames [34].

4.2.3.5. Discrete regime in a random particle distribution

The propagation of flames in media with randomly distributed sources has attracted significant attention due to its relevance to fields like forest fires [35, 36], the combustion of solid propellants [9], explosives [37], and sprays [8], as well as to solid-state high-temperature synthesis (SHS) processes [4]. The studies often employ simplified models to investigate the ability of the flame to cross the domain and to capture the characteristic features often

observed in experiments, such as the flame roughness. In particular, the nature of the propagation limit is of both practical and fundamental interest. The flame is often viewed as a network of successive ignition events, each of which occurs when the particle reaches its activation threshold, e.g., ignition temperature, and which are caused by heat transfer from previously ignited sources. The question then pertains to the scale of these interactions. Several studies attempt to understand the flame in terms of classical percolation or directed percolation models, in which the ignition of the particle usually depends on the presence of a burning source in its immediate proximity [4]. In such cases, close to the so-called percolation threshold, many variables, such as the rate of propagation, have been shown to evolve according to universal scaling laws defined by characteristic exponents [4]. Moreover, the front acquires a self-similar and possibly even fractal structure, as it propagates through the coarse domain.

However, this approach often neglects the "memory" of the field, as the rise in local temperature is a result of heat diffusion from hotter regions of previously ignited particles. Thus, rather than the effect of simple contact between contiguous sources, ignition events are generally the result of long-range contributions from other "hot spots" in the flame. Such interactions add significant complexity to the analysis of combustion systems, and it has been often argued that percolation cannot be used to explain extinction of such systems [4, 37]. Only the presence of heat losses or additional mechanisms of dissipation, which counter the effect of thermal diffusion over long distances, may give rise to percolation dynamics [38]. However, it has also been argued [36] that, while long-range interactions do not lead to percolation in the classical sense, they result in a percolation-like behaviour, in which the dynamic variables are still subject to scaling laws, albeit with variations in the value of

exponents as the percolation threshold is approached. While non-universal in its nature, this new type of percolation still presents a critical behaviour with possible analogies in other systems, such as the gelation transition in spin glasses [36]. It was also observed by Schiulaz *et al.* [37,38] that low-heat-loss and adiabatic systems appear to undergo a first-order phase transition. At the critical transition point, the system exhibits a jump, i.e., a shift from the propagation to no-propagation phase. Whether the flame spans an infinite domain is solely controlled by fluctuations, i.e., by the specific position of particles. While one configuration may lead to propagation, another one will not. Thus, at the critical point, the system exhibits a co-existence of phases — another attribute of first-order transitions. Only the removal of long-range connections can allow the transition to second-order behaviour. Even placing a two-dimensional system in a three-dimensional environment is not sufficient, as first-order behaviour is maintained. The system needs to be actively "drained" to exhibit second-order percolation transition [37].

The present work discusses the behaviour of discrete randomized systems and examines the nature of heat locking and propagation limits in terms of the model developed by Goroshin [19]. It has been shown [21,22] that flame propagation in random distributions overcomes many of the constraints caused by the rigidity of systems of regular lattices. The flame benefits from fluctuations in the particle number density, finding energetically advantageous paths through the domain. The stochastic nature of the propagation removes the synchronization required for the onset cascading period-doubling and chaotic behaviour. As a result, in two- and three-dimensional systems, the flame has been observed to propagate well beyond either the $\theta_{\mathrm{ign,qch}}$ or the $\theta_{\mathrm{ign,cr}}$ limits, with flames spanning computational domains at $\theta_{\mathrm{ign,2D}} \approx 0.65$ in two dimensions and $\theta_{\mathrm{ign,3D}} \approx 0.85$ in three dimensions for $\chi = 0$ [22].

For $\chi > 0$, Tang *et al.* have even observed flame propagation at $\theta_{\text{ign}} > 1$, i.e., for particles igniting at higher temperatures than the adiabatic temperature of the mixture. However, these observations must be validated in domains significantly larger than the boxes with $25 \times 25 \times 25$ particles used in the simulations.

Contrary to the analytical transparency of regular systems, which can be studied via one-dimensional models, flame propagation in randomly distributed particles require two- and three-dimensional numerical analysis. As the computational cost for 3D systems over sufficiently large domains remains prohibitive, most parametric studies have been performed in 2D, with some exceptions [39]. The dynamics of the present model were mainly investigated in [23]. The study focused on the range of ignition temperatures from 0.025 to 0.5 and found that flame propagation varies fundamentally for different input parameters. At low θ_{ign} and χ, the dynamics of the system, specifically the growth of front roughness, show good agreement with the Kardar-Parisi-Zhang (KPZ) model [40], often considered to be the field theory of many growth and deposition phenomena. Indeed, the low activation threshold (low θ_{ign}) and the fast energy release (low χ) favour short-range spatial and temporal correlations. Proximity to the flame, determined mostly by the local evolution of the front and the random position of the particles, is sufficient for particle ignition, which does not need to rely on accumulation of heat from distant sources. This is analogous to the growth of an interface from random deposition of particles. Raising χ or θ_{ign} results in increasing deviations from KPZ behaviour. In the first case, the growth of frontal roughness decreases towards zero as the flame becomes a smooth laminar front in the continuous limit (large χ). With an increase in θ_{ign}, the sources become gradually more difficult to ignite and rely progressively on thermal diffusion from more distant sources. The resulting extension of the

correlation length results in a shift in the size of frontal structures. As shown in the inset of Fig. 4–3a, at $\theta_{\text{ign}} = 0.1$, the size of frontal discontinuities is limited to the order of units of inter-particle distance. However, the range of scales noticeably increases at $\theta_{\text{ign}} = 0.4$, with hotter zones of different sizes. Finally, close to the 2D flame extinction limit ($\theta_{\text{ign}} = 0.63$), variations in the axial direction (y axis) of the flame bear signs of fluctuations of all sizes. In fact, according to Lam *et al.* [23], above $\theta_{\text{ign}} \approx 0.25$, initial conditions influence the dynamics of the flame over a significant part of the 200×200-particle computational domain. By the same token, boundary conditions play an increasing role.

Simulations shown in Fig. 4–3 have been achieved via a novel numerical approach, aimed at reducing the computational time required to solve the analytical model by Goroshin [19]. Similarly to previous versions in [22,23,39], the procedure uses eq.(4.4) with randomly positioned sources to evaluated whether a yet unburnt particle has ignited. The main difference consists in the selection of the particles to be evaluated for ignition. At each time step, equation (4.4) is used along with the contour function in MATLAB to find the location of the ignition isotherm. The front is then parcelled in the y-direction into small computational domains whose span in the x-direction is determined so as to ensure that the front will remain inside over the next computational step. During the subsequent steps, only particles located close to the front, i.e., within the unburnt regions of the computational domains, are evaluated for ignition via eq.(4.4). The procedure is based on the assumption of continuity of the isotherm, i.e., that the exponential decay of the sources will prevent the formation of a new "island" of burning sources away from the isotherm. Instead of scaling with the dimension of the system (power 2 for 2D and power 3 for 3D), the computational cost scales with the "fractal" dimension of the ignition isoline or isosurface, i.e. between 1 & 2, and 2 &

3, respectively. This should prove to be beneficial especially in 3D computations. The focus will be limited to the case with $\chi = 0$.

Several authors have noticed that an increase in ignition temperature leads to an increase of the length of influence in the flame, with the ignition of a particles depending on progressively more distant parts of the domain [23]. While the ignition of a particle is the result of the contributions of all ignited particles in the domain (eq. 4.4), insight is provided by representing the flame through single particle-to-particle connections. In the present work, for every igniting particle, such a link is provided by connecting it to the particle that contributed the most to its ignition, i.e., to the particle with the highest term in the summation in eq. 4.4. The resulting flame "history" is displayed in Fig. 4–3. In Fig. 4–3a. the links are coloured by the degree of branching, with darker links being outside branches and brighter links playing the role of connecting trunks. This representation has been chosen only to facilitate a qualitative analysis of the pictures. A more quantitative description is given in Fig 4–3b., in which the color scheme has been chosen to quantify the contribution to the "parent" source towards the ignition temperature, θ_{ign}. All three cases in Fig. 4–3 have been generated on the identical computational domain, and their orientation has been flipped vertically to allow for a better comparison.

At $\theta_{\text{ign}} = 0.1$, the flame exhibits strong connections, oriented mainly in the axial (i.e., x-) direction. This is in line with the dynamics of the KPZ model and strongly resembles the history of many phenomena associated with growth, deposition, or aggregation. The structure of the flame is somewhat modified at $\theta_{\text{ign}} = 0.4$, as the connections contribute noticeably less towards the ignition temperature, and their orientation is almost equally split between the x- and y-directions. A more significant branching in the y-direction reflects the

presence of larger structures in the flame. Finally, at $\theta_{\text{ign}} = 0.63$, the flame tree consists of weak connections, with particle ignition depending on the contribution even from distant sources. However, in spite of their weakness, the links form much larger structures than in the $\theta_{\text{ign}} = 0.1$ and $\theta_{\text{ign}} = 0.4$ cases: repeatedly, the tree is interrupted, with a single branch stemming from one link and spanning the entire domain laterally (in the y-direction). As can be seen in the 3D representation in Fig. 4–4, this behaviour occurs after a significant delay in time and corresponds to the entire flame propagation halting until a single particle ignites. This event provides a kernel for the subsequent expansion of the front, which occurs principally in the lateral direction, as particles situated close to the front are now located in a largely preheated zone. Such travelling waves appear at varying frequencies and span areas of varying sizes. However, their axial expansion appears to be always limited. As was noted by Schiulaz *et al.* [47] and Lam *et al.* [23], the system appears to be influenced by boundary conditions, with several kernels starting close to boundaries, in concave regions that are bound to be slowly heated due to the zero heat flux condition provided by the periodic boundary. This can be clearly seen by the border-to-border lateral propagation of the flame in Fig. 4–4 for $\theta_{\text{ign}} = 0.63$. The increase of the dependence of the ignition of a single particle is shown in the inset of Fig. 4–3a, with a significant transition between the neighbour-to-neighbour contact at $\theta_{\text{ign}} = 0.1$ to a large zone of dependence at $\theta_{\text{ign}} = 0.63$.

In Fig. 4–5, the rate of propagation of the three flames is represented by the evolution of number of ignited particles over time. The results, which are in agreement with calculations by Tang *et al.* [22], show that the 2D flame speed is relatively close to the predictions of the 1D regular model, with flame speeds higher at lower θ_{ign}, but decreasing with respect to predictions by eq. 4.7 at higher θ_{ign}. However, close to the propagation limit, at $\theta_{\text{ign}} = 0.63$,

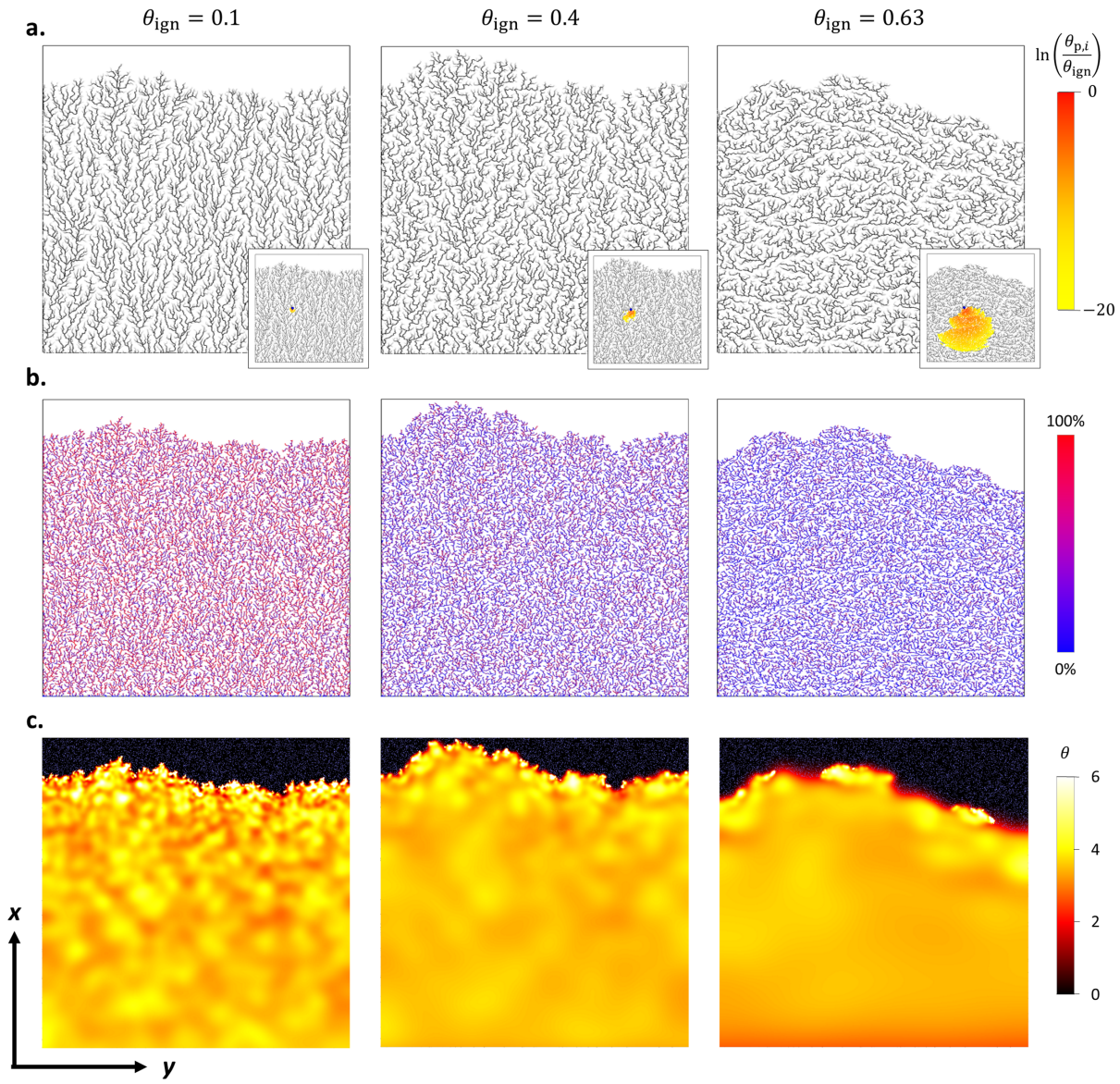

Figure 4–3: History of flame propagation coloured by: a. the strength determined by level of connectivity with inset indicating the length over which previous particles influence the ignition of the next one, b. the strength of connection, c. temperature profiles corresponding each flame configuration.

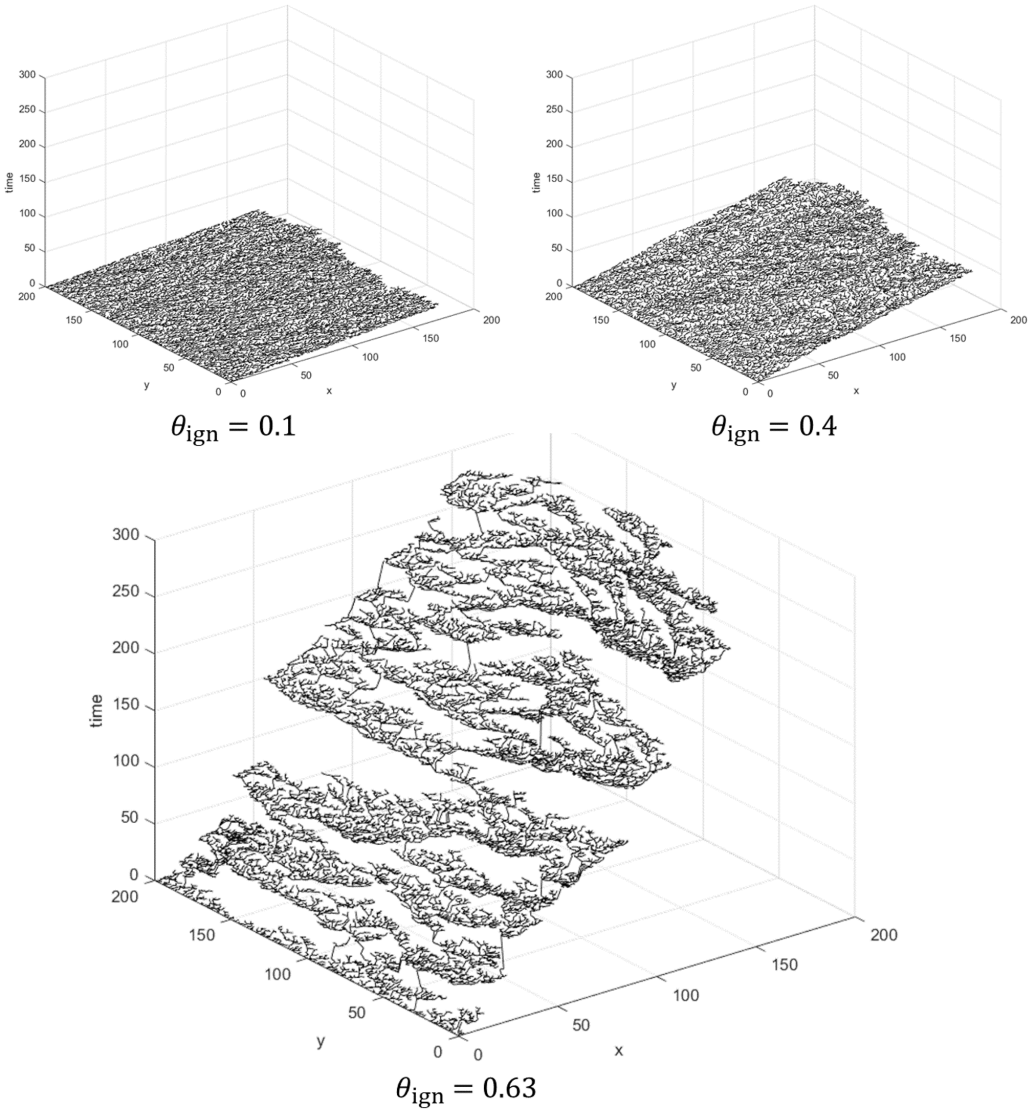

Figure 4–4: Comparison of the history of flames for three values of θ_{ign}, showing the emergence of large scale structures close to the propagation limit at θ_{ign}. The influence of the domain boundary can be seen for $\theta_{\text{ign}} = 0.63$.

the rate of flame propagation decreases over the course of the simulation, with uneven steps corresponding to the halting and formation of flame structures. The propagation limit of

$\theta_{\text{ign}} = 0.650$, reported by Tang *et al.* [22], was not reached in the present simulations. This may be caused by the sensitivity of the flame to initial conditions, with more initial "overdrive" needed for the flame [22].

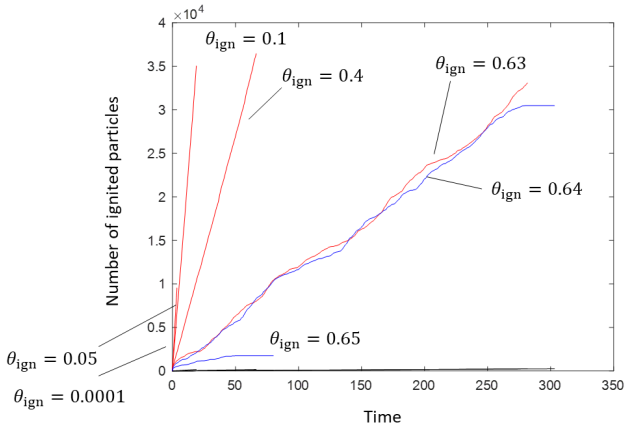

Figure 4–5: Propagation of flames for different ignition temperatures, showing the number of particles ignited over time.

It should be noted that the simulations involve particles with randomly generated x and y positions. However, the dynamics of propagation are likely to undergo significant changes if additional restrictions or rules are imposed on the positions of particles. For example, the imposition of minimal distances, which may correspond to suspensions of similarly charged particles, would prevent flame propagation from establishing clusters of closely spaced particles and the flame would rely more on mean-field effects. On the other hand, if inter-particle interactions may increase the incidence of strong connections between neighbouring particles, the system may be enticed to follow second-order percolation behaviour close to its propagation limit.

4.2.4 PERWAVES experiment aboard the ESA TEXUS-56 sounding rocket

Experimental studies of heat-locking phenomena are the focus of the Percolating Reactive Waves in Particulate Suspensions (PERWAVES) project. The experiments study the propagation of flames in micron-size iron suspensions in oxygen-xenon gas in transparent tube and are performed in a microgravity environment aboard European Space Agency (ESA) sounding rockets — the MAXUS-9 in April 2017 and TEXUS-56 in November 2019, respectively. While the first phase of the project confirmed the discrete nature of the propagation [41], the subsequent campaign is focused on the study of flames close to their limit of propagation [42].

4.2.4.1. Experimental details

Spherical and chemically pure (99.8% metal base) iron powder with an average particle Sauter mean diameter d_{32} of around 33 µm and a narrow particle size distribution was used in all experiments aboard sounding rockets and parabolic-flight aircraft [42]. The iron was chosen due to 1) its heterogeneous combustion that generates relatively small amounts of nano-oxides even in a 40%-oxygen gas mixture, 2) the relatively low ignition temperature for particles of this size (around 1000 K) [41, 43], and 3) its high density - all allowing to minimize the value of the discreteness parameter. Xenon was chosen as an inert diluent due to its low heat conductivity which reduces the value of discreteness parameter even further. The estimated value of the discreteness parameter χ for the iron suspension in 40% O_2 - 60% Xe gas mixture is only about $\chi \approx 0.063$ even at fuel concentration 1 g/L [41] suggesting discrete propagation regime in a whole range of fuel concentrations encountered experimentally. Experiments performed aboard the MAXUS-9 sounding rocket indeed confirmed the discrete

flame propagation regime, indicating practically identical flame velocities in oxygen-xenon mixtures with 20% and 40% oxygen despite a threefold difference in particle combustion times in these mixtures [41].

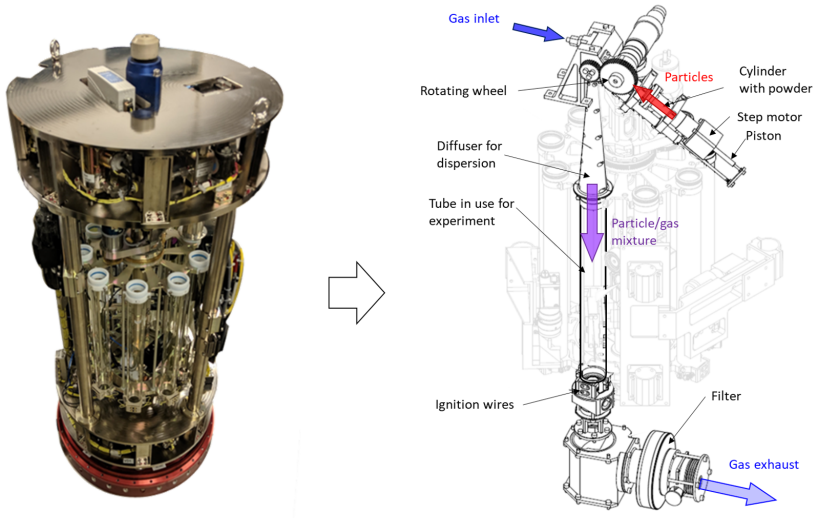

Figure 4–6: Picture and schematics of the experiment and the photo of TEXUS-56 PERWAVES combustion apparatus (see [47] for details). The drawing of the apparatus is a courtesy of Airbus Defence and Space.

With the discreteness regime of the flame propagation confirmed, the objectives of the follow-up experiments on board TEXUS-56 sounding rocket and parabolic flight aircraft reported in this paper were to observe the onset of the flame percolating behaviour. As discussed earlier, this transition is expected to occur while gradually reducing fuel concentration within the shaded area in Fig. 4–2.

The experimental apparatus whose detailed description is given in [42] was designed and built by Airbus Defence and Space (Bremen, Germany) and consists of 9 combustion tubes mounted on a carousel and ignited one-by-one when the tube is connected to the powder

dispersion system as shown in Fig. 4–6. The important changes introduced into the apparatus design in comparison to the previous MAXUS-9 sounding rocket experiment [42] were the replacement of the propane-based ignition system with an electrically heated tungsten wire allowing a gentler ignition without pressure and flow disturbance, the introduction of a high-speed camera operating at 1000 frames per second for observation of the flame structure, and a low-angle flow expansion cone connecting the combustion tube with the dispersion system that reduced particle accumulation [42].

In total, more than 30 flame propagation experiments were performed in two parabolic flight campaigns while testing the apparatus before and after the sounding-rocket flight and 11 combustion experiments were performed in a reduced-gravity environment ($10^{-5}g$) aboard the TEXUS-56 sounding rocket launched from Esrange Space center in Sweden on November 15^{th}, 2019. Considering the objectives of this paper, we report mostly data acquired with the high-speed camera.

4.2.4.2. Experimental observations

At reduced gravity, some of the dispersed iron powder was trapped in the vortex created by the rapid flow expansion and deposited on the wall of the expansion cone, connecting the powder dispersion unit to combustion tube [42]. The fuel concentration in the combustion tube could therefore not be simply calculated from the known powder and the gas feeding rates. Instead, it was monitored by counting particles in a thin laser sheet traversing the tube diameter about 50 mm from the open tube end (see Fig. 4–6). The average particle count, in turn, was related to the absolute value of the fuel concentration in the ground-based calibration procedure explained in detail in [42]. Here, we only mention that due to

the scattering of the particle count data, the accuracy of the concentration measurement is estimated to be about 0.4 g/L (± 0.2 g/L). As can be seen from the data presented below, the width of the fuel concentration range where transition between flame propagation regimes occurs is on par with this measurement accuracy. Thus, the observations presented below are more of a qualitative nature in relation to the fuel concentration.

The stoichiometric iron concentration in suspension with 40% O_2 is around 2 g/L. All combustion experiments were performed at fuel concentration below 1 g/L, i.e., in fuel-lean mixtures. At fuel concentrations above 0.6-0.7 g/L, the flame, as shown in Fig. 4–7a., was of conventional parabolic shape. Like in the previous MAXUS-9 sounding rocket experiments, the flame propagation speed was around 1 cm/s [41]. In general, the flame failed to propagate at fuel concentrations below 0.5 g/L. Though, in the vicinity of this concentration it

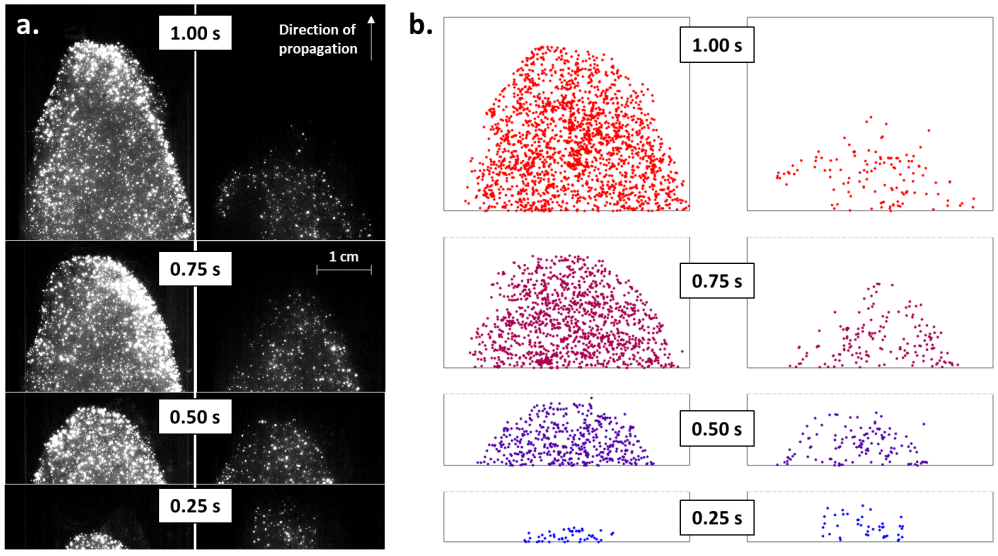

Figure 4–7: Parabolic and percolating flames: a. Still images of the flame captured by the high-speed camera, and b. corresponding plots showing particles that ignited within the last 3 ms. The figures were obtained during the parabolic campaign in May 2019.

sometimes did propagate for a few centimetres before quenching. The most dramatic change in the flame appearance and behaviour was observed in a narrow 0.5-0.7 g/L fuel concentrations range in the proximity to quenching. As can be seen from Fig. 4–7b, the flame in this range does not feature a frontal structure, i.e., there is no imaginary curve or a region clearly separating burned and unburned fuel. Instead, burning particles seem to be positioned at random and are often ignited far behind and on the sides of the flame leading edge giving appearance of the flame propagating backwards and sideways. It is difficult to represent the dynamics of such percolating flames by still frames.

Besides the appearance, the onset of the percolating-flame propagation regime is manifested by a drop in the flame speed and the number of the visible burning particles. This trend is most apparent in sounding rocket experiments where, with the appearance of the percolating regime, the flame speed and the density of burning particles drop 3- and 2-fold (2 experimental data points). In parabolic flight experiments, where the flame is strongly affected by varying levels of the residual gravity and frequent g-jitters [42], the scattering of the data makes this trend difficult to observe. The drop in the number of burning particles visible in the flame can be related to the emergence of the percolating cluster where ignition events are stretched over long spatial and time scales [24]. The behaviour has been observed in some videos, in which the speed dropped from 1.5 to 0.5 cm/s for a decrease in visible particle density from about 370 to 215 particles/cm^2.

As mentioned above, several authors who have recently theoretically investigated flames in random heterogeneous systems [12,37,38] have argued that the standard percolation, i.e., the second-order phase transition, can only be observed in a system with strong energy dissipation, i.e., heat loss. Strong heat loss prevents the accumulation of the heat released

by far-off sites, effectively cutting-off long-range communication between particles and thus reducing the problem to a standard site-percolation case. The external heat loss from the system in our experiments is, however, negligible. Indeed, the characteristic time of the heat loss for the flame in a tube, $\tau_l = R^2/\alpha$, is about 35 seconds (the thermal diffusivity of the oxygen-xenon mixture $\alpha = 0.065\,\mathrm{cm}^2/\mathrm{s}$) [41] and the tube radius $R = 1.5\,\mathrm{cm}$) suggesting that conductive heat loss does not affect even slow propagating percolating flames with the observed speed around $0.5\,\mathrm{cm/s}$. The radiation heat loss is estimated to be below 20% of the total energy release and primarily occurs during a brief high-temperature particle combustion stage. It is equivalent to the reduction of the fuel caloric output and thus does not influence the long-range thermal interaction between particles. This agrees with the statement by Khelloufi, Baara *et al.* [36], who argued that with the weighted long-range interactions between sites, the problem cannot be reduced to a standard percolation case showing universal critical exponents, i.e., which are independent of the nature of the interaction. In the case described in this paper, the thermal interaction between particles is described by the Green's function which, without strong heat loss, is indeed long-range and weighted both over distance and time. Thus, the critical exponents of the flame speed for the percolating flame in suspension may violate universality of the phase transition. This may also somewhat agree with the statement by Schiulaz *et al.* [37,38] that, in the absence of heat losses, the system exhibits a first-order phase transition, which is characterized by the prominent influence of the far-field temperature and the importance of fluctuations in the ability of the flame to propagate. Thus, it appears that the system undergoes a percolation-type transition, which is heavily influenced by heat-locking dynamics. However, it remains unclear which type of transition that is.

Additional effects are worth mentioning. During the sounding-rocket flight, the flame experienced instances during which a large part of the front underwent extinction, and only a small section propagated. In two tests, these small flames ultimately quenched. However, in one case, as Fig. 4–8 indicates, the flame managed to recover. It was observed that an initially parabolic front, stretching over the width of the tube, suddenly quenches, except for a localized kernel of particles, which sustain the propagation over a prolonged period of approximately 0.5 seconds, i.e., several hundreds of combustion times. However, unlike in the other cases ending in quenching, this small flame expands, igniting particles over a larger portion of the tube. The expansion of the flame seems to occur in all directions, with the reaction spreading laterally, forward, but also backwards, towards the ignition system. Around 4.5 seconds after the triggering of the video, the flame again spans the width of the tube. The particles appear to be relatively stationary during burning, which seem to exclude the effect of hydrodynamic phenomena. It is hypothesized that the initial flame experienced fluctuations in the distributions of particles which forced most of its surface to quench. It appears that only one region at the top of the picture benefited from a sufficient particle density, which allowed it to propagate.

4.2.5 Discussion and conclusions

The present work investigates the effect of discrete behaviour, which directly stems from the ability of particles to ignite. The segregated nature of the fuel and the associated need to diffuse thermal energy between individually igniting particles leads to heat-locking, i.e., the sacrifice of some thermal energy to sustain the process. As previous publications have shown, a simplified model, based on the linear superposition of heat diffusion from discrete

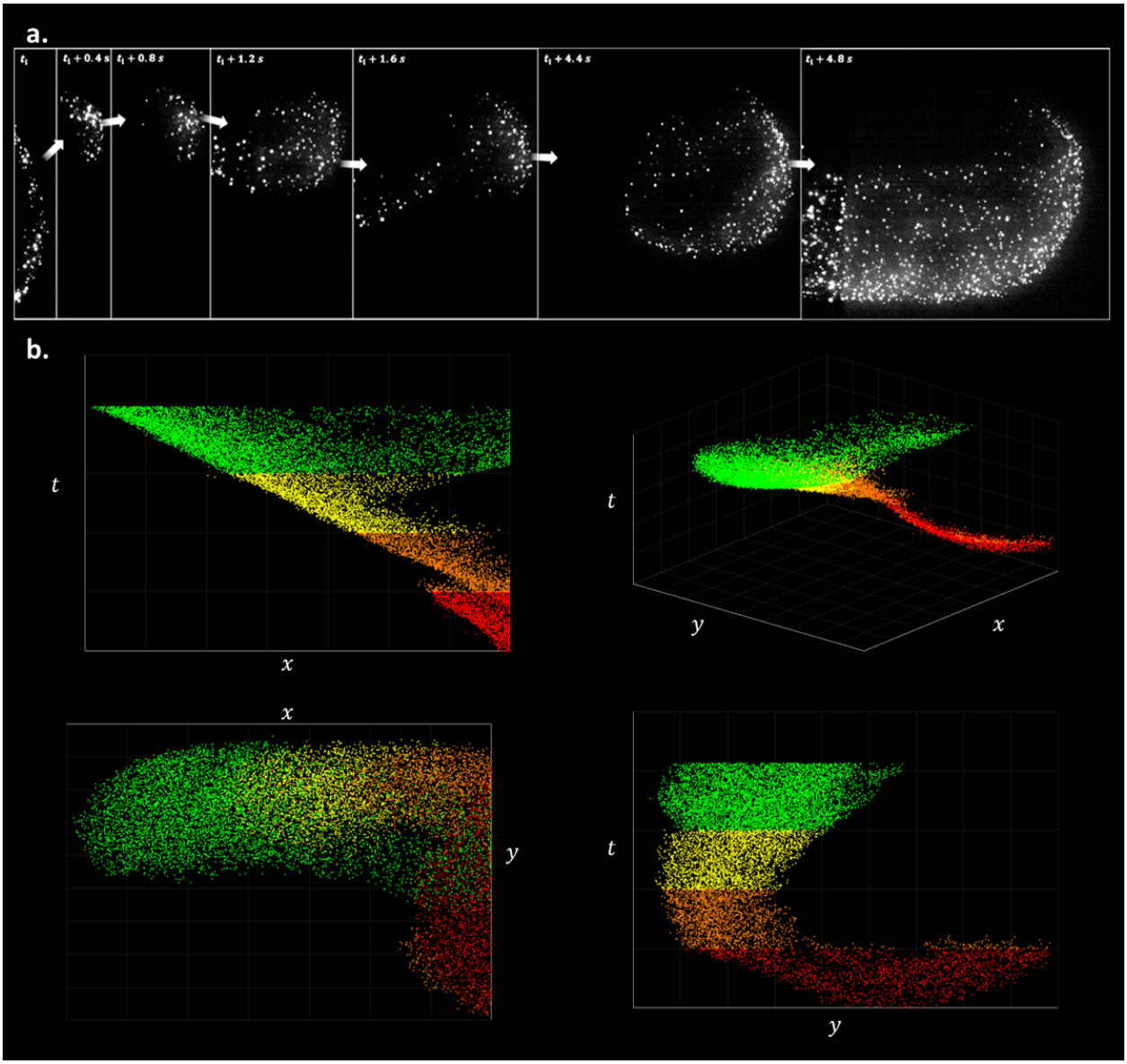

Figure 4–8: Partial quenching and recovery of flame: illustration of the quasi-extinction of a flame as observed by the high-speed camera. After almost disappearing, the flame gradually expands to occupy the width of the tube. a. camera frames, b. history of ignition events, with dots corresponding to instance where a particle ignited; the events are separated into four time ranges for easier visualization.

sources, illustrates the many ways heat locking can affect flame propagation. Both the rate of release from the sources as well as the activation threshold, i.e., the amount of energy that needs to be conveyed to the particle for it to ignite — are varied.

In previous work [20], activation has been shown to play a prominent role in the dynamics of flames propagating through regular lattices of particles. Fronts defined by low ignition temperatures are always stable and their speed is primarily controlled by the rate of heat release from particles and the rate of inter-particle heat transfer. For slowly reacting particles or fast-diffusion systems ($\chi \gg 1$), the effect of heat-locking is minimal, as continuous models capture well the dynamics of the front. However, when $\chi < 1$, diffusion locks the thermal energy around the particles, making the flame insensitive to the rate of the reaction. Conversely, at high activation thresholds (high θ_{ign}), the discrete nature of the sources destabilizes the flame. The fast reaction-long induction dynamics of instantaneously reacting particles lead to a period-doubling cascades and chaotic extinction. A more distributed heat release (increasing χ) suppresses the instability. However, at higher χ, the combination of rate of heat release and flame speed lead to the situation where a new layer ignites while the previous one is still releasing heat (at $\chi\eta \geq 1$). The co-existence of the two combustion processes seems to lead to a multiplicity of possible steady-state speeds and to a new possible destabilization of the flame.

It may seem that the dynamics of regular lattices are of little practical use, as such rigidity is practically impossible in real-life systems, usually characterized by a high-level of mixing. Such systems may, however, be subject to strong outside forcing, which can cause the preferential movement towards and the accumulation of particles in specific locations. For example, when flames in suspensions experience thermo-acoustic coupling in constrained

geometries, low-velocity high-pressure node regions represent such zones of attraction. In this case, discrete flames have been shown to interact with high-Lewis number instability mechanisms [44].

Heat-locking also plays an important role in the propagation of flames in mixtures with the random distribution of sources. One can again distinguish between the low- and high-activation behaviour. Low-activation flame dynamics are similar to growth phenomena with diffusion. The burning front resembles an interface that grows by accretion of new particles, as, in both cases, the growth occurs through local short-range interactions. An increase in the ignition temperature gradually raises the correlation lengths in the system until they span the whole domain, limited by its boundaries. When the θ_{ign} reaches a critical value, front propagation relies on fluctuations in the particle distribution, which lead to the creation of frontal structures at varying scales. When no such fluctuation is found in time, i.e., when no sufficient heat accumulation occurs around any unburnt particle before it is diffused away, the flame extinguishes. The system seems to exhibit first-order transition characteristics. These appear in several non-classical percolation models and are defined, among others, by a discontinuous order parameter behaviour at the critical point, cooperating effects, or phase coexistence [45].

Many propagating front systems have been studied in terms of classical (a.k.a ordinary) percolation, in which new particles are added to a combustion cluster through close contact with already burning particles. The accretion process is usually controlled by a set of rules that decide whether a particle will be added or not. The resulting structure then reflects the relative easiness of this accretion process. Easy activation results in clusters, which fill the space and propagate uniformly towards unburnt mixtures. Their roughness is defined

more by the coarseness of the medium rather than by dynamic effects. When the addition of a new particle to the cluster is more complex, through delays, higher activation, or other restrictive mechanisms, the cluster grows in a much more complex way. The resulting shape then usually reflects more the probabilistic nature of new connections, in line with classical percolation predictions. As it grows, the cluster explores paths and avoids regions of material on all scales, leading usually to relatively complex shapes of the burnt/unburnt interface, often qualified as "fractal". The downside of this approach is that it heavily relies on the type of rule used to determine whether a new particle will burn or not. Owing to the complicated structure of the mixtures studied, the activation of actual particles depends too much on local conditions at the time of ignition to be defined as an external input, making the rules more stochastic at best and outright arbitrary at worst. This is compounded by the experimental observation being difficult, depending both on the sensitivity of the diagnostic method and the choice of relevant parameters by the observer. And finally, the most important problem of these approaches is the choice to ignore any long-range effect. Typical combustion fronts are defined by global concentration and temperature fields, which keep a memory of past ignition events and thereby serve as mechanisms of long-range interaction. As discussed in [23] and in this work, activation through contact may still be the most determining factor at low ignition temperatures, where the major influence on particle ignition is from its closest neighbours. However, flames under these conditions are far from extinction conditions. Instead, flame extinction in adiabatic flames occurs when the activation threshold is raised. The propagation then relies more and more on mean-field support and, on average, less on direct contacts, as documented by the weakening neighbour-to-neighbour connections

as θ_{ign} increases. The extinction of such low-dissipation flames instead occurs through the mechanism described above.

The argument for ignoring long-range effects is the presence of dissipation mechanisms, such as heat losses, which lower the temperature, and force the flame to rely more on short-range interactions for particle activation. However, common dissipation mechanisms are seldom strong enough to lower the mean-field temperature so that it plays no significant role in the propagation. For example, heat losses to the surroundings appear not to be sufficient to cause a second-order transition [38], and heat dissipation through a highly conductive medium would most likely lead to the disappearance of discrete effects in the first place. Thus, especially in the combustion of metallic suspensions, the extinction of mixtures is not likely to follow classical continuous percolation extinction dynamics. This would also be in accordance with long-range models based on radiation in forest fires [36], which display such deviations from standard exponential behaviour. It is possible that heat-locking causes at least some of the first-order effects, described above, and which have been described in simulations in the present publication.

As seen in the experiments, flames in microgravity suspensions seem to exhibit phase transition behaviour close to their propagation limit, with some slowing down and the loss of a continuous frontal structure, with preferential propagation through certain parts of the suspension. It is, however, still unclear whether the dynamics are defined by a critical slowing down, described by universal exponents in second-order percolation systems, or whether the flame propagation is more influenced by local fluctuations and a first-order behaviour. The propagation patterns are also probably a strong function of the spatial distribution of particles, which may significantly differ from random particle distribution.

These theoretical aspects will be further investigated in the next TEXUS-58 sounding rocket flight experiment planned sometime in Fall 2022 or Spring 2023. With already ongoing apparatus modifications, the accuracy of concentration measurements and the uniformity of dust dispersion are expected to improve, allowing the estimation of the flame speed and of possible critical exponents experimentally. Implementation of the stereoscopic flame visualization system will also permit the reconstruction of the structure of the three-dimensional flame. It should also be pointed out that the discussions, presented in this and most publications pertain to two-dimensional systems, while the flames occur in three dimensions. While many considerations should still apply, a change in dimensions is sometimes accompanied with the appearance of qualitatively different behaviour. Thus, present studies should be expanded to 3-D.

4.2.6 Acknowledgments

We acknowledge the support of the Canadian Space Agency (CSA) [21FAMCGA17], the European Space Agency, the Natural Sciences & Engineering Research Council of Canada and the Fonds de recherche du Québec — Nature et technologies.

4.2.7 References

[1] D. A. Frank-Kamenetskii, N. Thon, Diffusion and Heat Exchange in Chemical Kinetics, Princeton University Press, New Jersey, 1955.

[2] S. Goroshin, J. Palecka, J. M. Bergthorson, Some fundamental aspects of laminar flames in nonvolatile solid fuel suspen sions, Progress in Energy and Combustion Science 91 (2022) 100994. doi:10.1016/J.PECS.2022.100994.

[3] A. Varma, A. S. Rogachev, A. S. Mukasyan, S. Hwang, Complex behavior of self-propagating reaction waves in heterogeneous media, Proceedings of the National Academy of Sciences of the United States of America 95 (19) (1998) 11053. doi:10.1073/PNAS.95.19.11053. 555.

[4] A. Mukasyan, A. Rogachev, Discrete reaction waves: Gasless combustion of solid powder mixtures, Progress in Energy and Combustion Science 34 (3) (2008) 377–416. doi:10.1016/j.pecs.2007.09.002.

[5] A. S. Mukasyan, S. Hwang, A. E. Sytchev, A. S. Rogachev, A. G. Merzhanov, A. Varma, Combustion wave mi 560 crostructure in heterogeneous gasless systems, Combustion Science and Technology 115 (4-6) (1996) 335–353. doi: 10.1080/00102209608935535.

[6] J. W. Essam, Percolation theory, Reports on Progress in Physics 43 (7) (1980) 833. doi:10.1088/0034-4885/43/7/001.

[7] A. R. Kerstein, C. K. Law, Percolation in combusting sprays I: Transition from cluster combustion to percolate combustion in non-premixed sprays, Symposium (International) on Combustion 19 (1) (1982) 961–969. doi:10.1016/S0082-0784(82) 80272-5.

[8] A. Umemura, S. Takamori, Percolation theory for flame propagation in non- or less-volatile fuel spray: A conceptual 570 analysis to group combustion excitation mechanism, Combustion and Flame 141 (4) (2005) 336–349. doi:10.1016/j. combustflame.2004.11.014.

[9] A. R. Kerstein, Percolation model of polydisperse composite solid propellant combustion, Combustion and Flame 69 (1) (1987) 95–112. doi:10.1016/0010-2180(87)90023-X. 575

[10] S. Gallier, J.-F. Guery, Regression fronts in random sphere packs: Application to composite solid propellant burning rate, Proceedings of the Combustion Institute 32 (2) (2009) 2115–2122. doi:10.1016/j.proci.2008.06.017.

[11] D. M. Grant, R. J. Pugmire, T. H. Fletcher, A. R. Kerstein, Chemical Model of Coal Devolatilization Using Percolation 580 Lattice Statistics, Energy and Fuels 3 (2) (1989) 175–186. doi:10.1021/EF00014A011/ASSET/EF00014A011.FP.PNGV03.

[12] O. Rabinovich, P. Grinchuk, B. Khina, A. Belyaev, Percolation combustion: Is it possible in SHS?, International Journal of Self Propagating High Temperature Synthesis 11 (3) (2002) 257–270.

[13] S. A. Rashkovskii, Hot-spot combustion of heterogeneous condensed mixtures. Thermal percolation, Combustion, Explo 585 sion, and Shock Waves 41 (1) (2005) 35–46. doi:10.1007/s10573-005-0004-4.

[14] P. S. Grinchuk, Combustion of heterogeneous systems with a stochastic spatial structure near the propagation limits, Journal of Engineering Physics and Thermophysics 86 (4) (2013) 875–887. doi:10.1007/s10891-013-0907-y.

[15] G. Grimmett, Percolation (1999) 447.

[16] G. MacKay, N. Jan, Forest fires as critical phenomena, Journal of Physics A: Mathematical and General 17 (14) (1984) L757. doi:10.1088/0305-4470/17/14/006.

[17] A. S. Rogachev, A. S. Mukas'yan, Experimental verification of discrete models for combustion of microheterogeneous compositions forming condensed combustion products (Review), Combustion, Explosion, and Shock Waves 51 (1) (2015) 53–62. doi:10.1134/S0010508215010050.

[18] Y. L. Shoshin, S. Goroshin, A. Zolotko, Flame in a medium with discrete sources, Dokl. Phys. Chem. (Engl. Transl.); 600 (United States) 291 (1987).

[19] S. Goroshin, J. Lee, Y. Shoshin, Effect of the discrete nature of heat sources on flame propagation in particulate suspensions, Symposium (International) on Combustion 27 (1) (1998) 743–749. doi:10.1016/S0082-0784(98)80468-2.

[20] F. D. Tang, A. J. Higgins, S. Goroshin, Effect of discreteness on heterogeneous flames: Propagation limits in regular and 605 random particle arrays, Combustion Theory and Modelling (2009). doi:10.1080/13647830802632184.

[21] S. Goroshin, F.-D. Tang, A. J. Higgins, Reaction-diffusion fronts in media with spatially discrete sources, Physical Review E 84 (2) (2011) 027301. doi:10.1103/PhysRevE.84.027301.

[22] F.-D. Tang, A. J. Higgins, S. Goroshin, Propagation limits and velocity of reaction-diffusion fronts in a system of discrete 19 random sources, Physical Review E 85 (3) (2012) 036311. doi:10.1103/PhysRevE.85.036311. 610

[23] F. Lam, X. Mi, A. J. Higgins, Front roughening of flames in discrete media, Physical Review E 96 (1) (2017) 013107. arXiv:1701.07167, doi:10.1103/PhysRevE.96.013107.

[24] D. Stauffer, A. Aharony, Introduction To Percolation Theory, Taylor & Francis, 2018. doi:10.1201/9781315274386.

[25] P. P. J. Daniell, The theory of flame motion, Proceedings of the Royal Society of London. Series A, Containing Papers of a Mathematical and Physical Character 126 (802) (1930) 393–405. doi:10.1098/RSPA.1930.0016.

[26] S. Goroshin, M. Bidabadi, J. Lee, Quenching distance of laminar flame in aluminum dust clouds, Combustion and Flame 105 (1-2) (1996) 147–160. doi:10.1016/0010-2180(95)00183-2. 635

[27] J. Palecka, S. Goroshin, J. M. Bergthorson, Propagation and quenching of dual-front flames in binary-fuel mixtures, Combustion Science and Technology 190 (9) (2018) 1557–1579. doi:10.1080/00102202.2018.1459583.

[28] A. G. Merzhanov, P. M. Krishenik, K. G. Shkadinski˘ı, A model of transverse flame propagation in alternating layers of combustible and inert solid substances, Doklady Physics 2001 46:9 46 (9) (2001) 619–623. doi:10.1134/1.1408988.

[29] P. M. Krishenik, A. G. Merzhanov, K. G. Shkadinskii, Nonstationary Regimes of Transformation of Multilayered Heteroge neous Systems, Combustion, Explosion and Shock Waves 2002 38:3 38 (3) (2002) 313–321. doi:10.1023/A:1015605920193. 645

[30] J. Beck, V. Volpert, Nonlinear dynamics in a simple model of solid flame microstructure, Physica D: Nonlinear Phenomena 182 (1-2) (2003) 86–102. doi:10.1016/S0167-2789(03)00119-2.

[31] P. M. Chaikin, T. C. Lubensky, Principles of Condensed Matter Physics, Principles of Condensed Matter Physics (jun 650 1995). doi:10.1017/CBO9780511813467.

[32] A. Wright, A. J. Higgins, S. Goroshin, The discrete regime of flame propagation in metal particulate clouds, Combustion Science and Technology 188 (11-12) (2016) 2178–2199. doi:10.1080/00102202.2016.1211877. 655

[33] G. I. SIVASHINSKY, Diffusional-Thermal Theory of Cellular Flames, Combustion Science and Technology 15 (3-4) (1977) 137–145. doi:10.1080/00102207708946779.

[34] A. G. Merzhanov, Self-propagating high-temperature synthesis: twenty years of search and findings, in: Combustion and Plasma Synthesis of High-Temperature Materials, VCH Publishers, New York, 1990, pp. 1–53.

[35] G. Caldarelli, R. Frondoni, A. Gabrielli, M. Montuori, R. Retzlaff, C. Ricotta, Percolation in real wildfires, Europhysics Letters (EPL) 56 (4) (2001) 510–516. arXiv:0108011, doi:10.1209/epl/i2001-00549-4.

[36] K. Khelloufi, Y. Baara, J. P. Clerc, B. Porterie, N. Zekri, Forest fire spread with non-universal critical behavior, Journal of Statistical Mechanics: Theory and Experiment 2013 (10) (2013) P10027. doi:10.1088/1742-5468/2013/10/P10027.

[37] M. Schiulaz, C. R. Laumann, A. V. Balatsky, B. Z. Spivak, Theory of deflagration in disordered media, Physical Review E 95 (3) (2017) 032103. arXiv:1612.00763, doi:10.1103/PhysRevE.95.032103. 670

[38] M. Schiulaz, C. R. Laumann, A. V. Balatsky, B. Z. Spivak, Theory of combustion in disordered media, Physical Review E 97 (6) (2018) 062133. arXiv:1803.10211, doi:10.1103/PhysRevE.97.062133.

[39] F. Y. Lam, X. Mi, A. J. Higgins, Dimensional scaling of flame propagation in discrete particulate clouds, Combustion 675 Theory and Modelling 24 (3) (2020) 486–509. arXiv:1906.01138, doi:10.1080/13647830.2019.1703044.

[40] M. Kardar, G. Parisi, Y.-C. Zhang, Dynamic scaling of growing interfaces, Physical Review Letters 56 (9) (1986) 889–892. doi:10.1103/PhysRevLett.56.889.

[41] J. Palecka, J. Sniatowsky, S. Goroshin, A. J. Higgins, J. M. Bergthorson, A new kind of flame: Observation of the discrete flame propagation regime in iron particle suspensions in microgravity, Combustion and Flame 209 (2019) 180– 186.

doi:10.1016/j.combustflame.2019.07.023.

[42] J. Palecka, S. Goroshin, A. J. Higgins, Y. Shoshin, P. de Goey, J.-R. Angilella, H. Oltmann, A. Stein, B. Schmitz, A. Verga, 685 S. Vincent-Bonnieu, W. Sillekens, J. M. Bergthorson, Percolating Reaction–Diffusion Waves (PERWAVES)—Sounding rocket combustion experiments, Acta Astronautica 177 (2020) 639–651. doi:10.1016/j.actaastro.2020.07.033.

[43] X. C. Mi, A. Fujinawa, J. M. Bergthorson, A quantitative analysis of the ignition characteristics of fine iron particles, Combustion and Flame 240 (2022) 112011. doi:10.1016/J.COMBUSTFLAME.2022.112011. 690

[44] X. C. Mi, A. J. Higgins, S. Goroshin, J. M. Bergthorson, The influence of spatial discreteness on the thermo-diffusive instability of flame propagation with infinite Lewis number, Proceedings of the Combustion Institute 36 (2) (2017) 2359– 2366. doi:10.1016/j.proci.2016.06.095.

[45] P. Grassberger, C. Christensen, G. Bizhani, S. W. Son, M. Paczuski, Explosive percolation is continuous, but with unusual finite size behavior, Physical Review Letters 106 (22) (2011) 225701. doi:10.1103/PHYSREVLETT.106. 695 225701/FIGURES/4/MEDIUM.

CHAPTER 5
Discussion

5.1 Advantages of a simplified analysis in heterogeneous combustion

Theoretical development in the combustion of non-volatile suspensions has always been challenged by a multiplicity and diversity of physical processes. Significant research has been conducted on the combustion of single isolated particles. While such studies provide important understanding of many characteristic features of ignition and combustion and are necessary for quantitative predictions, they are not sufficient to predict the behaviour of the dense suspensions encountered in nearly all practical applications of solid fuels, such as energetic materials (propellants, explosives etc.) or the newer use in carbon-free power-generation systems [12, 13]. These can only be understood through experiments and flame theory. However, the experimental difficulties associated to these large-scale systems limit the number of research groups capable of conducting such campaigns [6].

The resulting lack of experimental data means that, despite an increased activity over the last decade, the field of heterogeneous combustion is still in its early stages. Current understanding is too limited to support complex flame models comparable to the ones in gas combustion. Similar to the early developments in gas combustion theory, experimental work on heterogeneous flames must instead be backed by simplified models, in which qualitative understanding, based on a limited number of physically transparent parameters, is favoured over the need to obtain quantitative agreement through fitting parameters, whose selection

is often more arbitrary. These "toy" models should be based on fundamental consideration of flame dynamics and the simplifications should be physically justified. Such an approach defines the work in this thesis. The experiments are interpreted using models that reduce the usual complex formulations of combustion problems, often based on full sets of Navier-Stokes equations, down to a one-dimensional energy equation. In the latter, a series of simplifying assumptions justifies the use of constant externally defined ignition temperatures, at which combustion starts and proceeds over a constant reaction time at a constant rate. In addition, all gas properties are assumed to be constant. While such a formulation would be hard to defend for quantitative analyses, it offers the possibility of a full (often explicit) analytical treatment of the problem and provides a straightforward qualitative explanation of several complex phenomena.

The combustion of non-volatile suspensions does not involve a significant evaporation and premixing of the fuel with the gaseous oxidizer in the preheat zone. Thus, when simplified to a reaction-diffusion wave (neglecting the effect of convection), the flame is defined by an interaction between the reaction of the particles and the dynamics of the front, avoiding the added complexities of group or sheath combustion observed in sprays and volatile suspensions [171, 172]. As discussed in the introduction, the front may be formed by particles that have undergone ignition and burn in the diffusive regime as "flames within a flame". Conversely, the "collective effect" may be so strong that despite being controlled by slow kinetics, the heat production by the particles is sufficient to sustain a hot front. The second structure seems to occur in stoichiometric and fuel-rich hybrid flames (considering the gas fuel/oxidizer equivalence ration, ϕ), in which aluminum particles burn in slower reactions with the products of the hydrocarbon-air flames. Emission-absorption studies [35] seem to

suggest that, in this case, the particles in the aluminum front are likely to burn in the kinetic mode. This may also be supported by the experiments presented in this thesis, which show a faint aluminum front in rich propane-air mixtures. The availability of unreacted oxygen at $\phi < 1$ appears to enhance the combustion rate of particles. The resulting particle ignition is then responsible for the much brighter front and the significant reduction of the separation between the fronts. The "flame-within-a-flame" structure, in which the front is formed by particles burning in the diffusion-controlled regime with their own flame sheet on or around their surface, can be observed in Fig. 5–1. The close-up view shows the cusp region of a flame propagating in an aluminum-air suspension in the Hele-Shaw cell. The picture was obtained during a preliminary campaign for Publication 1 and raises many interesting points that will be discussed in the next section about instabilities.

5.2 Instabilities as a probing tool

When considering the effect of instabilities on flame propagation, studies of volatile fuels often identify pre-flame evaporation as a major mechanism that affects the propagation of the flame [91, 92, 93]. Instead, the lack of pre-flame evaporation in non-volatile fuels means that instabilities can instead affect the distribution of condensed particles/droplets entering the flame via acoustic interaction with particle kinematic lag in the preheat zone. The first mechanism was for example thought to segregate particles into laminae in lycopodium suspensions in Kundt's tube experiments [82], resulting in so-called "chattering flames". However, this has recently been put into question [92].

The other way instabilities can affect the flame is by directly controlling the reaction of particles, like in Fig. 5–1 where the intensity of combustion of individual aluminum particles

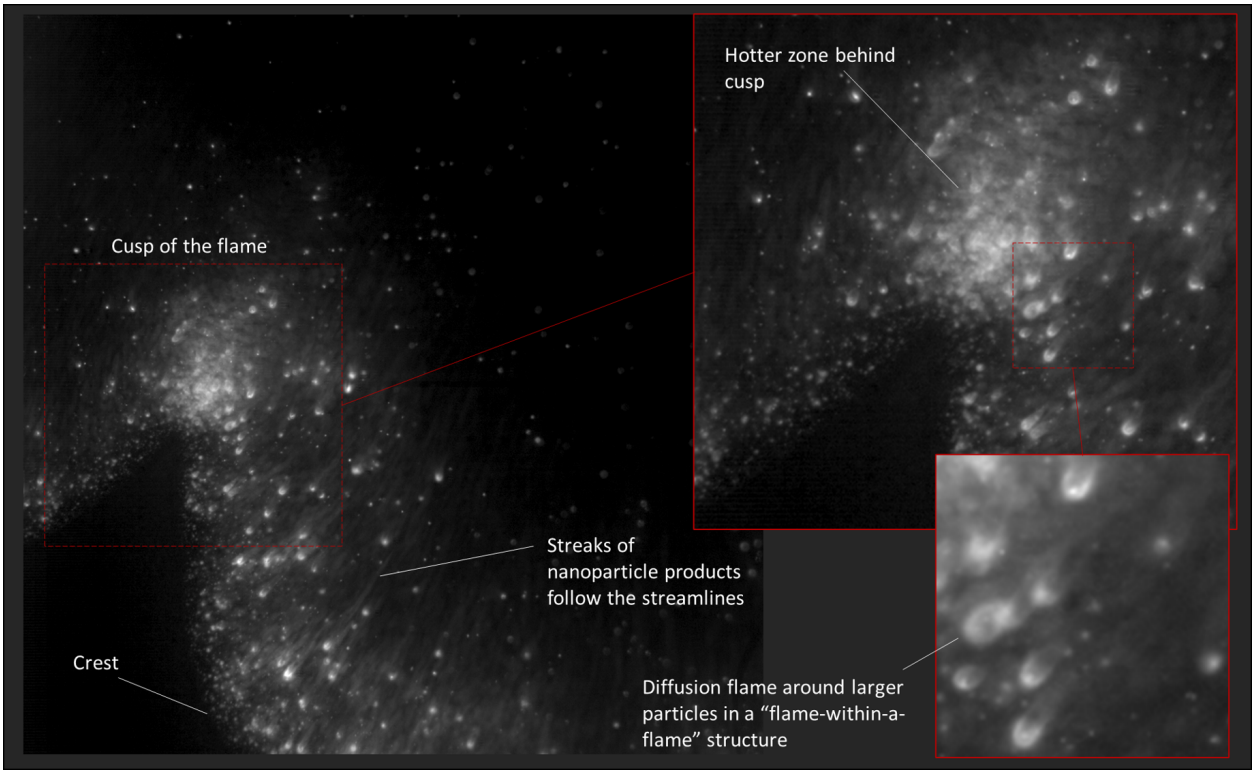

Figure 5–1: Close-up picture of a aluminum-air flame in the Hele-Shaw cell from publication 1, which illustrates the concept of "flame inside a flame". The burning streaks of nano-oxide products also indicate the approximate direction of the streamlines behind the curved front.

varies strongly between the crest and the cusp regions. The increased brightness of the flame sheets around the particles suggests that reaction rates are higher in the cusp regions. In addition, the streaklines of nano-oxides produced by the flame sheets around the particles seem to indicate that, though obviously evolving in time, the streamlines of the flow generally diverge from the cusp. With the help of Fig. 1–2, one may conjecture that, upstream of the flame, both the flow and, maybe to a lesser extent [4], the particles converge towards the cusp. This is also supported by the higher particle speed in these regions, observed in corresponding high-speed footage. While few definitive conclusions can be made about the concentration,

the temperature, and the general behaviour of the flame at this point, the picture and videos generate many questions whose answers should greatly improve our understanding of the dynamics of flame in suspensions, some of which are discussed below.

For example, experimental studies cite the effect of low Lewis number on the scale of the front to explain the formation of cellular structures in high-fuel-concentration flames [67]. One can hypothesize that the corresponding uneven diffusion of deficient oxygen reactants towards the flame may have much stronger effects in suspensions than in gases, as a low supply of oxygen to the cusp may cause particle extinction, i.e., the critical transition of the combustion mode from a diffusively to a kinetically controlled one. The question is even more puzzling when one considers the usually more intense reactions, observed at the flame cusps in the present experiments, which indicate, on the contrary, a stronger reaction there. Unfortunately, large uncertainties in the concentrations of particles currently prevent to determine whether such cases occur more in lean or in rich flames.

The effect on the dynamics of the flame may in particular be important if the combustion occurs in the discrete regime, as sharp variations of oxygen may lead to discrete effects with heat locking in high O_2 concentrations while, in O_2-deprived parts, the combustion may revert to the continuous regime. However, as shown in Chapter 2 and in Fig. 5–1, the effect may be balanced, compounded, or maybe even dominated by the convergence of streamlines towards the cusp of the flame, where the stronger thermal coupling, observed in Publication 1, suggests a stronger heat production of aluminum particles. This effect can itself be moderated by particle velocity slip [4].

5.3 Effect of fluid flow

So far, the discussion has been conducted in terms of mostly reaction-diffusion phenomena. However, suspensions, even in laminar flows such as the ones that were obtained in the Hele-Shaw cell, interact with fluid flows. For example, particle slip has been mentioned at different points. While, in the present work, estimations of the Stokes number of the particles as well as video footage indicate that the particles follow the gas flow towards the cusp, more dedicated studies, involving for example Particle Image Velocimetry (PIV) measurements, will be required to determined the degree of drift. Studies should also examine the effect of the solid phase on the gas flow and whether particles prevent or enhance the hydrodynamic formation of cellular structures. Another open ended question is the strong coupling between particle combustion and acoustics which has been observed, among others, in rocket motors [20, 121], and in tubes [54, 123, 108], as well as in the Hele-Shaw cells in Publication 1. The mechanism clearly differs from current descriptions in sprays and volatile suspensions [91, 92, 93]. As shown in Publication 1, in the case of hybrid flames, acoustics can probe the relative strength of thermal coupling. However, sometimes the interaction results in complex dynamics of the flame, as shown in Fig. 5–2. The varying strengths of thermal front coupling, subjected to acoustic forcing, produces complex patterns, suspected to generate intricate flows in a piston-like manner.

The effect of fluid dynamics is naturally much more important in turbulent conditions, present in many applications. Homogeneous turbulent flows already exhibit complex interactions and structures at many scales involved in the dissipation of energy [173]. The complexity only increases in the case of a gas turbulent flames [174, 175], and becomes very high in heterogeneous turbulent flames [176], where strong two-way particle-gas interactions

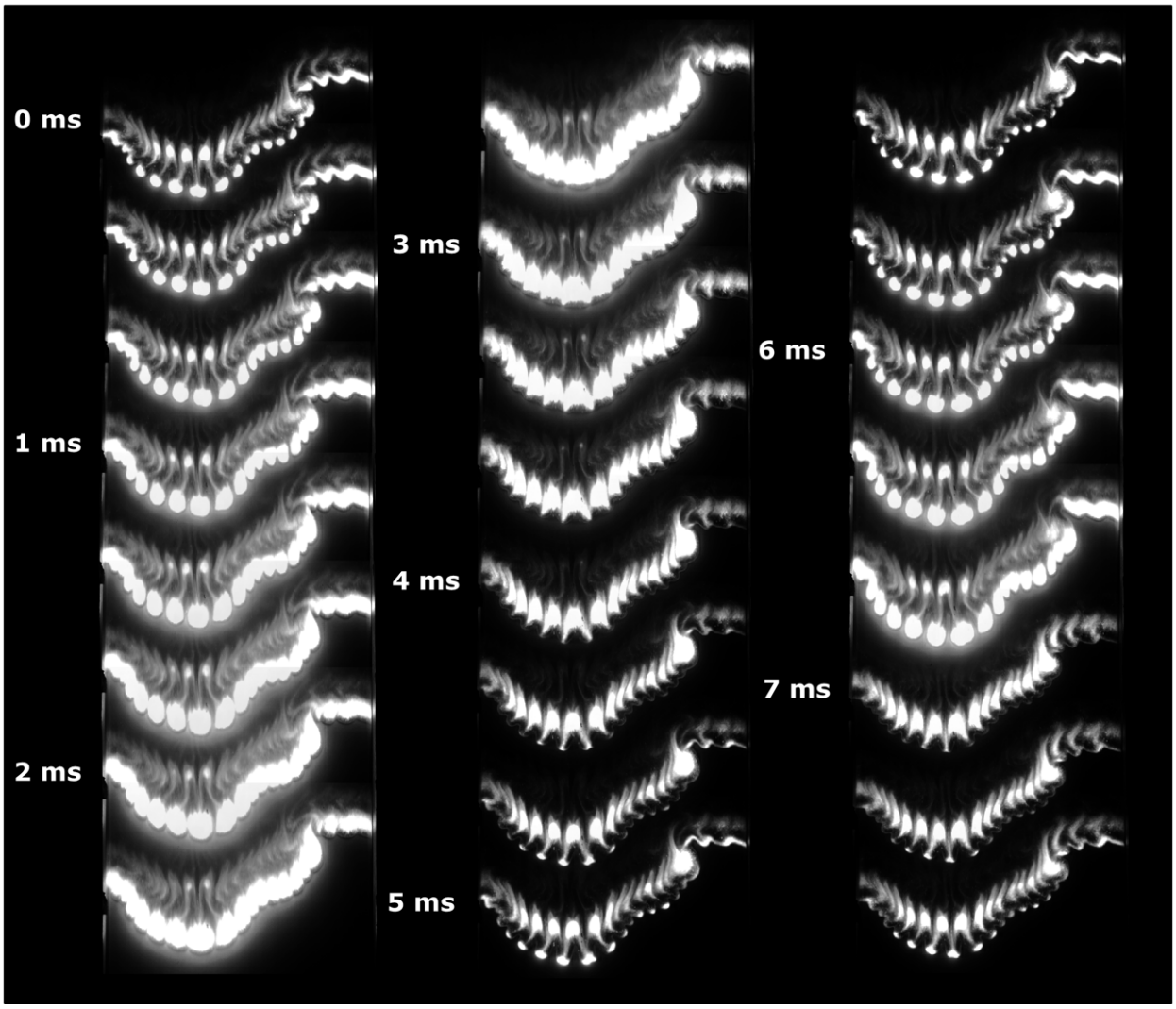

Figure 5–2: Manifestation of complex dynamics that result from the interaction of thermal coupling and acoustic forcing. Additional modes of instability appear and create complex flows between the individual structures. Each image corresponds to the 20-cm width of the window.

involve particle clustering and other complex phenomena with a major influence on the combustion process [177, 178]. Moreover, as discussed in [6], a further scale is added by significant radiation heat transfer, which mostly manifests as heat losses to the environment

but which may radically transform the combustion process if reflected back into the mixture from walls, for example when furnaces are covered with reflective deposits [179]. These are but few of the considerations that may strongly affect flame propagation and that need to be included in a quantitative analysis.

5.4 Effect of gravity

Gravity has a major effect on the combustion of solid suspensions. Fig. 5–3 illustrates the propagation of flames of the mixtures that were used during the TEXUS-56 campaign, i.e., of iron particles in 40% oxygen/60% xenon gas, on the ground at gravity g (Fig. 5–3a), aboard the parabolic flight aircraft (Falcon-20) where the gravity levels fluctuated between 0.02 and 0.05 g (Fig. 5–3b), and aboard the rocket where the gravity levels were maintained at $10^{-5}g$ (Fig. 5–3c). Fig. 5–3a clearly shows the effects of buoyancy that drives the fast propagation of the flame ($\sim$25 cm/s). The extremely uneven shape of the flame is caused both by the settling of the heavy particles, as well as by the flame following the recirculation zones, which are automatically generated during powder dispersion from the top of a tube, which were described by Mason *et al.* [180, 6]. In Fig. 5–3b, gravitational effects have been significantly reduced. However, the flame still possesses a characteristic parabolic shape [181], exacerbated by the effect of gravity [182]. The reduced effect of buoyancy leads to flame speeds of around 5-7 cm/s. The flame was also seen to experience g-jitters. Finally, in Fig. 5–3c, the virtual absence of gravitational effects leads to a much slower flame ($\sim$1 cm/s), which propagates steadily in the tube. The effect of gravity on the speed of flames propagating in tubes has been investigated in several studies.

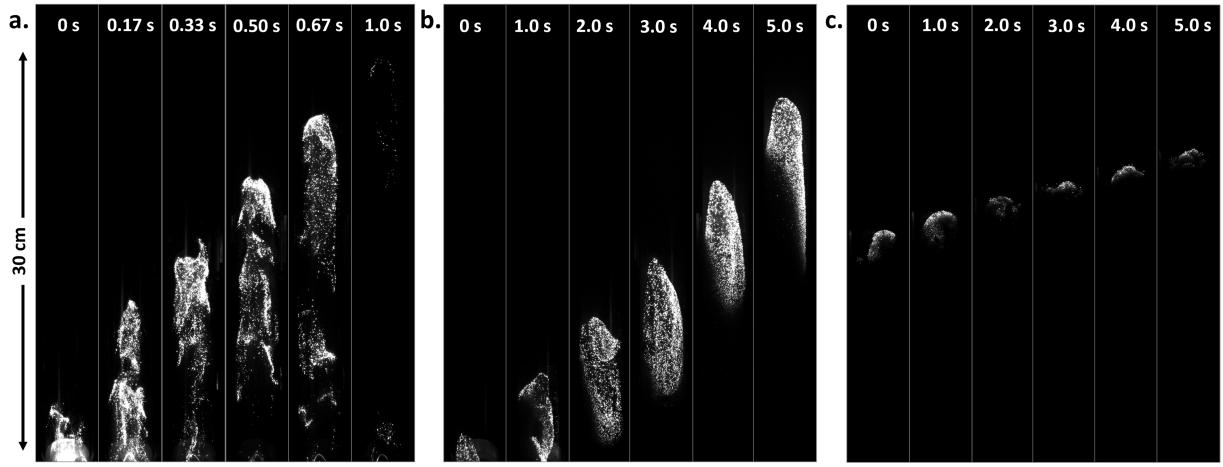

Figure 5–3: Propagation of flames in iron suspensions in xenon-oxygen gas mixtures at different levels of gravity: Frames taken at regular intervals of the flame propagating a. on the ground, b. in parabolic flights, c. aboard a sounding rocket. Reprinted with permission from [6].

While for flames in viscous flows, the velocity induced by buoyancy, v_b usually depends on $g^{1/3}$ [76], it was shown [183] that at least for slow gas flames propagating upwards, v_b, can be expressed as $v_\mathrm{b} \approx 0.3\sqrt{gD}$ [184, 76], where D is the diameter of the tube, which corresponds to the speed of an air bubble rising into a vertical tube filled with water [184]. Estimates showed that, in the PERWAVES apparatus ($D = 3\,\mathrm{cm}$) the $v_\mathrm{b} \sim \sqrt{gD}$ relationship follows the experimental trend, with buoyancy-induced velocities being minimal in the rocket (0.17 cm/s), slightly larger during the parabolic flights (7.7 cm/s), and significantly higher on the ground (54 cm/s). If one implements the factor of 0.3, the resulting velocities are 0.5 cm/s aboard the rocket, 2.3 cm/s aboard the parabolic flights, and 16.3 cm/s. These results are on the same order of magnitude as the experimental ones. However, one should keep in mind the added complexities in suspensions, e.g., the flow induced by falling particles, which, in the present case, is on the order 15-20 cm/s. Thus, more research will be

required to understand the effect of gravity on flames in suspensions.

5.5 Thermal coupling and flame speed

The presence of multiple reactants in a mixture usually increases the complexity of the combustion process. Indeed, in gas mixtures, the addition of reactive species introduces new reaction pathways and modifies the composition in the thin reaction zone. As the first publication shows, in heterogeneous flames, the disparity of fuel properties often involves delays in activation (or ignition) of individual fuel fractions. These lead to a separation into fronts, whose interaction is not dominated by chemistry but rather occurs over a larger diffusion scale through transport processes. This has been observed in several configurations [131, 67, 133] and has been visually confirmed in the Hele-Shaw cell for propane-aluminum-air mixtures, where the combustion between oxygen and the gaseous fuel is less activated and involves a faster onset of reaction than the one between oxygen and aluminum. It has been shown [130, 125, 57] that a similar front coupling mechanism also exists in binary suspensions of powders with significantly different properties. This raises an important question [6]: is it possible to use flame coupling in which a first front of fast-burning (usually fine) particles allows the propagation a more energetic yet typically slower-burning (large) powder? While such a system would benefit from an energetically very favourable combination of low activation and high energy content, it appears that the structure still primarily depends on the strength of the thermal coupling and on the dynamics of the more energetic — usually second — front. Thus if the stabilization of the second front is not possible, the result will be a single-front low-power (high-heat-capacity) flame.

5.6 Particle ignition and heat locking

Ignition is a prerequisite for heat locking. In fact, the ability of the particles to ignite and to transition to a mode in which the reaction rate is independent of the surrounding gas temperature is the key feature defining heterogeneous combustion [6]. The formation of "hot spots" of high temperature in a relatively colder gas leads to the presence of local gradients in the temperature field. As discussed in publications 2 and 3, the influence of these discrete features depends on the discreteness parameter χ, which compares the time required by the particle to deposit heat into the gas, simply referred to as the combustion time, and the characteristic time for inter-particle diffusion of heat. Thus, for slowly reacting particles in a medium with high thermal diffusivity, ($\chi > 1$), slowly forming gradients are immediately smoothed by fast diffusion, thus suppressing any discrete effects. On the other hand, for $\chi < 1$, a substantial amount of thermal energy accumulates in the vicinity of the particle. The heat is locked both because it needs to span a distance of inert material before it is used to ignite another source, and because this process takes a significant amount of time to achieve.

5.7 A new type of flame due to heat locking

As has been explored in Chapters 3 and 4 and publication 3, and in previous work [154, 87, 185, 155, 156], the transition to what has been called the discrete regime also results in a fundamental change in the physics of flame propagation. Flame behaviour is no longer obtained from simple averaging methods and instead must take into account the specificities of local and long-range interactions between particles. As previous studies [154, 87, 155, 185] and the present work show, a significant difference exists between the

propagation and extinction in regular arrays or lattices of particles and that of random systems. Regular spacing of particles results in a planar steady flame, which extinguishes in a highly organized way through a cascade of period-doubling events (for $\chi = 0$) or the growth of unbounded oscillations (for $\chi > 1$), possibly related to the number of simultaneously burning particles. Conversely, the propagation in random systems is defined by roughness growth, similar to deposition and accretion interfaces; and as the ignition temperature (activation threshold), T_{ign}, is raised, axial propagation gives way to longer period of hesitations and the reliance on random fluctuations of particles along the front that the flame explores for propagation.

The difference between the flames in regular grids and in random distributions may be analogous to a fundamental divide between the behaviour of low-dimensional systems, defined by few degrees of freedom, and high-dimensional ones [186]. The dynamics of the lattice are constrained by the imposed inter-particle distance: the position of all particles in the lattice can be defined by the coordinates of a single one (low degree of freedom). On the other hand, the position of a particle in a randomly distributed suspension does not imply anything about that of its neighbours. In non-linear systems, low-dimensional systems often give rise to chaotic behaviour [186]. On the contrary, high dimensionality is a feature of complex systems, which are usually composed of many interacting parts, whose collective behaviour leads to the spontaneous formation of temporal, spatial or functional structures [187]. The dimensionality seems to reflect on the propagation of the flame at high ignition temperatures. In rigid regular lattices, the reaction-diffusion wave cannot ignite periodically spaced particles at constant ignition times and has to compensate by increasing the degree of freedom by relying not on one but on two time-scales, i.e., by doubling the period. On

the other hand, in randomly distributed particles, the number of possible ways where the flame can propagate does not impose any such restrictions. As shown in publication 3, at high T_{ign}, the result is a temperature field in which gradients appear at many length scales, corresponding to the complex evolution of the ignition isotherm through clusters of particles of varying sizes. It is hypothesized that the difference between regular and random particle distributions may be understood in terms of the symmetry of the system, i.e., of its invariance to different types of transformation [188]. Irrespective of whether it undergoes rotation translation, or reflection, the random particle suspension still appears to be the same on average — a feature shared with the liquid or gas states of matter. Conversely, similar to a solid crystal, the regular system is invariant only with respect to translation equal to, or an integer multiple of, the inter-particle space, or to a rotation by 90, 180, etc. degrees. It is therefore at a lower-symmetry or even broken-symmetry state. In condensed matter, the loss of symmetry often associated with attempts of the system to restore it through periodic oscillations, perturbations etc. [188]. It should be noted that the present discussion is highly hypothetical and sound conclusions and analogies will require a more rigorous analysis. However, it is the author's opinion that, especially at this early stage of exploration of discrete systems, explorations of potential analogues in other fields, albeit highly qualitative, may be highly beneficial.

The propagation of flames in discrete suspensions of micron-sized particles in low-diffusivity gases is therefore presented here in the context of dynamics of complex systems and phase transitions. It has been debated [164, 163] whether, close to their propagation limit, discrete flames in reactive suspensions exhibit dynamics of classical percolations, which are defined by second-order phase transition behaviour, i.e., with dynamic variables behaving

according to universally shared power laws in the vicinity of the critical propagation limit. However, as mentioned in [164, 163] and in publication 3, this approach relies on strong inter-particle heat dissipation and completely ignores the long-distance interactions present in all combustion systems. Conversely, when the system is fully adiabatic, the propagation of the flame suggests first-order phase transition behaviour (discussed in Chapter 4.) It is therefore quite likely that, at its limit, the propagation is either a hybrid of both types or that the flame exhibits a new type of behaviour altogether. This question will require further experimental, numerical, and theoretical studies.

5.8 Front coupling and heat locking in applications

Front coupling and heat locking have been principally studied in the context of metal suspensions. Both effects are thus most likely to appear in applications related to the combustion of metals.

For thermally coupled flames, the change in the critical concentration for the stabilization of the second front and the variations of the separation distance, Z, with the gas equivalence ratio, as well as the complex interaction between the thermally coupled flame and pressure oscillations, are all dynamic phenomena, which may lead to new types of instabilities in applications. For example, as discussed already in [131], hydrocarbon-oxidizer-metal complex mixtures appear in the combustion of metallized propellants. In these complex mixtures, the oxidizer will react with the often complex organic binder in a gas flame or a leading-edge flame at the surface [189] formed by their evaporation, while the particles are often assumed to burn in the wake of the flame. However, even at relatively high aluminum concentration, many papers still assume that efficient combustion of aluminum only happens

when the particle reaches its high ignition temperature and see an obstacle in using metals in binder/oxidizer mixtures with too low temperatures [190]. The results presented in this thesis and in previous work [131, 133] disprove this understanding, as sufficient concentrations of aluminum particles are likely to form fronts, whose temperature is much higher than what is required for the ignition of a single particle [6]. It has also been shown that, depending on the size of the particles, an aluminum combustion zone forms at different distances from the gas front, sometimes as close as 3-4 mm [189]. It is thus quite likely that the effects of flame coupling may play a significant role in the combustion of hybrid metallized propellants and may strongly affect the stability of combustion.

Discrete combustion and heat locking are expected to have a somewhat more subtle effect in real-life applications. The findings of the theory may be relevant to a larger range of applications, in which the reactive components, such as the fuel and the oxidizer, are spatially segregated. Apart from multiphase mixtures, such as suspensions or powder compacts, it may be hypothesized that even in gas mixtures, incomplete mixing may give rise to some form of heat locking and heat diffusion across non-reactive regions. However, the latter point remains highly hypothetical.

CHAPTER 6
Conclusions and Future Work

The aim of the present body of work was to investigate thermal phenomena, which appear to govern the dynamics of flames in suspensions of non-volatile particles, with possible ramifications in the broader field of heterogeneous combustion. The objective of the study was to examine two such mechanisms. The first was front coupling, which controls the propagation of flames composed of multiple fronts, corresponding to separate reactions of dissimilar fuels. The second was heat locking, a direct consequence of particle ignition, in which thermal energy accumulation in large temperature gradients in the vicinity of the particle fundamentally modifies the physics of the flame in the so-called discrete regime. The analysis was performed on two separate experimental platforms. A Hele-Shaw cell, developed for laboratory combustion experiments, was used to study flame propagation in micron-sized aluminum suspensions in propane-air gas; it allowed the direct visualization and characterization of front coupling between the propane-air and aluminum fronts. The effect of heat locking was examined through direct observations of propagation of flames in tubes, filled with micron-sized iron particles in oxygen-xenon gas mixtures; test runs were performed in an automated experimental module at reduced-gravity conditions in sounding-rocket and parabolic-flight campaigns.

Experimental results showed that, in the aluminum-propane-air flame, variations in the fraction of each fuel, combined with the heat and momentum losses to the walls of the thin

Hele-Shaw channel, significantly modified the frontal structure of the flame, resulting in propagation of either the two fronts coupled together, only the propane front, or no front at all. Moreover coupling and separation of fronts were observed during the propagation through the action of intrinsic and acoustic instability mechanisms.

Experimental tests, performed during the first sounding rocket campaign aboard the European Space Agency (ESA) MAXUS-9, compared the propagation of flames in iron suspensions in two gas mixtures: 20% oxygen in xenon and 40% oxygen in xenon. Despite the combustion of particles being at least 3 times faster and at a significantly higher temperature, flames in both suspensions propagated slowly, at a speed close to 1 cm/s, in accordance with predictions of the discrete flame theory, based on the concept of heat locking.

In each case, simple models based on the diffusion equation with constant-ignition-temperature activation and constant or instantaneous heat release were successfully used to interpret the results. This underlines the primarily thermal nature of both front coupling and heat locking.

In a second sounding rocket campaign, which culminated with the flight of the ESA TEXUS-56 rocket, flames close to their low-concentration propagation limit were observed to exhibit a change in propagation patterns, suggesting the possibility of complex dynamics related to the discrete nature of the flame. While experiments were not able to confirm the nature of the phenomenon, prior simulations and experiments in other heterogeneous systems suggest a percolation-type limit occurring either with first- or second-order phase transition characteristics. These will be investigated in a future flight campaign aboard the ESA TEXUS-58 rocket, currently scheduled for Spring 2023, during which the experiment will be re-flown in an improved configuration. The new setup will be equipped with a more

accurate particle concentration system, as well as with a 3-D flame front visualization system, which will allow the researchers to observe the evolution of the frontal structure of the flame close to its propagation limit.

As outlined in a recent review publication [6], the presence of phenomena, such as front coupling and heat locking, indicates that, despite the complexity of the combustion systems, a common theoretical ground is possible and should be investigated. The review also provides a list of important questions, whose answer is likely to advance the fundamental understanding of non-volatile suspensions and should therefore motivate future work. For the flame coupling mechanism, the research should focus on the investigation of binary solid suspensions of two fuels with very dissimilar properties: either two fuels with the same chemical composition but significantly different particle sizes, or the mixture of one slow- and one fast-burning fuel with comparable particle sizes. In addition, investigations should focus on the impact of flame shape and flame stretch on front coupling.

A set of steps is also indicated for the study of discrete flames and heat locking. These include the investigation of 1) the nature of the propagation limit and its link to percolation, 2) the ability of adaptive behaviour of the flame, i.e., its ability to explore fluctuations in the concentration, to propagate even in mixtures, which are, on average, thermodynamically unfavourable, 3) the possibility of heat locking in fuel-rich conditions, 4) the hydrodynamic structure of discrete flames and their effective flame thickness, 5) the nature of the propagation in the presence of heat losses.

Answering these and other fundamental questions should lead to the development of a unified framework, in which the effect of more complex phenomena, such as turbulence or the scale-free effect of radiation, could be understood.

APPENDIX A
Hele-Shaw experimental apparatus

A.1 Design of the experimental unit

The Hele-Shaw-type cell was designed and constructed by a McGill CAPSTONE team [7]. The dimensions of the cell were dictated by the intended application – the observation of quasi-2D laminar heterogeneous flames in metallic suspensions. The purpose of this section is to provide additional details concerning the design and the function of the apparatus described in Publication 1. The cell consists of a high-aspect-ratio internal channel enclosed between two transparent windows, which:

- allows the development and observation of instabilities in both the axial (length) and one lateral (width) direction.
- minimizes the wavenumber of possible cells in the other lateral direction (depth).

Similar to experimental units used for gas flames [140, 139], the width of the channel was extended to 20 cm to minimize the effect of side walls on flame dynamics in the middle of the cell. As confirmed by the experiments, a length of 50 cm also allows enough time for the evolution of the flame structure before and during the thermo-acoustic oscillations.

For gas flames, the recommended channel width, h, is found by considering the Peclet number, $\mathrm{Pe} = \frac{h}{\delta_\mathrm{T}}$, where $\delta_\mathrm{T} = \frac{\alpha}{S_\mathrm{L}}$ is the thermal flame thickness, α is the thermal diffusivity, and S_L is the laminar flame speed. To avoid wrinkling in the direction normal to the cell windows (channel thickness), Pe should be kept significantly below 10^3 [137], while Pe> 10 is

required to avoid thermal quenching. In the case of metallic suspensions, such as aluminum-air mixtures, the existence of the discrete regime of combustion and its independence on the surrounding gas temperature reduces the dependence of the quenching distance on the flame thickness [6]. Thus, the channel thickness of 10 mm was designed to be larger than quenching distances measured in aluminum-hydrocarbon-air flames [133]. To further avoid boundary effects, the channel has a semi-circular profile on each edge of the 20-cm width. As shown in Fig. A–1, the cell consists of a central aluminum frame with large lateral slots on each side. Two side sections, each composed of glass pane glued to an aluminum structure, can then be fastened to the central section, with the glass forming the sides of the central channel. This design permits an easy removal and cleaning of the windows after each experimental run.

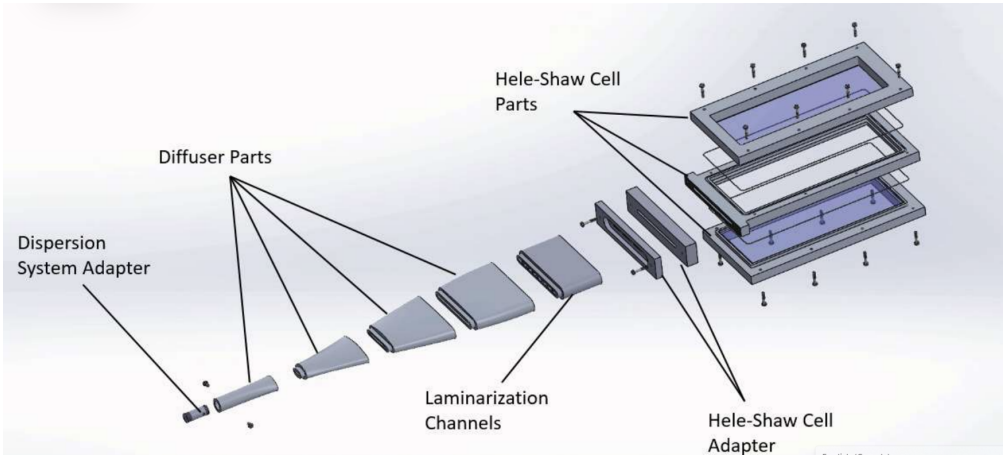

Figure A–1: Exploded view of the diffuser, adapter, and cell [7].

The apparatus also consists of a conical diffuser, connected to the cell through an adapter part, and which provides a smooth transition from the circular dispersion system, the latter described in detail in previous work [133]. The profile of the diffuser has been chosen to minimize the diffusing angle (and prevent flow separation) as well as a tangential transition

to both the inlet and the outlet. The simplest profile which satisfies these requirements is a 3^{rd}-order spline of the form:

$$f(x) = \frac{2}{L^3}(R_1 - R_2)\left(x^3 - \frac{3}{2}Lx^2\right) + R_1 \tag{A.1}$$

where R_1 is the radius of the inlet, R_2 the width of the cell channel, and L the length of the diffuser, which was limited by the overall height of the apparatus. RANS $(k-\epsilon)$ simulations, performed with ANSYS Fluent, showed that, without restrictions between the diffuser and the cell, this configuration does not lead to a uniform distribution of the powder and instead generates an unstable jet. This was confirmed with subsequent experiments. Several alternative designs were tested with no significant success – always leading to the formation of recirculation zones in the diffuser or the cell. The solution was provided by placing laminarizing channels in the adapter between the diffuser and the cell sections. Both the simulations and subsequent tests yielded a relatively stable laminar flow of particles.

The concentration of powders is provided by the attenuation of a laser beam crossing the flow which exits the upper end of the cell. A photo-diode then records the variations in light intensities, displayed through a voltage signal. The concentration measurement system, along with the calibration procedure is described in our previous work [56, 6]. It should be noted, however, that due to the weak attenuation by the thin layer of powder, the laser beam was oriented at an angle, providing a longer path length through the attenuating powder medium. Unlike in experiments with stabilized flames [56, 131], the experimental unit only allows the measurements of the concentration up to the ignition event. Moreover, the measurements are also performed outside of the cell. This leads to both spatial and temporal differences between the measured concentration and that within the cell which

account for the large errors reported in the publication. To minimize the latter, the ignition of each run is delayed until the powder concentration/voltage signal reaches a plateau, which indicates a relatively stable concentration. Fig. A–2 shows a typical concentration evolution.

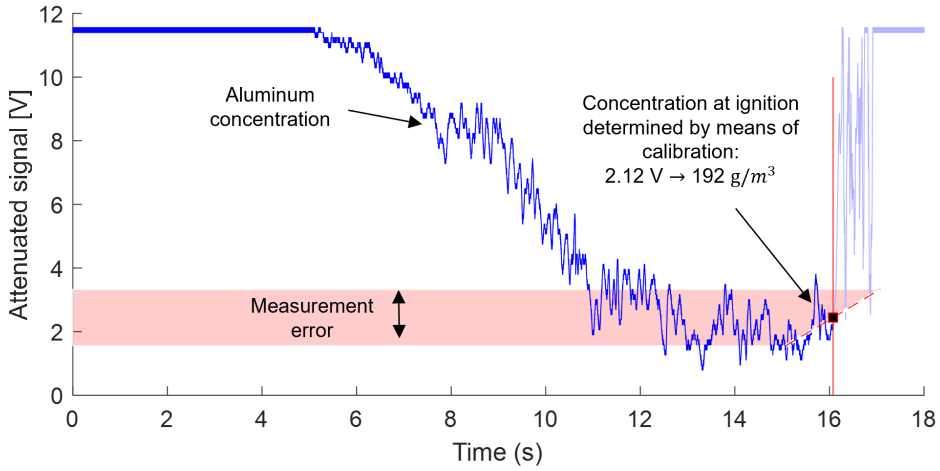

Figure A–2: Laser attenuation signal used to determine the concentration of particles in the flow exiting the Hele-Shaw cell.

The adapter section is also provided with a blast gate with a slot, which allows the flow to reach the cell during the dispersion. Before the experimental run, an electronically activated solenoid valves pulls the gate, removing the slot and stopping the flow to the cell. This measure (along with a simultaneous stopping of the flow and actuator motion) allows the suspension to become quiescent and prevents flame propagation back into the diffuser.

A.2 Analysis of flame propagation

The section below provides an overview of some of the tools that were used to examine the propagation of flames in Hele-Shaw cells in suspensions. Unlike gas mixtures, which burn in smooth fronts with a relatively uniform brightness, defining fronts in burning suspensions

is more challenging, as these present large variations in light intensity and a significantly rougher structure.

In the scope of the work performed for Publication 1, a validation of the apparatus was performed with gas flames. Fig. A–3 illustrates flames propagating in propane/air gas mixtures for different equivalence ratios. As expected, close to the fuel-lean propagation limit at $\phi = 0.58$, the dominance of thermal diffusion in the high-Lewis number mixture produces a smooth flame. As the Lewis number decreases with increasing equivalence ratio, cells of progressively smaller wavelength corrugate the flame. It is also worth noting that, close to the fuel-rich propagation limit ($\phi = 1.40$), a prominent structure with a strong cusp at the tip, which have been referred to as flame fingers [191], and have been observed in previous experiments in Hele-Shaw cells.

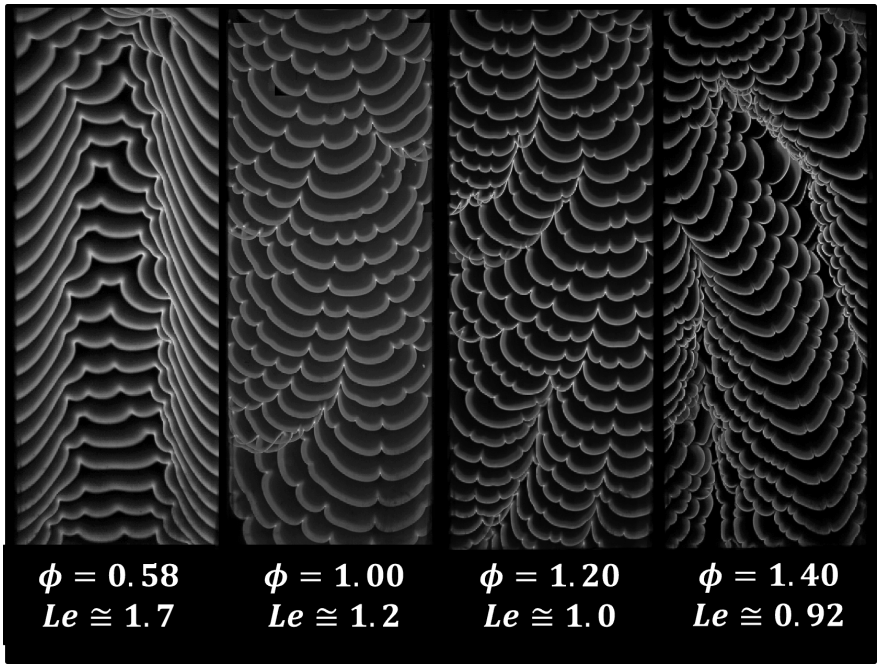

Figure A–3: Propagation of propane-air flames obtained by the superimposition of frames at varying equivalence ratios.

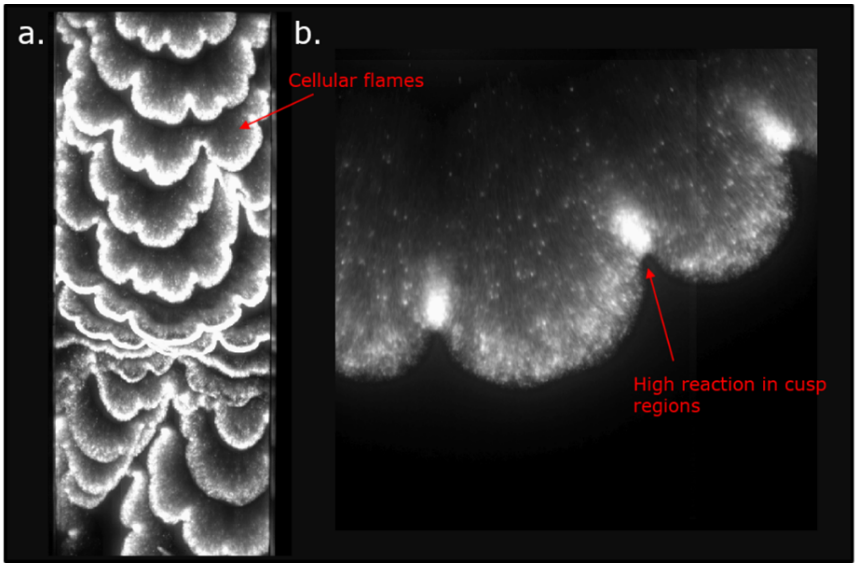

Figure A–4: Aluminum-air flame in a Hele-Shaw cell: a. Propagation of the flame obtained by the superimposition of frames, b. close-up showing a higher luminosity of reaction in the flame cusp regions.

Compared to the relative simplicity of front localization in gas mixtures, flames in metallic suspensions present a larger challenge, with large variations of luminosity across the front and over time (Fig. A–4a). As Fig. A–4b shows, an aluminum-air flame exhibits larger intensities in the cusp regions, where the reaction is presumed to occur at higher rates than in the convex crest regions.

Variations of the luminosity also present a unique challenge in two-front propane-aluminum-air flames. While, to an observer, the dimmer gas flame front appears smooth and continuous, illumination from the metal front significantly alters the brightness of different segments of the dimmer gas front, which, unlike the pure gas flame, becomes more difficult to identify. The front is usually found by combining flame contours found with different intensity thresholds.

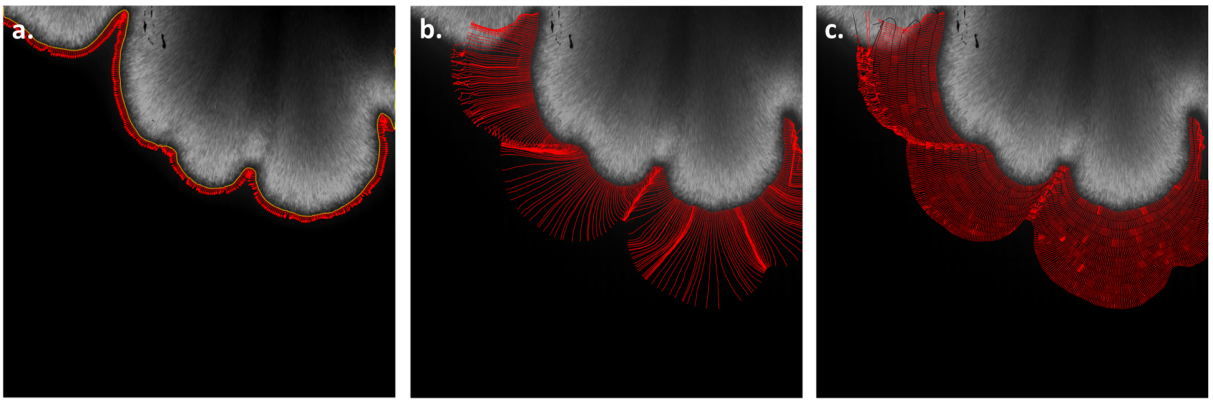

Figure A–5: Algorithm for tracking the evolution of the flame front: a. determination of vectors normal to the flame surface evolution of the cells without (b.) and with (c.) updating the location of the normal vector.

Smoothing of the front then allows to obtain the distribution of the vector normal to the surface of the flame (Fig. A–5a), which, combined over successive frames, can provide the path travelled by the flame (Fig. A–5b). The figure illustrates the progressive growth of cells and the appearance of cusps. However, as the lines, produced by combining vectors normal to the flame over successive frames, quickly diverge according to the Huygens principle towards the cusp, better flame tracking can be achieved by periodically redistributing the normal vectors over the flame surface (Fig. A–5c).

The normal direction to the flame is used to identify the distance between the fronts, Z, in publication 1. The light intensity distribution, represented as a surface plot for the entire flame in Fig. A–6, is used to determine the location of the second front. Uncertainties in the measurements are also caused by the inherently granular nature of the front, as luminous particle agglomerates ignite unevenly along the front.

Finally, an interesting visualisation describing the flame behaviour can be obtained by using the transparency settings in software like MATLAB, showing only regions with

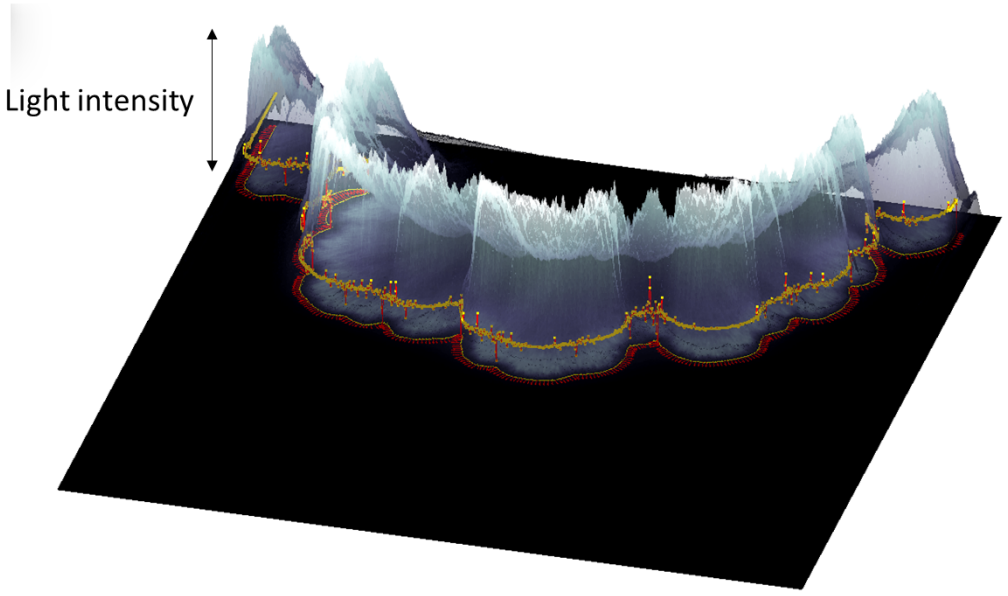

Figure A–6: Distribution of light intensity along the flame front of a hybrid propane-aluminum-air flame.

intensities above a certain threshold. These can then be superimposed to provide a 3D reconstruction of the flame dynamics in time. An aluminum/air flame is shown in Fig. A–7, along with the main dynamic features.

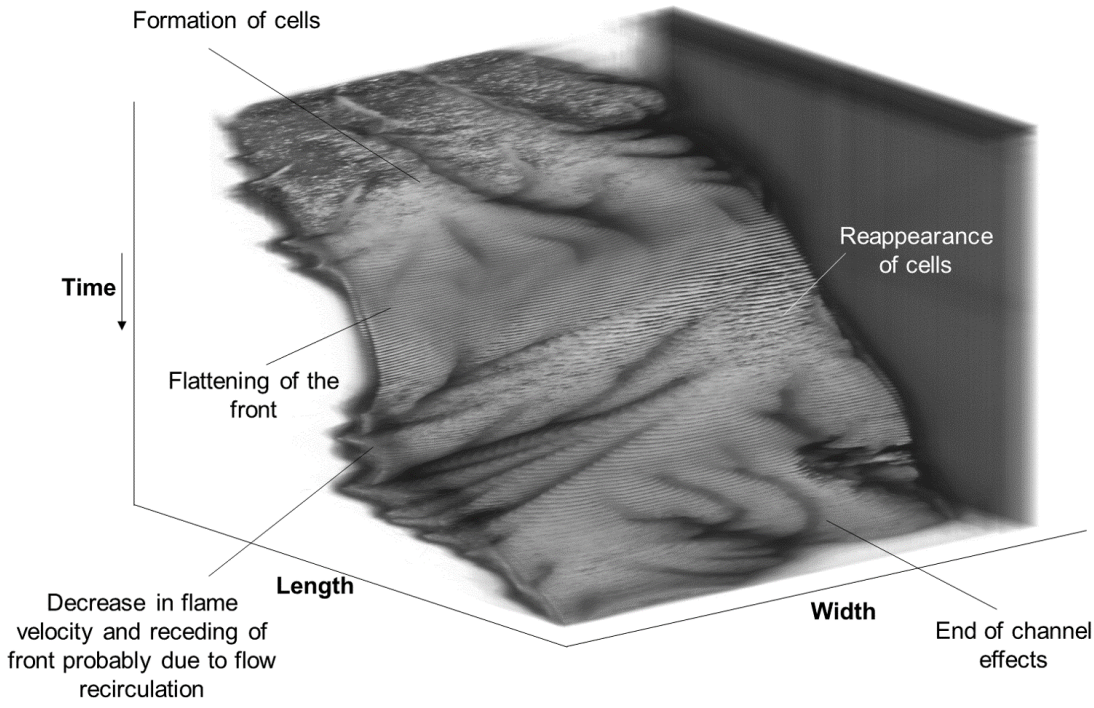

Figure A–7: Evolution of the flame shape and position in time with regions of varying stability.

APPENDIX B
PERWAVES project: Experimental apparatus and analysis

B.1 Experimental apparatus

B.1.1 History of the apparatus

The working principle of the PERWAVES experimental module is based on the flame propagating in a semi-open tube. The design was successfully used since the 1990's by McGill researchers for experiments with metal flames aboard parabolic flight aircraft [88]. The autonomous sounding-rocket module was designed and built by Airbus Defence and Space Germany for the MAXUS and later adapted for the TEXUS sounding rocket platforms.

B.1.2 Test sequence and apparatus functionalities

As illustrated in Fig. B–1, a laminar flame is initiated at the open end of a glass tube and propagates towards the closed end through a quiescent metal suspension at constant ambient pressure, allowing easy observation of the flame. The overall design of the PERWAVES sounding rocket experimental module is shown in Fig. B–2 along with key modifications between the MAXUS-9 and TEXUS-56 campaigns.

B.1.3 Dispersion system

The oxidizing gas mixtures are stored in high-pressure reservoirs and are supplied to the test sections through pressure regulators. The gas, maintained at a steady flow by a flowmeter, enters the dispersion system through a narrow rectangular channel. The metal powder, stored in a cylindrical reservoir, is pushed towards the channel by a piston connected to a linear actuator driven by a variable-speed step motor (see Fig. B–1). The particles, fed

onto and collected by a rotating wheel with a rough surface, are deposited into the gas flow in the narrow channel. After expansion in a conical diffuser, the flow of suspended particles enters a quartz tube (inner diameter: 30 mm, length: 332 mm). As discussed in [134], due to the possibility of recirculation zones, created by the bell-shaped diffuser profile during the MAXUS-9 campaign, the design was modified to provide a smoother transition between the dispersion channel and the tube, through a longer straight diffuser with a small expansion angle.

B.1.4 Ignition system

After dispersing the volume equivalent of about two full tubes, the gas flow is interrupted. The mixture is then ignited. During the MAXUS-9 campaign, this was done by injecting a small volume ($< 1\,\mathrm{cm}^3$) of propane which was subsequently ignited by an electric arc close to the open end of the tube. However, this led to relatively violent ignition events, which significantly affected flame propagation. As will later be shown, this required discarding the first 3 seconds of the run and was also the cause of some of the subsequent flame stalling. Thus, the system was replace in the TEXUS-56 campaign by a tungsten-wire ignition system, used to ignite propagating flames in our experiments [88]. In the current setup, the mixture is ignited by a 0.125-mm-thick tungsten wire, fixed on a ring, and stretched across the tube open end, which is heated resistively by a 20-VDC electrical source, until it undergoes self-sustained combustion at temperatures exceeding 3000 K. Each reaction tube is equipped with two ignition wires to allow multiple runs.

B.1.5 Exhaust system

Both the gas/particle mixture before ignition, and the combustion products leaving the tube, are picked up by the exhaust flow, driven by the fan, through a multilayered exhaust

HEPA filter, which collects all micron- and submicron-sized solid particles. Due to some deposition of combustion products on tube walls a tube remains transparent only for the first two runs. Thus, to ensure an unobstructed observation of flame propagation in every test, the 9 tubes are arranged in a carousel, which rotates and connects a clean tube to the dispersion and the ignition units after two consecutive combustion runs. The overall process occurs at constant absolute pressure maintained in the dome, which encloses the apparatus and constitutes a section of the rocket payload.

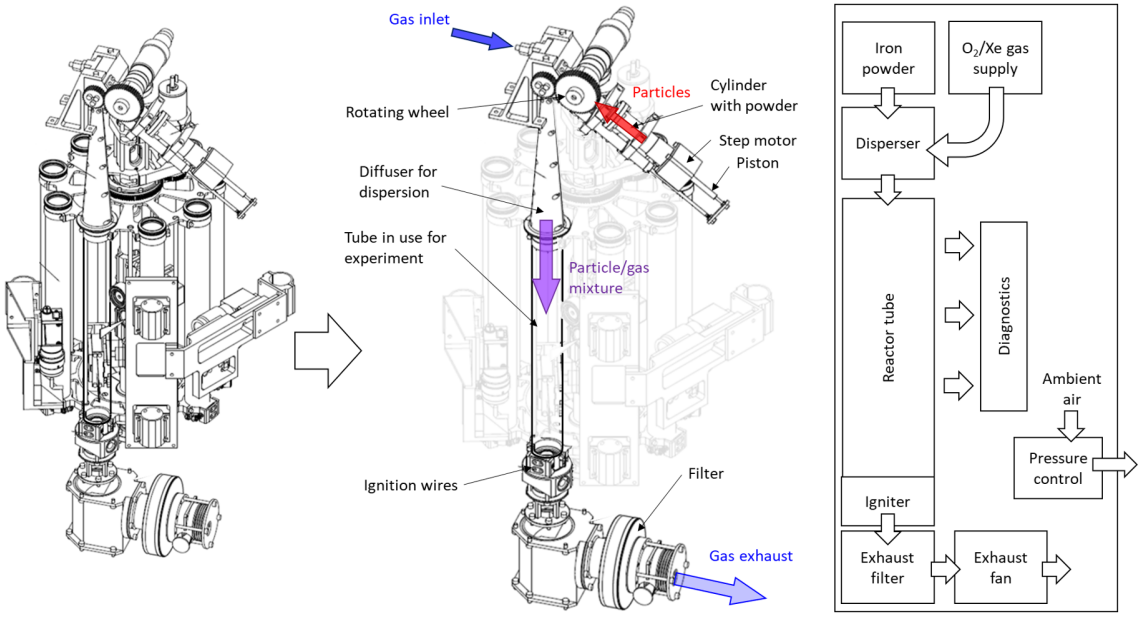

Figure B–1: Operating principle of the PERWAVES apparatus. The schematics of the apparatus were provided by Airbus Defence and Space Germany. Drawings of the apparatus are a courtesy of Airbus Defence and Space.

B.1.6 Reaction tube cleaning process

To fully evacuate the tube after each test and to extinguish and purge any reactive materials inside, the tube is filled with inert argon gas, which is stored in the gas reservoir 2.

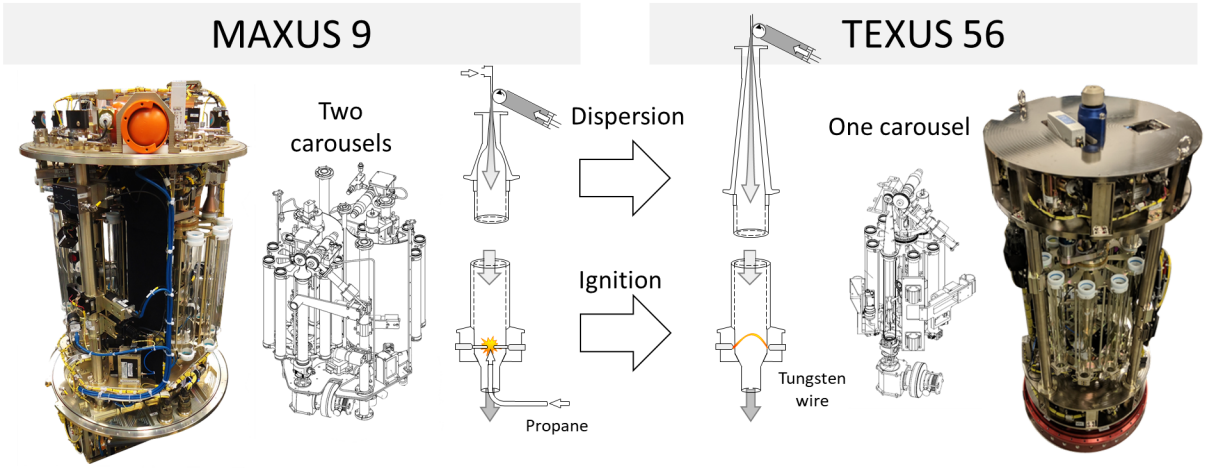

Figure B–2: Modifications of the PERWAVES apparatus in the transition between MAXUS-9 and TEXUS-56. The schematics of the apparatus were provided by Airbus Defence and Space Germany. Drawings of the apparatus are a courtesy of Airbus Defence and Space.

The argon gas is flown through a separate branch, consisting of a pressure reduction valve, an adjustable flow control valve, and a shut-off valve, and is delivered into the tube.

B.1.7 Operation of apparatus

The experimental setup is designed to run in a fully automatic mode starting with high fuel concentrations and decreasing concentration by pre-programmed steps until no flame propagation event is observed. The operator aboard the Falcon aircraft, however, can override the pre-set automatic procedure by observing flame propagation events on monitors and sending command to increase, decrease, or maintain the current powder concentration.

B.2 Data analysis

B.2.1 Particle counting and particle concentration

The concentration of iron particles in suspension is determined by a direct count of particles from a central section of volume illuminated by the laser sheet. The overall procedure

that was used to convert particle counts is shown in Fig. B–3. It should be noted that the final plot of flame speed versus concentration slightly differs from the figure in publication 2. It was created before a minor adjustment, which made the starting frame for particle counts uniform for all runs. The difference between the two Figures is included in the uncertainties reported for the data.

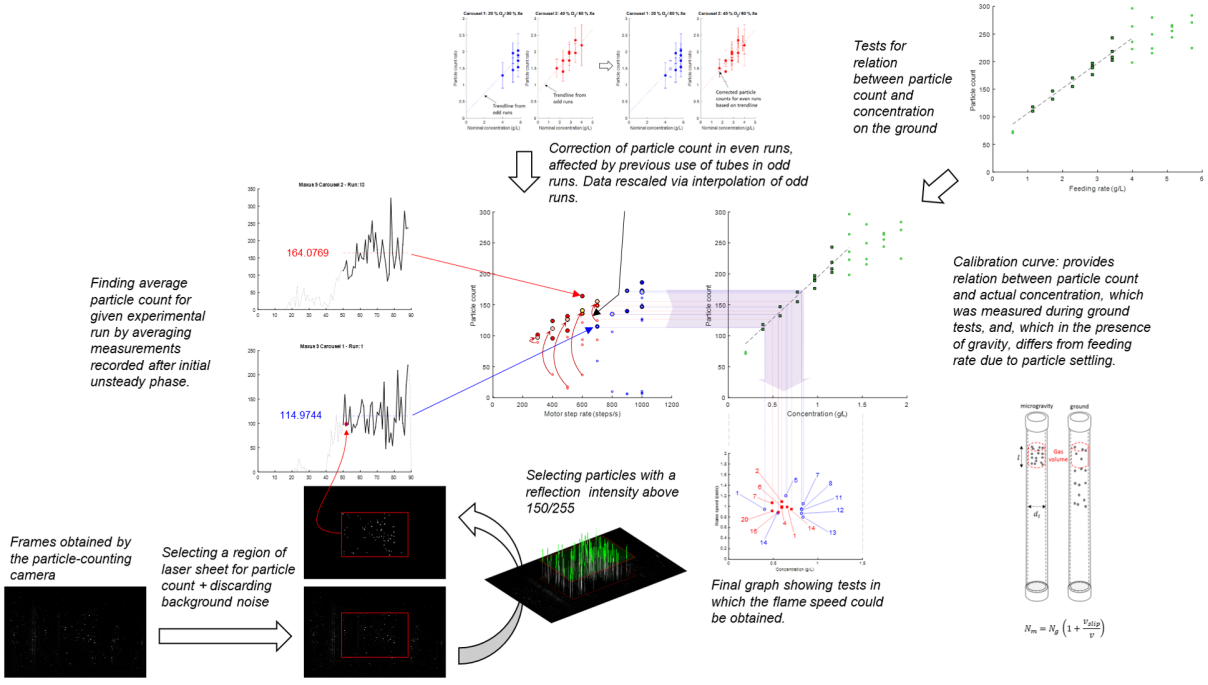

Figure B–3: Procedure used to determine the concentration during experiments during the MAXUS-9 flight.

During the MAXUS campaign, the particle count was found to be a relatively strong function of the camera sensitivity threshold. This was mainly due to a Gaussian intensity profile of the laser sheet exacerbated by far-field Fraunhofer diffraction from the light sheet-forming slit. The intensity profile of the laser sheet, which has no well-defined borders, made the counting volume a function of the camera sensitivity, as increasing the camera

sensitivity led to an increase of the volume from which particles were counted. This is illustrated in Fig. B–4a., along with the difference in average particle count with intensity threshold (Fig. B–4b.).

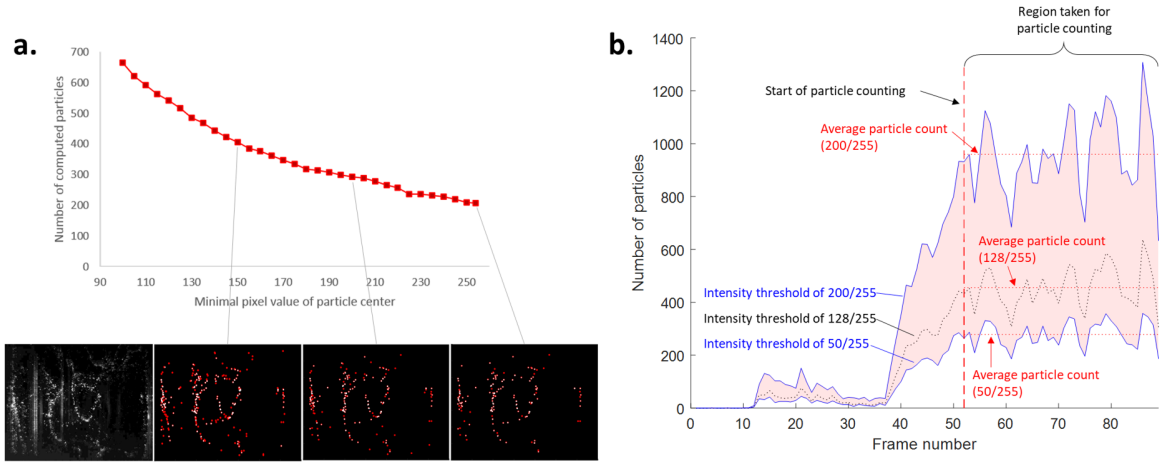

Figure B–4: Effect of choice of intensity threshold: dependence of the particle count (a) and measured average particle number (b).

As Figs. B–5 and B–6 indicate, a correction had to be applied to the even runs from the MAXUS-9 experiment. As every tube was used for two consecutive runs, particle deposition from every odd run obscured the signal of the particle counting system in the subsequent even run. This can be observed through the sawtooth-like profile on the particle count versus run number (Fig B–5a) and led to a low correlation between the particle count and the feeding rate.

The much more linear relationship observed for the odd runs (Fig. B–5b) was therefore used to calibrate the concentrations of the even runs (Fig. B–5). The significant reduction of gravity during the quasi-free-fall conditions aboard the sounding rockets leads to the prominence of other forces, which influence particle dispersion and deposition on the walls.

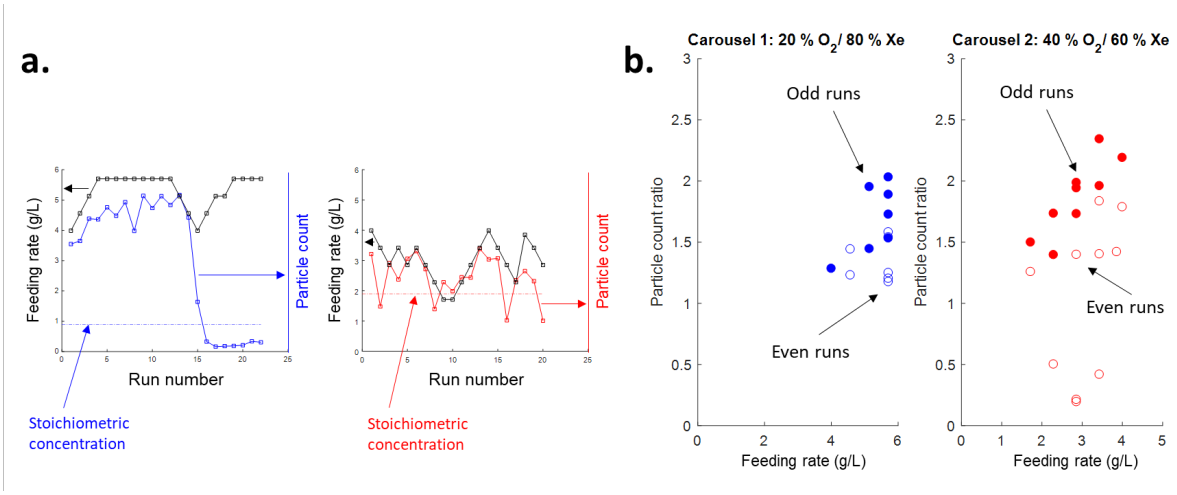

Figure B–5: Illustration of the systematically lower particle counts in all even runs over run number (a) and feeding rate (b).

Thus, the particle concentration cannot be inferred from the feeding rate. A post-flight ground calibration of the particle counting system was therefore necessary. The purpose of such campaigns was to produce a calibration curve relating the measured particle count to the concentration of particles in the tube. During experiments, performed in the laboratory, particle counts were obtained for different feeding rates, obtained by placing a scale under the open end of the tube and measuring the constant mass flow rate corresponding to the plateau in the particle counts, which was then divided by the known volume flow rate of the gas.

Neglecting complex particle-to-particle fluid effects in these relatively sparse suspensions, one can then obtain a correction factor, comparing the expected concentration with respect to the feeding rate. As shown in Fig.B–7, the system feeds a particle of mass m_{part} for every volume $V_{\mathrm{gas}} = A \times l$ to the tube. The feeding rate, F_{R}, can be expressed as the ratio

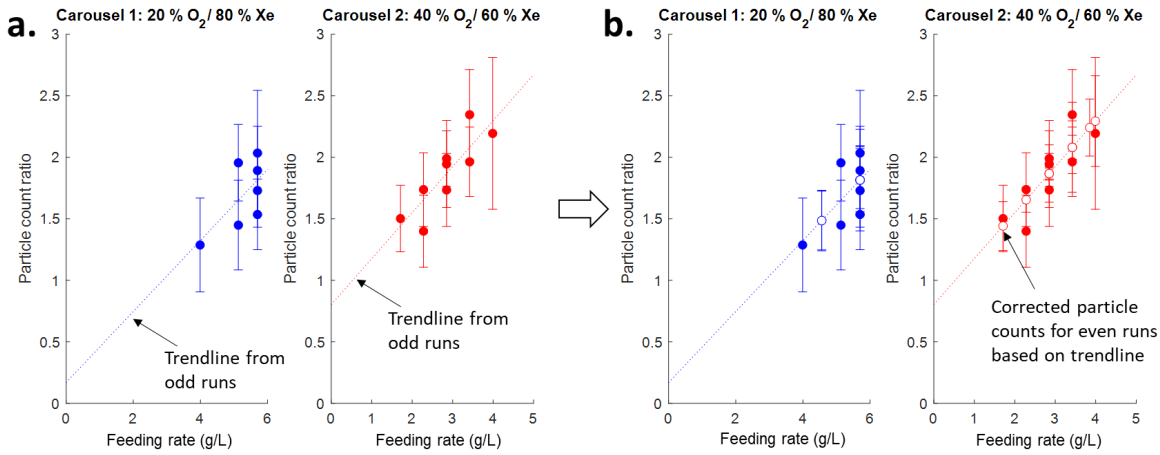

Figure B–6: Modification of the particle count of even runs through extrapolation of odd ones.

of the mass flow rate of particles, $\dot{m} = \frac{m}{\Delta t}$, and the volume flow rate of the gas, $\dot{Q} = \frac{V_{\text{gas}}}{\Delta t}$:

$$F_{\text{R}} = \frac{\dot{m}}{\dot{Q}} = \frac{m_{\text{part}}/\Delta t}{V_{\text{gas}}/\Delta t} = \frac{m_{\text{part}}}{V_{\text{gas}}} = \frac{m_{\text{part}}}{A \times l} \tag{B.1}$$

The unit volume of gas, flowing at a speed v_{gas}, travels the distance l in a time Δt. The particles experience slip, i.e., a velocity $v_{\text{part}} = v_{\text{gas}} + v_{\text{slip}}$, and cover a longer distance, $l_{\text{p}} = l + l_{\text{slip}}$. As the picture shows, the concentration, C, can then be expressed as:

$$C = \frac{m_{\text{part}}}{l^2\,(l + l_{\text{slip}})} = \frac{m_{\text{part}}}{l^3}\frac{l}{l + l_{\text{slip}}} = F_{\text{R}}\frac{v_{\text{gas}}\Delta t}{(v_{\text{gas}} + v_{\text{slip}})\,\Delta t} = F_{\text{R}}\frac{1}{1 + v_{\text{slip}}/v_{\text{gas}}} = \frac{F_{\text{R}}}{F_{\text{slip}}} \tag{B.2}$$

Thus, the calibration curve can now be expressed in terms of the estimated concentration (g/L) in the tube, as shown in Fig. B–7b.

As the effect of gravity becomes negligible aboard the sounding rocket, no scaling factor is necessary, and the calibration curve can be directly used to obtain concentration from particle counts.

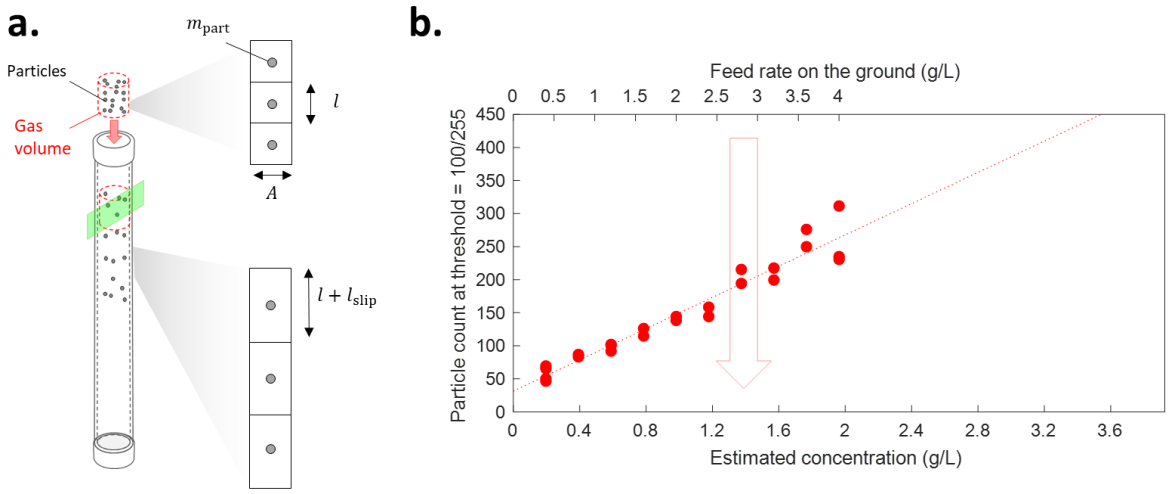

Figure B–7: Effect of gravity on particle count: a. illustration of the principle; b. calibration curve relating particle count, feed rate on the ground, and estimated concentration at a pixel intensity threshold for image binarization of 100/255.

B.2.2 Flame speed measurements

The flame speed is determined from the CMOS camera recordings using a filming rate of 60 frames per second. The field-of-view of the camera encompasses the entire length of the combustion tube. The position of the flame front on each frame is thus determined by taking the location of the farthest pixel that was illuminated above a specified threshold. The resulting curve is then usually smoothed by means of a simple algorithm. The procedure is shown in Fig. B–8.

B.2.3 High-speed imaging

High-quality close-up imaging was available for the second campaign aboard the TEXUS-56 rocket. Images of the flame front are recorded a high-speed camera (Miro C210) at the rate of 1000 fps. The 1280 × 1024 resolution allows recording of a field-of-view of

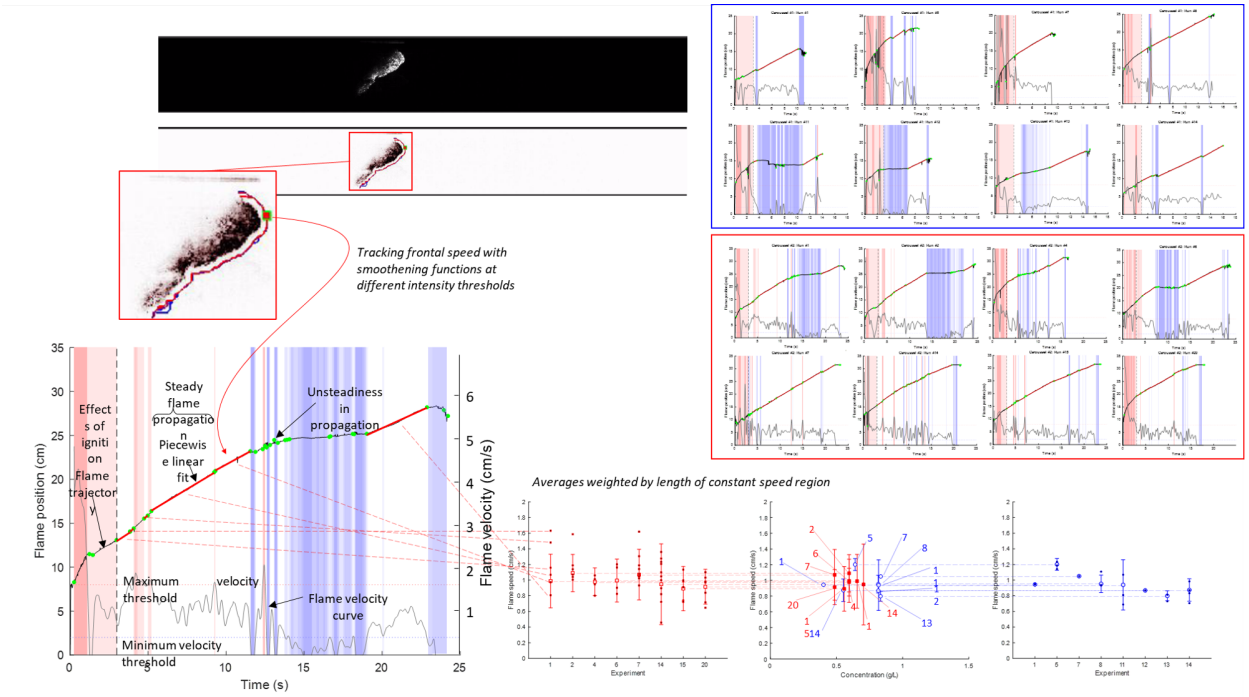

Figure B–8: Procedure used to determine the flame speed during experiments during the MAXUS-9 flight.

37.5 mm × 30 mm, spanning the entire width of the tube and at the same time recording individual particles (each pixel represents about 30 micrometers, i.e., the diameter of a particle). While the camera is equipped with a relatively large RAM memory (8 GB), the whole process is limited by the need to continuously save images into the on-board permanent memory. Thus, the RAM is split into four compartments, which allow the videos to be recorded, stored, and uploaded into the permanent memory continuously. Consequently, each high-speed video is limited to a little more than 2 seconds of recording. This also requires the videos to be triggered at the right time. The triggering occurs through direct analysis of the number of illuminated pixels on a region of the camera screen. When the

flame reaches the field of view, the video is recorded. An illustration of the position of the high-speed camera is shown in Figure B–9.

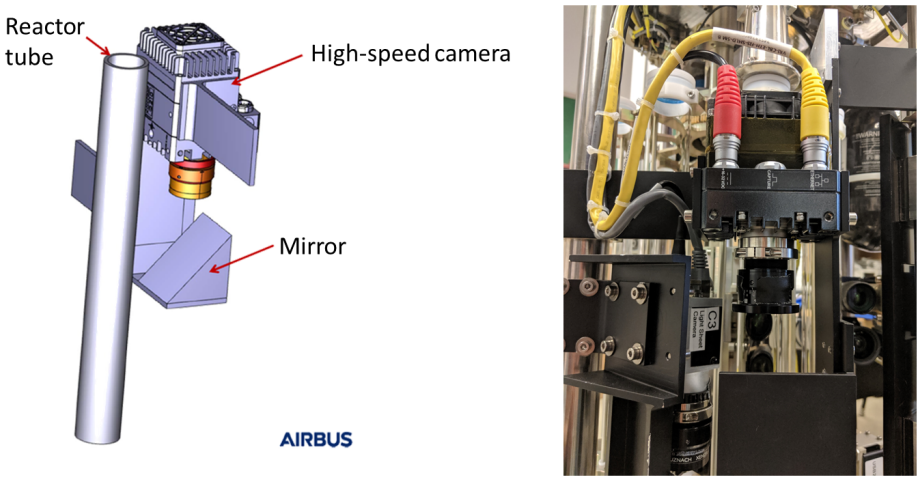

Figure B–9: Schematics and picture of the position of the high-speed camera on the apparatus. The CAD rendering is a courtesy of Airbus Defence and Space Germany.

B.2.4 Particle combustion time measurements and particle tracking

The particle combustion times were measured on the ground by means of a tube apparatus described in Publication 2. Fig. B–10 shows the typical image obtained with the high-speed camera in both the 20% O_2/80% Xe and the 40% O_2/60% Xe gas mixtures.

The combustion times were obtained by superimposing images of subsequent frames and counting the number of frames involved in the combustion of the particle. In these measurements, the combustion time was defined as the period, over which the particle exhibited an increased reaction. As illustrated by the 3D reconstruction of the evolution of the pixel area occupied by the particles in Fig. B–11, the particle combustion process consists of three phases: a pre-ignition induction phase, a fast-reaction phase, and a relatively long cooling phase. In the present work, only the fast-reaction region was used for the combustion time.

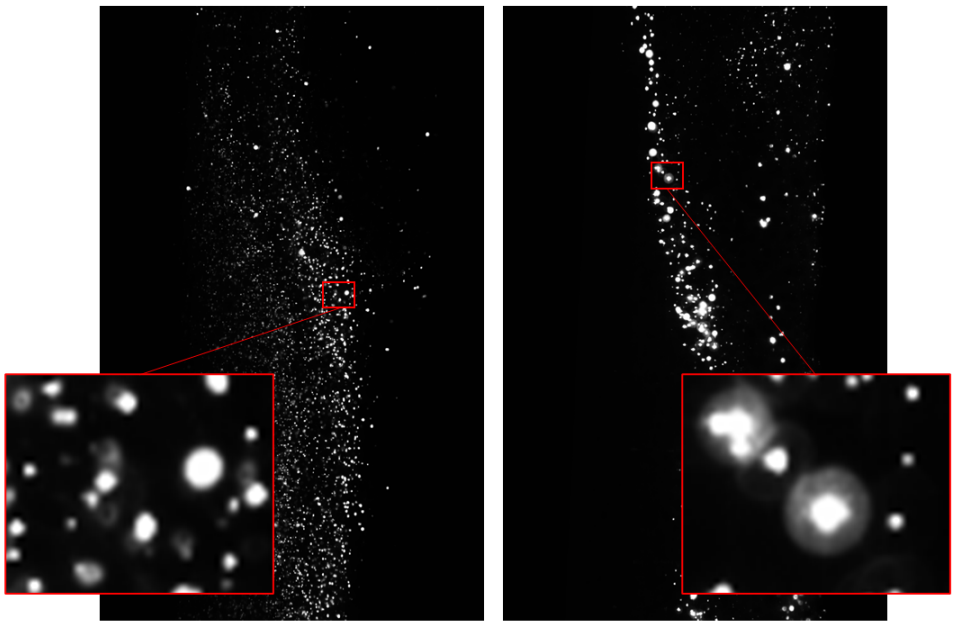

Figure B–10: Frames used for particle combustion time measurements for both the 20% O_2/80% Xe and the 40% O_2/60% Xe gas mixtures.

The main reason is that, in discrete flames, only the heat delivered during this phase plays a significant role in the propagation of the flame. The remaining thermal energy, produced slowly during a longer cool-off period, only contributes to the mean field relatively far behind the front. The intensity of the reaction was defined by an increased luminosity and a larger pixel area covered by the particle. Due to the well-defined contours of the particles, the selection of the appropriate intensity threshold was rather straightforward.

The selection of bounds for combustion time measurements was much easier in the 40%-O_2 mixture, in which the fast-reaction period was shorter and defined with a more abrupt increase and decrease in the pixel area occupied by the particle. In the 20%-O_2 mixture, the selection was more difficult, as the area covered by the particle evolved much more smoothly. While the pre-ignition phase was comparable to the 40%-O_2 case, the decrease in the pixel

area was significantly more gradual, making the determination of the end of reaction more challenging and uncertain.

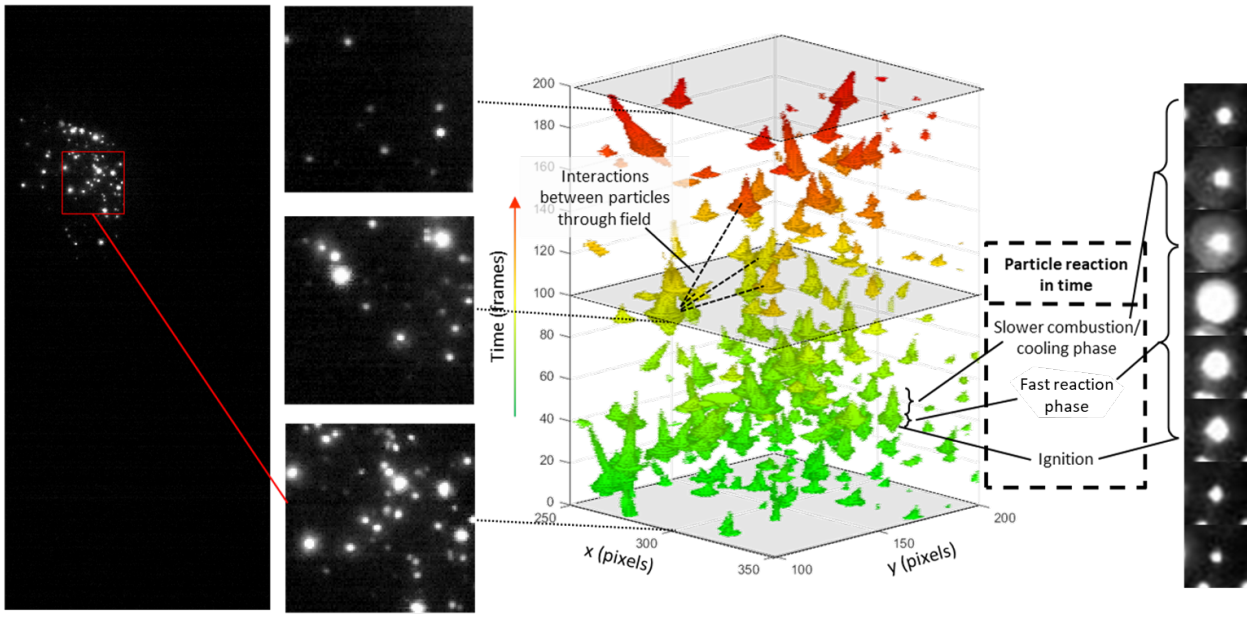

Figure B–11: Algorithm to determine the combustion time and ignition temperature of the particles.

Algorithms for particle tracking were developed in the context of the analysis of the TEXUS-56. The code, developed in the MATLAB, consists in several steps. First, to avoid significant difficulties associated with brighter clusters and overlapping particle, the contour() function is used with pixel intensity data to obtain a smoothed topographical map of intensity for a given frame. The map is then used to identify all the peaks, i.e., all the closed contour regions containing no higher-intensity contours. This algorithm provided a high accuracy in the determination of the centroid of practically all particles in the frame. The edge of the particle was determined as the lowest intensity contour containing only one particle. An algorithm based on the superposition of consecutive particle images between

frames was then used to provide particle tracking. As can be seen from Fig. B–11, the images of the particle over time then form the complete trace of the particle from its first appearance on the screen until its complete extinction.

References

[1] J. Palečka, J. Park, S. Goroshin, and J. M. Bergthorson, "Aluminum-propane-air hybrid flames in a Hele-Shaw cell," *Proceedings of the Combustion Institute*, vol. 38, no. 3, pp. 4461–4468, 2021.

[2] J. Palečka, J. Sniatowsky, S. Goroshin, A. J. Higgins, and J. M. Bergthorson, "A new kind of flame: Observation of the discrete flame propagation regime in iron particle suspensions in microgravity," *Combustion and Flame*, vol. 209, pp. 180–186, nov 2019.

[3] M. Soo, S. Goroshin, J. M. Bergthorson, and D. L. Frost, "Reaction of a particle suspension in a rapidly-heated oxidizing gas," *Propellants, Explosives, Pyrotechnics*, vol. 40, pp. 604–612, aug 2015.

[4] A. Y. Korol'chenko and N. L. Poletaev, "Stability of a limiting flame in an aerosol," *Combustion, Explosion, and Shock Waves*, vol. 20, pp. 366–371, jul 1984.

[5] J. Palecka, S. Goroshin, and J. M. Bergthorson, "Propagation and quenching of dual-front flames in binary-fuel mixtures," *Combustion Science and Technology*, vol. 190, pp. 1557–1579, sep 2018.

[6] S. Goroshin, J. Palečka, and J. M. Bergthorson, "Some fundamental aspects of laminar flames in nonvolatile solid fuel suspensions," *Progress in Energy and Combustion Science*, vol. 91, p. 100994, jul 2022.

[7] J. Arsenault, R. Aucoin, M. Toufaili, and Y. Zhang, "Dispersion System for Study of Flames in Particulate Suspensions in a 2-D Channel," tech. rep., McGill University, Montreal, Canada, 2017.

[8] I. Glassman, "Metal Combustion Processes," tech. rep., 1959.

[9] G. H. Markstein, "Combustion of metals," *AIAA Journal*, vol. 1, pp. 550–562, mar 1963.

[10] A. Merzhanov, "History and recent developments in SHS," *Ceramics International*, vol. 21, pp. 371–379, jan 1995.

[11] G. S. Upadhyaya, *Powder Metallurgy Technology*. Cambridge International Science Publishing, 2014.

[12] J. Bergthorson, S. Goroshin, M. Soo, P. Julien, J. Palecka, D. Frost, and D. Jarvis, "Direct combustion of recyclable metal fuels for zero-carbon heat and power," *Applied Energy*, vol. 160, pp. 368–382, dec 2015.

[13] J. M. Bergthorson, "Recyclable metal fuels for clean and compact zero-carbon power," *Progress in Energy and Combustion Science*, vol. 68, pp. 169–196, sep 2018.

[14] A. F. Hepp, D. L. Linne, J. E. Colvin, M. F. Wade, and J. E. Colvin, "Production and use of metals and oxygen for lunar propulsion," *Journal of Propulsion and Power*, 1994.

[15] U. S. Meyer, Mike L. (NASA Lewis Research Center Cleveland, OH, "Powdered aluminum and oxygen rocket propellants: Subscale combustion experiments," in *30th JANNAF Combustion Subcommittee Meeting,*, no. NASA Technical Memorandum 106439, (Monterey, California, USA), 1993.

[16] R. K. Eckhoff, *Dust Explosions in the Process Industries*. Elsevier, 2003.

[17] R. K. Eckhoff, *Explosion Hazards in the Process Industries*. Elsevier, 2006.

[18] R. H. Essenhigh, "Combustion and flame propagation in coal systems: A review," 1977.

[19] H. M. Cassel, "Fundamental Aspects of Dust Flames," tech. rep., Bureau of Mines Report of Investigations 6551, 1964.

[20] E. W. Price, "Recent advances in solid propellant combustion instability," *Symposium (International) on Combustion*, vol. 12, no. 1, pp. 101–113, 1969.

[21] A. G. Merzhanov, "Self-propagating high-temperature synthesis: twenty years of search and findings," in *Combustion and Plasma Synthesis of High-Temperature Materials*, pp. 1–53, New York: VCH Publishers, 1990.

[22] J. W. Martin, M. Salamanca, and M. Kraft, "Soot inception: Carbonaceous nanoparticle formation in flames," *Progress in Energy and Combustion Science*, vol. 88, p. 100956, jan 2022.

[23] M. Matalon, "Flame dynamics," *Proceedings of the Combustion Institute*, vol. 32, pp. 57–82, jan 2009.

[24] L. P. Yarin, G. Hetsroni, and A. Mosyak, *Combustion of two-phase reactive media*. Springer Science \& Business Media, 2004.

[25] C. K. Law, "A Simplified Theoretical Model for the Vapor-Phase Combustion of Metal Particles†," *http://dx.doi.org/10.1080/00102207308952359*, vol. 7, pp. 197–212, jul 2007.

[26] G. Faeth, "Evaporation and combustion of sprays," *Progress in Energy and Combustion Science*, vol. 9, pp. 1–76, jan 1983.

[27] X. Zhang, J. Yu, W. Gao, D. Zhang, J. Sun, S. Guo, and R. Dobashi, "Effects of particle size distributions on PMMA dust flame propagation behaviors," *Powder Technology*, vol. 317, pp. 197–208, jul 2017.

[28] L. D. Smoot and P. J. Smith, *Coal Combustion and Gasification*. Boston, MA: Springer US, 1985.

[29] D. Bradley, M. Lawes, H.-Y. Park, and N. Usta, "Modeling of laminar pulverized coal flames with speciated devolatilization and comparisons with experiments," *Combustion and Flame*, vol. 144, pp. 190–204, jan 2006.

[30] I. Glassman and R. A. Yetter, *Combustion*. Elsevier, 1996.

[31] A. Fontijn, *Gas Phase Metal Reactions*. Elsevier, 1992.

[32] L. A. Vulis, *Thermal Regimes of Combustion*. New York: McGraw-Hill, 1961.

[33] D. A. Frank-Kamenetskii and N. Thon, *Diffusion and Heat Exchange in Chemical Kinetics*. New Jersey: Princeton University Press, 1955.

[34] N. N. Semenov, "Chemical Kinetics & chain reactions," 1935.

[35] M. J. Soo, K. Kumashiro, S. Goroshin, D. L. Frost, and J. M. Bergthorson, "Thermal structure and burning velocity of flames in non-volatile fuel suspensions," *Proceedings of the Combustion Institute*, 2017.

[36] T. A. Steinberg, D. B. Wilson, and F. Benz, "The combustion phase of burning metals," *Combustion and Flame*, vol. 91, pp. 200–208, nov 1992.

[37] A. Y. Lukin and A. M. Stepanov, "Dispersity of the combustion products of metal particles," *Combustion, Explosion and Shock Waves 1983 19:3*, vol. 19, pp. 287–295, may 1983.

[38] A. Maček, "Fundamentals of combustion of single aluminum and beryllium particles," in *Symposium (International) on Combustion*, vol. 11, pp. 203–217, 1967.

[39] E. L. Dreizin and M. A. Trunov, "Surface phenomena in aluminum combustion," *Combustion and Flame*, vol. 101, no. 3, pp. 378–382, 1995.

[40] P. Bucher, R. A. Yetter, F. L. Dryer, E. P. Vicenzi, T. P. Parr, and D. M. Hanson-Parr, "Condensed-phase species distributions about Al particles reacting in various oxidizers," *Combustion and Flame*, 1999.

[41] M. W. Beckstead, "Correlating aluminum burning times," *Combustion, Explosion, and Shock Waves*, vol. 41, pp. 533–546, sep 2005.

[42] P. Lynch, H. Krier, and N. Glumac, "A correlation for burn time of aluminum particles in the transition regime," *Proceedings of the Combustion Institute*, vol. 32 II, no. 2, pp. 1887–1893, 2009.

[43] D. Ning, Y. Shoshin, J. van Oijen, G. Finotello, and L. de Goey, "Burn time and combustion regime of laser-ignited single iron particle," *Combustion and Flame*, vol. 230, p. 111424, aug 2021.

[44] X. Mi, A. Fujinawa, and J. M. Bergthorson, "A quantitative analysis of the ignition characteristics of fine iron particles," *Combustion and Flame*, vol. 240, p. 112011, jun 2022.

[45] A. Panahi, D. Chang, M. Schiemann, A. Fujinawa, X. Mi, J. M. Bergthorson, and Y. A. Levendis, "Combustion behavior of single iron particles-part I: An experimental study in a drop-tube furnace under high heating rates and high temperatures," *Applications in Energy and Combustion Science*, vol. 13, p. 100097, mar 2023.

[46] A. Fujinawa, J. Jean-Philyppe, A. Panahi, D. Chang, M. Schiemann, Y. Levendis, J. M. Bergthorson, and X. Mi, "Combustion behavior of single iron particles - Part II: A theoretical analysis based on a zero-dimensional model," 2022.

[47] H. M. Cassel and I. Liebman, "The cooperative mechanism in the ignition of dust dispersions," *Combustion and Flame*, vol. 3, no. 2, pp. 467–475, 1959.

[48] E. N. Rumanov and B. I. Khaikin, "Critical autoignition conditions for a system of particles," *Combustion, Explosion and Shock Waves 1969 5:1*, vol. 5, pp. 88–91, jan 1969.

[49] S. Goroshin, J. Mamen, A. Higgins, T. Bazyn, N. Glumac, and H. Krier, "Emission spectroscopy of flame fronts in aluminum suspensions," *Proceedings of the Combustion Institute*, vol. 31, pp. 2011–2019, jan 2007.

[50] R. Eschenbach and J. Agnew, "Use of the constant-volume bomb technique for measuring burning velocity," *Combustion and Flame*, vol. 2, pp. 273–285, sep 1958.

[51] D. B. Mercer, P. R. Amyotte, D. J. Dupuis, M. J. Pegg, A. Dahoe, W. B. de Heij, J. F. Zevenbergen, and B. Scarlett, "The influence of injector design on the decay of pre-ignition turbulence in a spherical explosion chamber," *Journal of Loss Prevention in the Process Industries*, vol. 14, pp. 269–282, jul 2001.

[52] A. Dahoe and L. de Goey, "On the determination of the laminar burning velocity from closed vessel gas explosions," *Journal of Loss Prevention in the Process Industries*, vol. 16, pp. 457–478, nov 2003.

[53] W. Nusselt, "Der Verbrennungsvorgang in der Kohlenstaubfeuerung," *Ver. Deut. Ing*, vol. 68, pp. 124–128, 1924.

[54] H. M. Cassel, A. K. Das Gupta, and S. Guruswamy, "Factors affecting flame propagation through dust clouds," in *Symposium on Combustion and Flame and Explosion Phenomena*, 1948.

[55] S. Goroshin, Y. L. Shoshin, N. D. Ageyev, and N. I. Poletaev, "The Premixed Aluminium Dust Flame Structure," *Flame Structure*, pp. 213–218, 1991.

[56] S. Goroshin, I. Fomenko, and J. H. S. Lee, "Burning velocities in fuel-rich aluminum dust clouds," *Symposium (International) on Combustion*, vol. 26, pp. 1961–1967, 1996.

[57] Y. Huang, G. A. Risha, V. Yang, and R. A. Yetter, "Combustion of bimodal nano/micron-sized aluminum particle dust in air," *Proceedings of the Combustion Institute*, vol. 31, pp. 2001–2009, jan 2007.

[58] R. Lomba, P. Laboureur, C. Dumand, C. Chauveau, and F. Halter, "Determination of aluminum-air burning velocities using PIV and Laser sheet tomography," *Proceedings of the Combustion Institute*, vol. 37, no. 3, pp. 3143–3150, 2019.

[59] Y. L. Shoshin and E. L. Dreizin, "Laminar Lifted Flame Speed Measurements for Aerosols of Metals and Mechanical Alloys," *AIAA Journal*, vol. 42, pp. 1416–1426, jul 2004.

[60] P. Julien, S. Whiteley, M. Soo, S. Goroshin, D. L. Frost, and J. M. Bergthorson, "Flame speed measurements in aluminum suspensions using a counterflow burner," *Proceedings of the Combustion Institute*, vol. 36, no. 2, pp. 2291–2298, 2017.

[61] M. McRae, P. Julien, S. Salvo, S. Goroshin, D. L. Frost, and J. M. Bergthorson, "Stabilized, flat iron flames on a hot counterflow burner," *Proceedings of the Combustion Institute*, vol. 37, no. 3, pp. 3185–3191, 2019.

[62] O. C. Kwon, G. Rozenchan, and C. K. Law, "Cellular instabilities and self-acceleration of outwardly propagating spherical flames," *Proceedings of the Combustion Institute*, vol. 29, no. 2, pp. 1775–1783, 2002.

[63] C. Law, G. Jomaas, and J. Bechtold, "Cellular instabilities of expanding hydrogen/propane spherical flames at elevated pressures: theory and experiment," *Proceedings of the Combustion Institute*, vol. 30, pp. 159–167, jan 2005.

[64] A. Omari and L. Tartakovsky, "Measurement of the laminar burning velocity using the confined and unconfined spherical flame methods – A comparative analysis," *Combustion and Flame*, vol. 168, pp. 127–137, jun 2016.

[65] E. F. Fiock and C. F. Marvin, "The Measurement of Flame Speeds.," *Chemical Reviews*, vol. 21, pp. 367–387, dec 1937.

[66] T. Skjold, K. L. Olsen, and D. Castellanos, "A constant pressure dust explosion experiment," *Journal of Loss Prevention in the Process Industries*, vol. 26, pp. 562–570, may 2013.

[67] P. Julien, J. Vickery, S. Goroshin, D. L. Frost, and J. M. Bergthorson, "Freely-propagating flames in aluminum dust clouds," *Combustion and Flame*, 2015.

[68] M. Matalon, "Intrinsic flame instabilities in premixed and nonpremixed combustion," *Annual Review of Fluid Mechanics*, vol. 39, pp. 163–191, jan 2007.

[69] H. D. Ross and S. R. Gollahalli, "Microgravity Combustion: Fire in Free Fall," *Applied Mechanics Reviews*, vol. 55, no. 6, p. B116, 2002.

[70] R. A. Strehlow, "Flammability Limits in a Standard Tube," in *Combustion Experiments in a Zero-Gravity Laboratory*, pp. 61–89, New York: American Institute of Aeronautics and Astronautics, jan 1981.

[71] A. Abbud-Madrid and P. D. Ronney, "Effects of radiative and diffusive transport processes on premixed flames near flammability limits," *Symposium (International) on Combustion*, vol. 23, pp. 423–431, jan 1991.

[72] C. M. Dunsky and A. C. Fernandez-Pello, "Gravitational effects on cellular flame structure," *Symposium (International) on Combustion*, vol. 23, pp. 1657–1662, jan 1991.

[73] H. G. Pearlman and P. D. Ronney, "Near-limit behavior of high-Lewis number premixed flames in tubes at normal and low gravity," *Physics of Fluids*, vol. 6, pp. 4009–4018, dec 1994.

[74] H. G. Pearlman, "Low-temperature oxidation reactions and cool flames at earth and reduced gravity," *Combustion and Flame*, vol. 121, pp. 390–393, apr 2000.

[75] P. D. Ronney, "Near-limit flame structures at low Lewis number," *Combustion and Flame*, vol. 82, pp. 1–14, oct 1990.

[76] P. D. Ronney, "Understanding combustion processes through microgravity research," *Symposium (International) on Combustion*, vol. 27, pp. 2485–2506, jan 1998.

[77] S. Kumagai, T. Sakai, and S. Okajima, "Combustion of free fuel droplets in a freely falling chamber," *Symposium (International) on Combustion*, vol. 13, pp. 779–785, jan 1971.

[78] D. R. Ballal, "Flame propagation through dust clouds of carbon, coal, aluminium and magnesium in an environment of zero gravity," *Proceedings of the Royal Society of London. A. Mathematical and Physical Sciences*, vol. 385, pp. 21–51, jan 1983.

[79] A. L. Berlad, "Combustion of particle clouds," in *Combustion Experiments in a Zero-Gravity Laboratory* (T. H. Cochran, ed.), pp. 91–127, New York: AIAA Progress in Astronautics and Aeronautics, 1981.

[80] H. Kobayashi, N. Ono, Y. Okuyama, and T. Nioka, "Flame propagation experiment of PMMA particle cloud in a microgravity environment," *Symposium (International) on Combustion*, vol. 25, no. 1, pp. 1693–1699, 1994.

[81] H. D. Ross, L. T. Facca, A. L. Berlad, and V. Tangirala, "Feasibility of reduced gravity experiments involving quiescent, uniform particle cloud combustion," *NASA Tech. Memo*, vol. 101371, 1989.

[82] A. L. Berlad, H. D. Ross, L. Facca, and V. Tangirala, "Particle cloud flames in acoustic fields," *Combustion and Flame*, vol. 82, pp. 448–450, dec 1990.

[83] J. Lee, O. Peraldi, and R. Knystautas, "Microgravity combustion of dust suspension," in *31st Aerospace Sciences Meeting*, (Reston, Virigina), American Institute of Aeronautics and Astronautics, jan 1993.

[84] S. Goroshin, M. Kolbe, J. Bellerose, and J. Lee, "Microgravity apparatus and ground-based study of the flame propagation and quenching in metal dust suspensions.," in *Seventh International Workshop on Microgravity Combustion and Chemically Reacting Systems*, p. 341, 2003.

[85] E. L. Dreizin and V. K. Hoffmann, "Constant pressure combustion of aerosol of coarse magnesium particles in microgravity," *Combustion and Flame*, vol. 118, pp. 262–280, jul 1999.

[86] E. L. Dreizin and V. K. Hoffmann, "Experiments on magnesium aerosol combustion in microgravity," *Combustion and Flame*, vol. 122, pp. 20–29, jul 2000.

[87] F.-D. Tang, S. Goroshin, A. Higgins, and J. Lee, "Flame propagation and quenching in iron dust clouds," *Proceedings of the Combustion Institute*, vol. 32, no. 2, pp. 1905–1912, 2009.

[88] S. Goroshin, F.-D. Tang, A. J. Higgins, and J. H. Lee, "Laminar dust flames in a reduced-gravity environment," *Acta Astronautica*, vol. 68, pp. 656–666, apr 2011.

[89] G. I. Sivashinski, "Diffusional-Thermal Theory of Cellular Flames," *Combustion Science and Technology*, vol. 15, pp. 137–145, jan 1977.

[90] G. I. Sivashinsky, "Instabilities, pattern formation, and turbulence in flames," *Annual Review of Fluid Mechanics*, 1983.

[91] P. Clavin and J. Sun, "Theory of acoustic instabilities of planar flames propagating in sprays or particle-laden gases," *Combustion Science and Technology*, vol. 78, pp. 265–288, aug 1991.

[92] J. Buckmaster and P. Clavin, "An acoustic-instability theory for particle-cloud flames," *Symposium (International) on Combustion*, vol. 24, pp. 29–36, jan 1992.

[93] C. Clanet, G. Searby, and P. Clavin, "Primary acoustic instability of flames propagating in tubes: cases of spray and premixed gas combustion," *Journal of Fluid Mechanics*, vol. 385, pp. 157–197, apr 1999.

[94] A. G. Merzhanov and E. N. Rumanov, "Physics of reaction waves," *Reviews of Modern Physics*, 1999.

[95] A. I. Vol'pert, V. A. Volpert, and V. A. Volpert, *Traveling wave solutions of parabolic systems*, vol. 140. American Mathematical Soc., 1994.

[96] A. Bayliss, B. J. Matkowsky, and V. A. Volpert, "Spatiotemporal pattern formation in solid fuel combustion," in *Advances in Sensing with Security Applications*, pp. 247–282, Dordrecht: Kluwer Academic Publishers, 2006.

[97] G. Darrieus, "Propagation d'un front de flamme, presented at La Technique Moderne," in *La Technique Moderne*, (Paris), 1938.

[98] L. Landau, "On the theory of slow combustion," *Acta Physicochim. USSR*, vol. 19, no. 77, 1944.

[99] M. Matalon, "The Darrieus–Landau instability of premixed flames," *Fluid Dynamics Research*, vol. 50, p. 051412, aug 2018.

[100] M. L. Frankel and G. I. Sivashinsky, "The Effect of Viscosity on Hydrodynamic Stability of a Plane Flame Front," *http://dx.doi.org/10.1080/00102208208923598*, vol. 29, pp. 207–224, dec 2007.

[101] G. H. Markstein, *Nonsteady Flame Propagation*. Elsevier, 1964.

[102] P. Pelce and P. Clavin, "Influence of hydrodynamics and diffusion upon the stability limits of laminar premixed flames," *Journal of Fluid Mechanics*, vol. 124, pp. 219–237, 1982.

[103] M. Matalon and B. J. Matkowsky, "Flames as gasdynamic discontinuities," *Journal of Fluid Mechanics*, vol. 124, pp. 239–259, 1982.

[104] H. G. Pearlman, "Excitability in high-lewis number premixed gas combustion," *Combustion and Flame*, vol. 109, no. 3, pp. 382–398, 1997.

[105] G. Jomaas, J. K. Bechtold, and C. K. Law, "Spiral waves in expanding hydrogen–air flames: Experiment and theory," *Proceedings of the Combustion Institute*, vol. 31, pp. 1039–1046, jan 2007.

[106] G. Jomaas and C. K. Law, "Observation and regime classification of pulsation patterns in expanding spherical flames," *Physics of Fluids*, vol. 22, p. 124102, dec 2010.

[107] F.-D. Tang, S. Goroshin, and A. J. Higgins, "Modes of particle combustion in iron dust flames," *Proceedings of the Combustion Institute*, vol. 33, pp. 1975–1982, jan 2011.

[108] A. Wright, A. J. Higgins, and S. Goroshin, "The discrete regime of flame propagation in metal particulate clouds," *Combustion Science and Technology*, vol. 188, pp. 2178–2199, dec 2016.

[109] H. Hanai, K. Maruta, H. Kobayashi, and T. Niioka, "Pulsating flame propagation of PMMA particle cloud in microgravity," *Symposium (International) on Combustion*, vol. 27, pp. 2675–2681, jan 1998.

[110] C. Nicoli, P. Haldenwang, and S. Suard, "Analysis of pulsating spray flames propagating in lean two-phase mixtures with unity Lewis number," *Combustion and Flame*, 2005.

[111] P. M. Krishenik, E. N. Rumanov, and K. G. Shkadinskii, "Modeling of combustion wave propagation in a carbon dust/gas mixture," *Combustion and Flame*, vol. 99, pp. 713–722, dec 1994.

[112] X. Mi, A. J. Higgins, S. Goroshin, and J. M. Bergthorson, "The influence of spatial discreteness on the thermo-diffusive instability of flame propagation with infinite Lewis number," *Proceedings of the Combustion Institute*, vol. 36, no. 2, pp. 2359–2366, 2017.

[113] S. Candel, "Combustion dynamics and control: Progress and challenges," *Proceedings of the Combustion Institute*, 2002.

[114] J. W. S. Lord Rayleigh, "The explanation of certain acoustical phenomena," *Nature*, vol. 18, pp. 319–321, jul 1878.

[115] G. Searby, "Acoustic Instability in Premixed Flames," *Combustion Science and Technology*, vol. 81, pp. 221–231, feb 1992.

[116] G. H. E. Markstein, "Instability phenomena in combustion waves," *Symposium (International) on Combustion*, vol. 4, pp. 44–59, jan 1953.

[117] W. Kaskan, "An investigation of vibrating flames," *Symposium (International) on Combustion*, vol. 4, pp. 575–591, jan 1953.

[118] S. H. Yoon, T. J. Noh, and O. Fujita, "Onset mechanism of primary acoustic instability in downward-propagating flames," *Combustion and Flame*, vol. 170, pp. 1–11, aug 2016.

[119] A. K. Dubey, Y. Koyama, S. H. Yoon, N. Hashimoto, and O. Fujita, "Range of "complete" instability of flat flames propagating downward in the acoustic field in combustion tube: Lewis number effect," *Combustion and Flame*, vol. 216, pp. 326–337, jun 2020.

[120] R. L. Raun and M. W. Beckstead, "A numerical model for temperature gradient and particle effects on Rijke burner oscillations," *Combustion and Flame*, 1993.

[121] S. Gallier and F. Godfroy, "Aluminum combustion driven instabilities in solid rocket motors," *Journal of Propulsion and Power*, 2009.

[122] S. K. Aslanov, V. G. Shevchuk, Y. N. Kostyshin, L. V. Boichuk, and S. V. Goroshin, "Oscillatory combustion of air suspensions," *Combustion, Explosion, and Shock Waves*, vol. 29, no. 2, pp. 163–169, 1993.

[123] S. V. Goroshin, V. G. Shevchuk, and N. D. Ageev, "Oscillatory combustion of gaseous suspensions," *Combustion, Explosion, and Shock Waves*, vol. 17, pp. 595–600, nov 1981.

[124] M. C. Branch, M. E. Sadequ, A. A. Alfarayedhi, and P. J. Van Tiggelen, "Measurements of the structure of laminar, premixed flames of CH4/NO2/O2 and CH2O/NO2/O2 Mixtures," *Combustion and Flame*, vol. 83, no. 3–4, pp. 228–239, 1991.

[125] S. Goroshin, M. Kolbe, and J. H. Lee, "Flame speed in a binary suspension of solid fuel particles," *Proceedings of the Combustion Institute*, vol. 28, pp. 2811–2817, jan 2000.

[126] B. I. Khaikin, A. K. Filonenko, and S. I. Khudyaev, "Flame propagation in the presence of two successive gas-phase reactions," *Combustion, Explosion, and Shock Waves*, vol. 4, pp. 343–348, oct 1968.

[127] B. I. Khaikin, A. K. Filonenko, S. I. Khudyaev, and T. M. Martem'yanova, "Stagewise combustion of nonvolatile easily dispersed substances," *Combustion, Explosion and Shock Waves 1975 9:2*, vol. 9, pp. 144–156, mar 1973.

[128] V. S. Berman and Y. S. Ryazantsev, "Asymptotic analysis of stationary distribution of the front of a two-stage consecutive exothermic reaction in a condensed medium," *Journal of Applied Mechanics and Technical Physics 1975 14:1*, vol. 14, pp. 60–70, jan 1973.

[129] V. S. Berman, Y. S. Ryazantsev, and V. M. Shevtsova, "Nonsteady propagation of two-stage sequential reaction in the condensed phase," *Combustion, Explosion and Shock Waves 1982 17:6*, vol. 17, pp. 646–649, nov 1981.

[130] S. Goroshin, M. Bidabadi, and J. Lee, "Quenching distance of laminar flame in aluminum dust clouds," *Combustion and Flame*, vol. 105, pp. 147–160, apr 1996.

[131] M. Soo, P. Julien, S. Goroshin, J. M. Bergthorson, and D. L. Frost, "Stabilized flames in hybrid aluminum-methane-air mixtures," *Proceedings of the Combustion Institute*, vol. 34, pp. 2213–2220, jan 2013.

[132] P. Julien, S. Whiteley, S. Goroshin, M. J. Soo, D. L. Frost, and J. M. Bergthorson, "Flame structure and particle-combustion regimes in premixed methane–iron–air suspensions," *Proceedings of the Combustion Institute*, vol. 35, no. 2, pp. 2431–2438, 2015.

[133] J. Palecka, P. Julien, S. Goroshin, J. M. Bergthorson, D. L. Frost, and A. J. Higgins, "Quenching distance of flames in hybrid methane–aluminum mixtures," *Proceedings of the Combustion Institute*, vol. 35, no. 2, pp. 2463–2470, 2015.

[134] J. Palečka, S. Goroshin, A. J. Higgins, Y. Shoshin, P. de Goey, J.-R. Angilella, H. Oltmann, A. Stein, B. Schmitz, A. Verga, S. Vincent-Bonnieu, W. Sillekens, and J. M. Bergthorson, "Percolating Reaction–Diffusion Waves (PERWAVES)—Sounding rocket combustion experiments," *Acta Astronautica*, vol. 177, pp. 639–651, dec 2020.

[135] J. Vickery, P. Julien, S. Goroshin, J. M. Bergthorson, and D. L. Frost, "Propagation of isobaric spherical flames in hybrid aluminum-methane fuel mixtures," *Journal of Loss Prevention in the Process Industries*, vol. 49, pp. 472–480, sep 2017.

[136] P. G. Saffman and G. Taylor, "The Penetration of a Fluid into a Porous Medium or Hele-Shaw Cell Containing a More Viscous Liquid," *Proceedings of the Royal Society A: Mathematical, Physical and Engineering Sciences*, vol. 245, no. 1242, pp. 312–329, 1958.

[137] G. Joulin and G. Sivashinsky, "Influence of Momentum and Heat Losses on the Large-Scale Stability of Quasi-2D Premixed Flames," *Combustion Science and Technology*, vol. 98, pp. 11–23, jun 1994.

[138] J. Sharif, M. Abid, and P. D. Ronney, "Premixed-gas flame propagation in Hele-Shaw cells," in *1st Joint U.S. Sections Combustion Institute Meeting*, (Washington DC), NASA, 1999.

[139] C. Almarcha, J. Quinard, B. Denet, E. Al-Sarraf, J. M. Laugier, and E. Villermaux, "Experimental two dimensional cellular flames," *Physics of Fluids*, vol. 27, no. 9, pp. 9–11, 2015.

[140] J. Wongwiwat, J. Gross, and P. Ronney, "Flame Propagation in Narrow Channels at Varying Lewis Number," in *25th International Colloquium on the Dynamics of Explosions and Reactive Systems*, 2015.

[141] E. A. Sarraf, C. Almarcha, J. Quinard, B. Radisson, and B. Denet, "Quantitative Analysis of Flame Instabilities in a Hele-Shaw Burner," *Flow, Turbulence and Combustion*, vol. 101, pp. 851–868, oct 2018.

[142] F. Veiga-López, D. Martínez-Ruiz, E. Fernández-Tarrazo, and M. Sánchez-Sanz, "Experimental analysis of oscillatory premixed flames in a Hele-Shaw cell propagating towards a closed end," *Combustion and Flame*, 2019.

[143] B. Radisson, J. Piketty-Moine, and C. Almarcha, "Coupling of vibro-acoustic waves with premixed flame," *Physical Review Fluids*, vol. 4, p. 121201, dec 2019.

[144] D. Martínez-Ruiz, F. Veiga-López, D. Fernández-Galisteo, V. N. Kurdyumov, and M. Sánchez-Sanz, "The role of conductive heat losses on the formation of isolated flame cells in Hele-Shaw chambers," *Combustion and Flame*, vol. 209, pp. 187–199, nov 2019.

[145] D. Fernández-Galisteo, V. N. Kurdyumov, and P. D. Ronney, "Analysis of premixed flame propagation between two closely-spaced parallel plates," *Combustion and Flame*, 2018.

[146] A. P. Aldushin, "Stationary propagation of an exothermic-reaction front in a condensed medium," *Journal of Applied Mechanics and Technical Physics 1975 15:3*, vol. 15, pp. 363–370, may 1974.

[147] A. P. Hardt and P. V. Phung, "Propagation of gasless reactions in solids—I. Analytical study of exothermic intermetallic reaction rates," *Combustion and Flame*, vol. 21, pp. 77–89, aug 1973.

[148] A. S. Mukasyan and A. S. Rogachev, "Discrete reaction waves: Gasless combustion of solid powder mixtures," *Progress in Energy and Combustion Science*, vol. 34, pp. 377–416, jun 2008.

[149] A. S. Mukasyan, S. Hwang, A. E. Sytchev, A. S. Rogachev, A. G. Merzhanov, and A. Varma, "Combustion wave microstructure in heterogeneous gasless systems," *Combustion Science and Technology*, vol. 115, pp. 335–353, jun 1996.

[150] T. L. Jackson and J. Buckmaster, "Heterogeneous Propellant Combustion," *https://doi.org/10.2514/2.1761*, vol. 40, pp. 1122–1130, may 2012.

[151] M. N. Chee, S. G. Whittington, and R. Kapral, "A model of wave propagation in an inhomogeneous excitable meduim," *Physica D: Nonlinear Phenomena*, vol. 32, pp. 437–450, dec 1988.

[152] A. R. Kerstein, "Percolation model of polydisperse composite solid propellant combustion," *Combustion and Flame*, vol. 69, pp. 95–112, jul 1987.

[153] Y. L. Shoshin, S. Goroshin, and A. Zolotko, "Flame in a medium with discrete sources," *Dokl. Phys. Chem. (Engl. Transl.); (United States)*, vol. 291, 1987.

[154] S. Goroshin, J. Lee, and Y. Shoshin, "Effect of the discrete nature of heat sources on flame propagation in particulate suspensions," *Symposium (International) on Combustion*, vol. 27, pp. 743–749, jan 1998.

[155] F.-D. Tang, A. J. Higgins, and S. Goroshin, "Propagation limits and velocity of reaction-diffusion fronts in a system of discrete random sources," *Physical Review E*, vol. 85, p. 036311, mar 2012.

[156] F. Lam, X. Mi, and A. J. Higgins, "Front roughening of flames in discrete media," *Physical Review E*, vol. 96, p. 013107, jan 2017.

[157] F. Y. Lam, X. Mi, and A. J. Higgins, "Dimensional scaling of flame propagation in discrete particulate clouds," *Combustion Theory and Modelling*, vol. 24, pp. 486–509, may 2020.

[158] N. Provatas, T. Ala-Nissila, M. Grant, K. R. Elder, and L. Piché, "Scaling, propagation, and kinetic roughening of flame fronts in random media," *Journal of Statistical Physics*, vol. 81, pp. 737–759, nov 1995.

[159] N. Provatas, T. Ala-Nissila, M. Grant, K. R. Elder, and L. Piché, "Flame propagation in random media," *Physical Review E*, vol. 51, pp. 4232–4236, may 1995.

[160] V. G. Ivancevic and T. T. Ivancevic, "Complex Nonlinearity," 2008.

[161] M. M. Henkel, H. Hinrichsen, and S. Lubeck, "Non-equilibrium phase transitions. Volume I, Absorbing phase transitions," 2008.

[162] V. S. Zykov and E. Bodenschatz, "Wave Propagation in Inhomogeneous Excitable Media," *https://doi.org/10.1146/annurev-conmatphys-033117-054300*, vol. 9, pp. 435–461, mar 2018.

[163] M. Schiulaz, C. R. Laumann, A. V. Balatsky, and B. Z. Spivak, "Theory of combustion in disordered media," *Physical Review E*, vol. 97, p. 062133, jun 2018.

[164] M. Schiulaz, C. R. Laumann, A. V. Balatsky, and B. Z. Spivak, "Theory of deflagration in disordered media," *Physical Review E*, vol. 95, p. 032103, mar 2017.

[165] F. Peruggi, "First-order transitions in percolation models," *Physica A: Statistical Mechanics and its Applications*, vol. 141, pp. 140–150, feb 1987.

[166] A. Piscitelli, A. Coniglio, A. Fierro, and M. P. Ciamarra, "Jamming as a random first-order percolation transition," *Physica A: Statistical Mechanics and its Applications*, vol. 569, p. 125796, may 2021.

[167] G. Grimmett, "Percolation," p. 447, 1999.

[168] M. Sahimi, "Percolation, Introduction to," *Encyclopedia of Complexity and Systems Science*, pp. 6518–6521, 2009.

[169] P. De Gregorio, A. Lawlor, and K. A. Dawson, "Bootstrap Percolation," *Encyclopedia of Complexity and Systems Science*, pp. 608–626, 2009.

[170] M. Knackstedt and L. Paterson, "Invasion percolation," *Encyclopedia of Complexity and Systems Science*, pp. 4947–4960, 2009.

[171] H. H. CHIU and T. M. LIU, "Group Combustion of Liquid Droplets," *Combustion Science and Technology*, vol. 17, pp. 127–142, dec 1977.

[172] W. A. Sirignano, "Advances in droplet array combustion theory and modeling," *Progress in Energy and Combustion Science*, vol. 42, no. 1, pp. 54–86, 2014.

[173] F. Durst, "Fluid mechanics : an introduction to the theory of fluid flows.," 2010.

[174] A. N. Lipatnikov and J. Chomiak, "Turbulent flame speed and thickness: phenomenology, evaluation, and application in multi-dimensional simulations," *Progress in Energy and Combustion Science*, vol. 28, pp. 1–74, jan 2002.

[175] J. F. Driscoll, "Turbulent premixed combustion: Flamelet structure and its effect on turbulent burning velocities," *Progress in Energy and Combustion Science*, vol. 34, pp. 91–134, feb 2008.

[176] K. K. Kuo and R. Acharya, "Applications of Turbulent and Multiphase Combustion," *Applications of Turbulent and Multiphase Combustion*, apr 2012.

[177] S. Elghobashi and G. C. Truesdell, "On the two-way interaction between homogeneous turbulence and dispersed solid particles. I: Turbulence modification," *Physics of Fluids A: Fluid Dynamics*, vol. 5, p. 1790, sep 1998.

[178] C. Peng, O. M. Ayala, and L. P. Wang, "A direct numerical investigation of two-way interactions in a particle-laden turbulent channel flow," *Journal of Fluid Mechanics*, vol. 875, pp. 1096–1144, sep 2019.

[179] T. F. Wall, S. P. Bhattacharya, L. L. Baxter, G. Richards, and J. N. Harb, "The character of ash deposits and the thermal performance of furnaces," *Fuel Processing Technology*, vol. 44, pp. 143–153, sep 1995.

[180] W. Mason and K. Saunders, "Recirculating flow in vertical columns of gas-solid suspension," *Journal of Physics D: Applied Physics*, vol. 8, no. 14, p. 1674, 1975.

[181] Y. B. Zeldovich, A. Istratov, N. Kidin, and V. Librovich, "Flame Propagation in Tubes: Hydrodynamics and Stability," *Dynamics of Curved Fronts*, pp. 499–511, jan 1988.

[182] D. Bradley, "Combustion Instabilities," in *Turbulent Premixed Flames*, 2011.

[183] A. Levy, "An Optical Study of Flammability Limits," *Proceedings of the Royal Society of London A*, vol. 283, no. 1392, pp. 134–145, 1965.

[184] F. A. Williams, *Combustion Theory : The Fundamental Theory of Chemically Reacting Flow Systems*. Menlo Park, California: The Benjamin /Cummings, 1985.

[185] S. Goroshin, F.-D. Tang, and A. J. Higgins, "Reaction-diffusion fronts in media with spatially discrete sources," *Physical Review E*, vol. 84, p. 027301, aug 2011.

[186] W. Banzhaf, "Self-organizing Systems," in *Encyclopedia of Complexity and Systems Science*, pp. 8040–8050, New York, NY: Springer New York, 2009.

[187] R. A. Meyers, ed., *Encyclopedia of Complexity and Systems Science*. New York, NY: Springer New York, 2009.

[188] P. M. Chaikin and T. C. Lubensky, "Principles of Condensed Matter Physics," *Principles of Condensed Matter Physics*, jun 1995.

[189] A. Dokhan, E. W. Price, J. M. Seitzman, and R. K. Sigman, "The ignition of ultra-fine aluminum in ammonium perchlorate solid propellant flames," *39th AIAA/ASME/SAE/ASEE Joint Propulsion Conference and Exhibit*, 2003.

[190] P. F. Pokhil, A. F. Belyaev, Y. V. Frolov, V. S. Logachev, and A. I. Korotkov, "Combustion of metal powders in active media," *Defense Technical Information Center, Technical Report AD0769576*, 1972.

[191] L. Berger, K. Kleinheinz, A. Attili, and H. Pitsch, "Characteristic patterns of thermodiffusively unstable premixed lean hydrogen flames," *Proceedings of the Combustion Institute*, vol. 37, pp. 1879–1886, jan 2019.